ELECTRICAL CHARACTERIZATION OF GaAs MATERIALS AND DEVICES

DAVID C. LOOK
Wright State University, USA

JOHN WILEY & SONS
Chichester · New York · Brisbane · Toronto · Singapore

Chapter 1

THE HALL EFFECT AND MAGNETORESISTANCE

At the close of his famous paper announcing the discovery of what we now know as the *Hall effect,* E. H. Hall (1879) surmised that, 'To make a more complete and accurate study of the phenomenon described in the preceding pages, availing myself of the advice and assistance of Prof. Rowland, will probably occupy me for some months to come.' Indeed, that phenomenon was not only to occupy his time, but also that of multitudes of other researchers in the intervening years. Virtually every major semicondutor laboratory, and even most smaller ones, make use of the Hall effect regularly, both because of the simplicity of the technique, and the central importance of the parameters it measures, namely carrier concentration n (or p) and mobility μ. (The latter, of course, also requires a conductivity measurment.) However, the simplicity can sometimes perhaps be a disadvantage, because of subtle pitfalls, which are present in every technique but are not always studied and taken seriously, and also because the potential to get much more information than just n and μ is often not recognized. In this chapter, we hope to address both of these problems.

We will first consider matters of a very practical, mundane nature, e.g. the best contacting materials for both conductive and semi-insulating (SI) materials, the kinds of apparatus which are commercially available, the sample geometries which give the most accurate results, and the best techniques for preparing the surface of an SI GaAs sample for measurement. The latter two discussions are supplemented by very recent round-robin studies. On the other hand, we feel that problems of a theoretical nature are also important, such as the approximations which are explicitly or implicitly part of the equations which are commonly used. Some theoretical topics, such as mixed conductivity and impurity (or defect) statistics, are covered more thoroughly here (including the Appendices) than in most other treatises on this subject. Also, depth-profiling techniques are considered in detail here because of their importance in thin-layer devices. Other subjects, such as a.c. Hall techniques, are not covered as thoroughly, because they are not widely used for GaAs and also because

:y are covered sufficiently in other works (Wieder, 1979). There is, of ırse, some duplication of material found in other books because a ınograph such as this should be fairly complete. However, we believe that : emphasis on GaAs and the strong coverage of both practical and :oretical matters make the subject matter here distinct from other atments. For a good background on electrical measurements in semicon- ctors, the reader can consult Putley (1960), Beer (1963), Blood and ton (1978), Wieder (1979), and Nag (1980).

1.1 PRACTICAL CONSIDERATIONS

.1 General working equations: Hall-bar structures

: begin with a discussion of the basic formulas necessary to carry out a ıple Hall-effect analysis. Detailed derivations of these formulas, and their ationships to the various physical parameters of interest, are given later. e prototype structure for the Hall-effect experiment, herein called a 'Hall r', is shown in Fig. 1.1.1. The chief advantages of the Hall bar are ease of

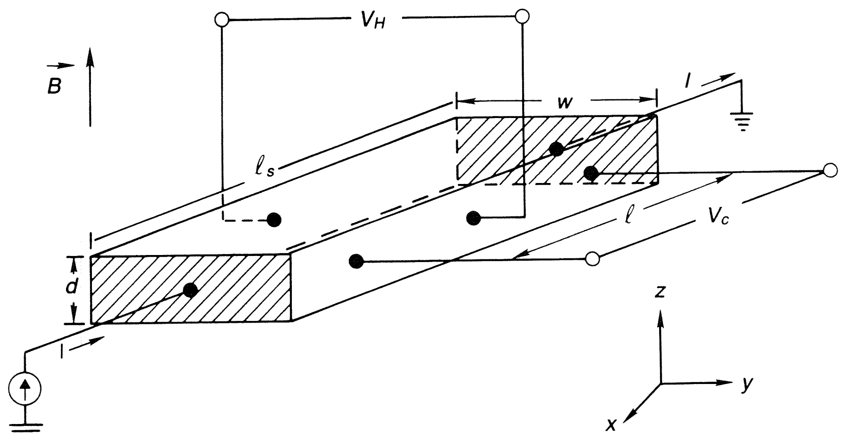

Fig. 1.1.1 The Hall-bar configuration for resistivity and Hall-effect measurements

brication and simplicity of analysis due to the uniformity of electric field ıes along the length of the sample. Although in the past this structure was e most commonly used pattern, that is no longer true; some of the more ›pular structures will be considered later. Assume that the charge carriers e electrons and that they are all traveling with a velocity v in the x rection, before application of a magnetic field, $\mathbf{B} = B\hat{\mathbf{z}}$. In actuality, the ectrons will have random thermal velocities of about 10^7 cm/s (at 296 K), ith only a small *net* velocity in the x direction ($v_x \simeq 10^4$ cm/s for an electric :ld of about 1 V/cm). However, the random velocity is not important in ıis simple model.

Upon application of a magnetic field in the z direction, the electrons experience a force $-e\mathbf{v} \times \mathbf{B}$, which will have a y component $-e(\mathbf{v} \times \mathbf{B})_y = -e(v_z B_x - v_x B_z) = ev_x B_z$. The electronic charge will build up on the $+y$ face of the sample until an opposing force $-eE_y$ just balances the $ev_x B_y$ force. With this balance, the electrons again have no y component of velocity, just as was the case when $B = 0$. The total current density is of course $j_x = -nev_x$, so that $eE_y = ev_x B = -eBj_x/ne$. The Hall coefficient R_H is defined as

$$R_H = \frac{E_y}{j_x B} = -\frac{1}{ne} \tag{1.1.1}$$

Although the above picture is far too simple, in fact Eq. (1.1.1) is close to reality for most semiconductor materials, and in particular GaAs. A more accurate analysis gives $R_H = -r/ne$ where r, the *Hall factor*, typically varies between 1.0 and 1.3 for GaAs, under a wide variety of temperatures, sample purities, and other factors.

We might expect that for low values of $\mathbf{E}$, the velocity v_x would vary linearly with E_x, i.e., $v_x = \mu E_x$. This is the true definition of *ohmic* current flow, which will be assumed to hold in all the examples discussed in this chapter. (However, other more 'practical' definitions will also be discussed.) The coefficient of proportionality between $\mathbf{v}$ and $\mathbf{E}$, called the *mobility* μ, is nearly isotropic for GaAs. The mobility can then be measured as follows:

$$\mu \equiv \frac{v_x}{E_x} = -\frac{j_x}{neE_x} = \frac{j_x}{E_x}\frac{E_y}{j_x B} = \frac{1}{B}\frac{E_y}{E_x} = \frac{1}{B}\frac{V_c}{V_H}\frac{w}{l} \tag{1.1.2}$$

where, in Fig. 1.1.1, $V_c = E_x l$ is the *conductivity* voltage, i.e., the voltage between the contacts parallel to the current flow, and $V_H = E_y w$ is the voltage between the contacts perpendicular to the current flow, the *Hall voltage*. Equations (1.1.1) and (1.1.2) constitute the working equations for the Hall-bar experiment. However, in terminology, we usually call μ the *conductivity mobility*, and designate the quantity measured by Eq. (1.1.2) as the *Hall mobility*, μ_H. The conductivity mobility is defined by the equation $\sigma = ne\mu$, where σ is the conductivity. When the electrons all have the same magnitude of x-axis velocity, as in our simple example, then $\mu_H = \mu$, as will be shown later. Also, in general, Eq. (1.1.1) should read $R_H = -1/n_H e$, where n_H is the *Hall concentration*. Again, for electrons all of the same velocity, $n_H = n$.

At this point, units should be discussed. There are four systems of units currently in vogue: (1) esu, (2), emu, (3) MKS, and (4) laboratory. The latter two seem to be the preferred systems for semiconductor work so that we will not use the others here. (Actually, the laboratory system of units includes elements of the other three.) In succeeding chapters of this book, all equations and expressions will be in MKS units unless specifically stated otherwise. A conversion table for some of the common quantities is given in Table 1.1.1. With the aid of this table, we can write the Hall-bar working

1.1.1 Units in th .KS and laboratory systems. [To convert, use 1 MKS (multiplication factor) × 1 laboratory unit. For example, 1 ampere/m^2 = npere/cm^2]

Quantity	Symbol	MKS	= Factor ×	Laboratory
acitance	C	farad	1	farad
rier concentration	c, n, p	m^{-3}	10^{-6}	cm^{-3}
rge	q, e	coulomb	1	coulomb
ıductivity (volume)	σ	(ohm-m)$^{-1}$	10^{-2}	(ohm-cm)$^{-1}$
rent	I	ampere	1	ampere
rent density	j	ampere/m^2	10^{-4}	ampere/cm^2
ctric field intensity	E	volt/m	10^{-2}	volt/cm
l coefficient	R	m^3/coulomb	10^6	cm^3
gnetic induction	B	V-s/m^2	10^4	gauss
bility	μ	m^2/V-s	10^4	cm^2/V-s
istivity	ρ	ohm-m	10^2	ohm-cm

tions in both systems:

$$\rho = \sigma^{-1} = \frac{E_x}{j_x} = \frac{V_c(\mathrm{V})\, w(\mathrm{m}) d(\mathrm{m})}{I(\mathrm{A})\quad l(\mathrm{m})}\ \Omega\text{-m} \qquad (1.1.3a)$$

$$= \frac{V_c(\mathrm{V})\, w(\mathrm{cm}) d(\mathrm{cm})}{I(\mathrm{A})\quad l(\mathrm{cm})}\ \Omega\text{-cm} \qquad (1.1.3b)$$

$$\mu_H = |R_H \sigma| = \frac{1}{B}\frac{E_y}{E_x} = \frac{1}{B(\mathrm{V\text{-}s/m^2})}\frac{V_H(\mathrm{V})}{V_c(\mathrm{V})}\frac{l(\mathrm{m})}{w(\mathrm{m})}\frac{\mathrm{m}^2}{\mathrm{V\text{-}s}} \qquad (1.1.4a)$$

$$= \frac{10^8}{B(\mathrm{gauss})}\frac{V_H(\mathrm{V})}{V_c(\mathrm{V})}\frac{l(\mathrm{cm})}{w(\mathrm{cm})}\frac{\mathrm{cm}^2}{\mathrm{V\text{-}s}} \qquad (1.1.4b)$$

$$n_H = \frac{1}{|eR_H|} = \frac{j_x B}{eE_y} = 6.25 \times 10^{18}\frac{I(\mathrm{A})B(\mathrm{V\text{-}s/m^2})}{V_H(\mathrm{V})d(\mathrm{m})}\ \mathrm{m}^{-3} \qquad (1.1.5a)$$

$$= 6.25 \times 10^{10}\frac{I(\mathrm{A})B(\mathrm{gauss})}{V_H(\mathrm{V})d(\mathrm{cm})}\ \mathrm{cm}^{-3} \qquad (1.1.5b)$$

? Geometrical effects: Hall-bar structures

sider the structures shown in Fig. 1.1.2, for which a Hall voltage is sured across the sample dimension which is perpendicular to the ent. Figure 1.1.2(a) is the preferred structure, with $l_s/w \gtrsim 3$. Figure 2(b) has an opposite l/w aspect ratio, with $l_s/w \ll 1$. As $l_s \to 0$, it is clear the Hall voltage cannot be maintained, because the large-area current acts will tend to short out this voltage. The magnitude of the shorting ct is shown in Fig. 1.1.3 (Isenberg *et al.*, 1948), in which the ratio of the erved and true Hall voltages is plotted as a function of l_s/w. It is ımed here that the voltage contacts are in the middle of the sample. As

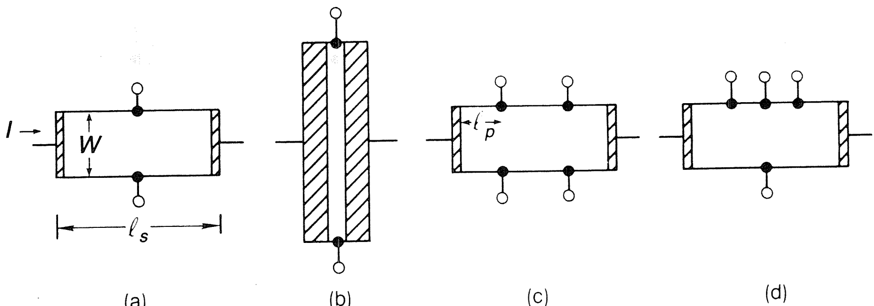

Fig. 1.1.2 Various contact arrangements for measurement of the Hall voltage: (a) preferred aspect ratio; (b) opposite aspect ratio, which shorts Hall voltage; (c) and (d) configurations which permit resistivity measurements also

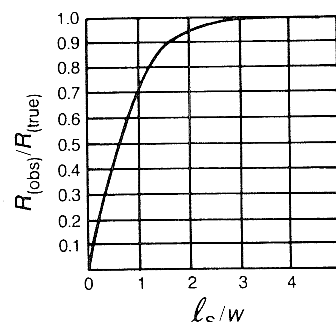

Fig. 1.1.3 Shorting effect of large-area current contacts on Hall voltage. The parameters are defined in Fig. 1.1.2(a). (After Isenberg *et al.* (1948). Reproduced by permission of The American Institute of Physics)

can be seen, if $l_s/w \gtrsim 3$, then the shorting effect reduces V_H by less than 1%, whereas if $l_s/w = 1$, the effect is about 30%. Thus, it is recommended that a structure of type (a) be prepared with $l_s/w \gtrsim 3$.

Another commonly used structure is shown in Fig. 1.1.2(c). The advantage of this configuration is that a conductivity can also be determined since the parallel voltage V_c can be measured between two of the contacts on one side or the other. However, one must again be careful of Hall-voltage shorting effects, as illustrated in Fig. 1.1.4 (Volger, 1950). For example, if $l_s/w = 4$, then l_p/w (see Fig. 1.1.2c) must be greater than 1, or $\frac{1}{4}l_s/w$. For smaller values of l_s/w it becomes progressively more difficult to measure a true Hall voltage, and by the time $l_s/w \lesssim 2$, it is impossible.

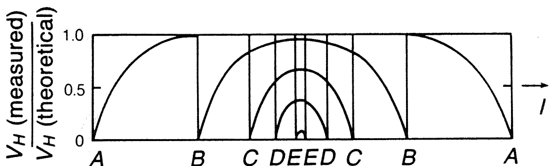

Fig. 1.1.4 Ratio of the experimentally measured Hall voltage to the Hall voltage calculated theoretically for an ideal configuration as a function of the geometry of the experimental configuration. The solid vertical lines represent the ends of five different experimental samples, AA to EE, corresponding to progressively smaller ratios of length to width from 4/1 for AA to 1/8 for EE. Horizontal distance corresponds to the placement of the Hall probes on the sample. For example, for a sample with the length/width ratio of AA, Hall probes must be at least one fourth the length of the crystal in from the ends, in order for the true theoretical Hall voltage to be measured. For length/width ratios of 2/1 or less, no position of the Hall probes gives the theoretical Hall voltage. (After Volger (1950). Reproduced by permission of Philips Research Laboratories)

rhaps the most convenient Hall-bar structure is the one shown in Fig. l.2(d), in which the Hall voltage V_H is measured in the middle, and the nductivity (parallel) voltage V_c between the two outer contacts on one e. This configuration has been used in an on-chip test pattern, to be esented later (Fig. 1.1.17).

Up to now we have assumed that the experimenter has been able to make int contacts of vanishing width. Obviously this is impossible, and the ite contact dimension, illustrated in Fig. 1.1.5, must be taken into nsideration. Haeusler and Lippman (1968) have shown that the degrada- n in Hall mobility can be approximated, for $\mu B \ll 1$, by

$$\frac{\Delta\mu_H}{\mu_H} = 1 - (1 - \mathrm{e}^{-\pi l_s/2w})(1 - 2l_c/\pi w) \qquad (1.1.6)$$

ıere $\Delta\mu_H$ is the amount μ_H must be *increased* to obtain the true value. ppose, for example, $l_s/w = 3$. Then $\Delta\mu_H/\mu_H \simeq 0.0090 + 0.631 l_c/w$, or $\iota_H/\mu_H \simeq 0.13$ for $l_c/w \simeq 0.2$. Thus, errors due to finite contact size can be preciable and must be taken into account, especially in small samples.

To circumvent the contact-size problem, but retain the advantages of a ıll-bar, side arms can be added, as shown in Fig. 1.1.6. Here, as long as $\lesssim l_w$, $l_w \lesssim w/3$, and $l \gtrsim 4w$, the deviation from the rectangular sample with ıe point contacts is not large (Jandl *et al.*, 1974). However, such a ucture is obviously much more difficult to fabricate, and finds its greatest e with thin-film samples, when photolithographic techniques can be

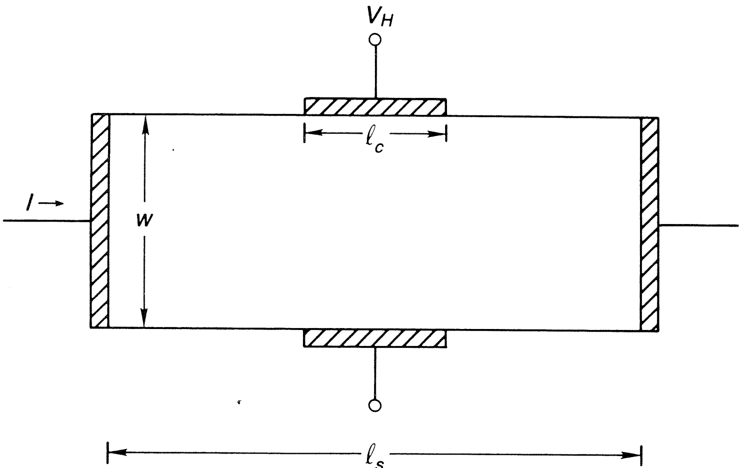

Fig. 1.1.5 A Hall bar with finite Hall-voltage contact dimensions

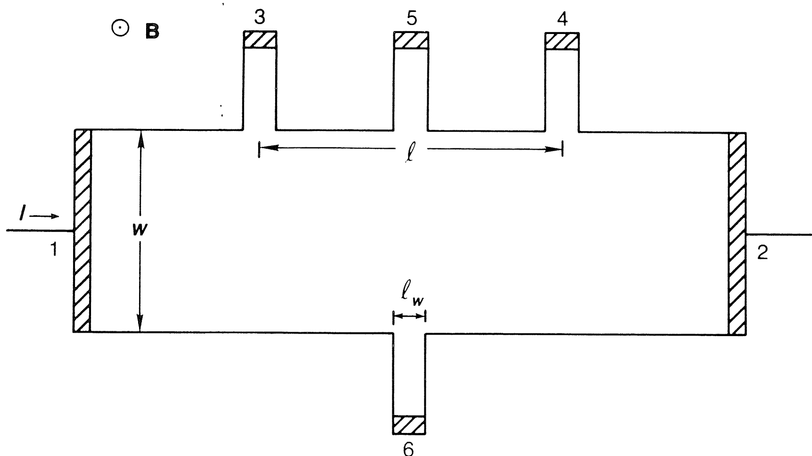

Fig. 1.1.6 A Hall bar with contact arms

applied. With an ultrasonic cutting tool it is also possible to create the pattern in bulk samples.

It is useful to average voltage readings over the four combinations of current and magnetic-field polarities, for reasons discussed below. Thus, in reference to the contact numbering of Fig. 1.1.6, ρ and R_H become

$$\rho = \frac{wd}{l}\tfrac{1}{2}[R_{12,34} - R_{21,34}] \qquad (1.1.7)$$

$$R_H = \frac{d}{b}\tfrac{1}{4}[R_{12,65}(+B) - R_{21,65}(+B) + R_{21,65}(-B) - R_{12,65}(-B)] \qquad (1.1.8)$$

where $R_{ij,kl} \equiv V_{kl}/I_{ij}$. Then $\mu_H = R_H/\rho$ and $n_H = -1/eR_H$.

ıough averaging over current and magnetic-field polarities seems tedious time consuming, it is a useful way to eliminate certain additional e.m.f.s :h can obscure the true Hall voltage. Several such spurious e.m.f.s are fly discussed below.

One obvious source of error is misalignment of contacts 5 and 6 in Fig. 1.1.6, which can lead to a significant effect if $V_c \gg V_H$. The misalignment voltage, designated V_M, reverses with current.

Suppose that the sample is mounted on a slab which itself has a temperature gradient transverse to the direction of current flow. Then, the metal/semiconductor junctions on arms 5 and 6 will constitute a thermoelectric couple, and will give rise to an e.m.f., designated by V_S, because of the Seebeck effect. This e.m.f. is not affected by current or magnetic field, to first order.

Even if no *external* transverse temperature gradient exists, the sample can set up its own, because slow (cool) and fast (hot) electrons are shunted to the sides in different numbers by the $e\mathbf{v} \times \mathbf{B}$ force. Thus, an *internally* generated Seebeck effect is set up, but in contrast to the *external* Seebeck effect it produces a voltage (V_E) which is proportional to both current and magnetic field. This phenomenon is known as the Ettingshausen effect.

If instead of an externally imposed current, a longitudinal temperature gradient exists, then electrons tend to diffuse from the hot end of the sample to the cold end, and this diffusion current experiences a 'Hall effect' in the presence of a magnetic field. The phenomenon is known as the Nernst or Nernst–Ettingshausen effect, and the resulting e.m.f. (V_N) is proportional to magnetic field, but not to external current.

Finally, the Nernst (diffusion) electrons will also experience an Ettingshausen-type effect, in that their spread of velocities will result in hot and cold sides, and thus again set up a transverse Seebeck voltage, known as the Righi–Leduc voltage, V_R. The Righi–Leduc voltage is also proportional to magnetic field, but not external current.

The variations of these various voltages with current and magnetic-field larities, along with the variations of the Hall voltage, are listed in Table 1.2. Let

$$V_{Ha} = V_H + V_M + V_S + V_E + V_N + V_R$$

ıere V_{Ha} is the *apparent* Hall voltage. It is clear from Table 1.1.2 that each oice of current and magnetic-field polarities will give a different V_{Ha} than y other choice. However, there is a particularly useful combination

$$\tfrac{1}{4}[V_{Ha}(+,+) - V_{Ha}(+,-) - V_{Ha}(-,+) + V_{Ha}(-,-)] = V_H + V_E \quad (1.1.9)$$

ıich eliminates all spurious e.m.f.s except that due to the Ettingshausen fect. Thus, the apparent Hall coefficient under adiabatic conditions (R_{Ha})

Table 1.1.2 Dependences of various thermal, thermomagnetic, and galvanomagnetic voltages on magnetic-field and current polarities

	I	B	V_H	V_M	V_S	V_E	V_N	V_R
1.	+	+	+	+	+	+	+	+
2.	+	−	−	+	+	−	−	−
3.	−	+	−	−	+	−	+	+
4.	−	−	+	−	+	+	−	−
$\tfrac{1}{4}(V_1 - V_2 - V_3 + V_4)$:			V_H	0	0	V_E	0	0

always involves both the true Hall and Ettingshausen coefficients, and in fact can be written, $R_{HA} = R_H + P\Theta$, where P is the Ettingshausen coefficient, and Θ is the thermo-electric power. Fortunately, $P\Theta \ll R_H$ in most circumstances, although this inequality obviously does not hold in mixed conductors near a point at which R_H goes through zero as a function of some parameter.

It is also of interest to note, by referring to Table 1.1.2, that the Seebeck voltage could presumably be determined by *adding* all four combinations of $V_{Ha}(i, j)$.

1.1.4 General working equations: van der Pauw structures

Although the Hall-bar configuration discussed above is the simplest and most straightforward geometry to analyze, it is not the most popular shape in use today. The reason stems from a very convenient formulation by van der Pauw (1958) in which he solved the potential problem in a thin layer of *arbitrary* shape. At that time (1958), it was not as easy to make a symmetrical pattern, such as a Hall bar, and so the van der Pauw technique caught on quickly and has increased in popularity over the years. One of the convenient features of this technique is that no dimension need be measured for the calculation of *sheet* resistance or sheet carrier concentration, although a thickness must of course be known for *volume* resistivity and concentration. Basically, the validity of the van der Pauw method requires that the sample be flat, homogeneous and isotropic, a singly connected domain (no holes), and have line electrodes on the periphery, projecting to point contacts on the surface, or true point contacts on the surface. The last requirement is the most difficult to satisfy, so much work has gone into determining the effects of finite contact size and will be discussed later.

Consider the sample shown in Fig. 1.1.7(a). Here a current I flows between contacts 1 and 2, and a voltage V_c is measured between contacts 3 and 4. The relationship between V_c and I is determined by first mapping the given sample geometry, which in general is complex, onto a geometry which

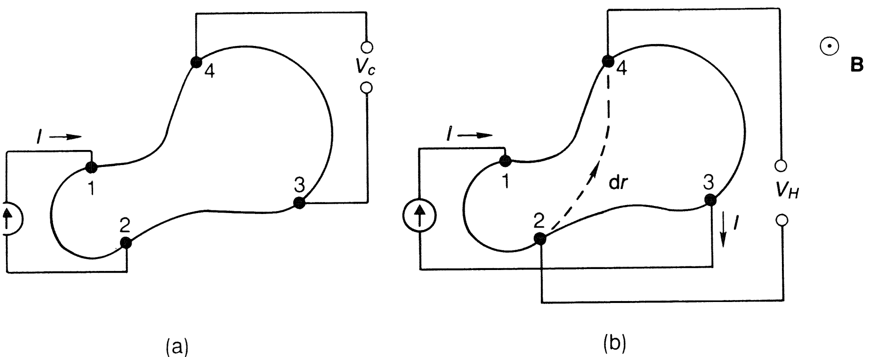

g. 1.1.7 An arbitrary shape for van der Pauw measurements: (a) resistivity; (b) ıll effect. A current-integration path is shown from r_2 to r_4, as discussed in the text

more regular and easier to analyze. The Laplace equation is then solved r the simpler geometry. We will give only the results of van der Pauw's lculations here. Let $R_{ij,kl} \equiv V_{kl}/I_{ij}$, where the current enters contact i and aves contact j, and $V_{kl} = V_k - V_l$. (These definitions, as well as the contact ımbering, correspond to ASTM Standard F76.) The resistivity ρ, with $= 0$, is then calculated as follows:

$$\rho = \frac{\pi d}{\ln 2}\left[\frac{R_{21,34} + R_{32,41}}{2}\right] f \qquad (1.1.10)$$

here f is determined from a transcendental equation:

$$\frac{Q-1}{Q+1} = \frac{f}{\ln 2} \operatorname{arccosh}\left\{\tfrac{1}{2}\exp\left[\frac{\ln 2}{f}\right]\right\} \qquad (1.1.11)$$

ere $Q = R_{21,34}/R_{32,41}$, if this ratio is greater than unity; otherwise $= R_{32,41}/R_{21,34}$. A curve of f vs Q, accurate to acout 2%, is presented in ig. 1.1.8 (van der Pauw, 1958). Also useful is a somewhat simpler

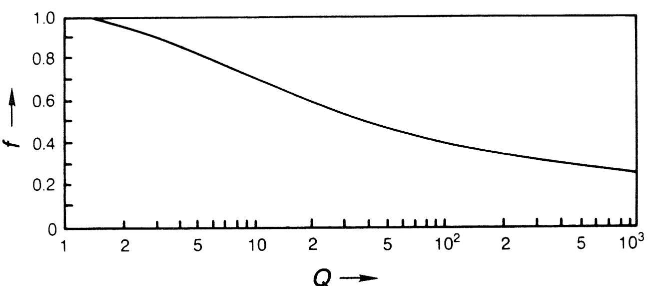

Fig. 1.1.8 The resistivity-ratio function used to correct the van der Pauw results for asymmetric sample shape. (After van der Pauw (1958). Reproduced by permission of Philips Research Laboratories)

analytical procedure for determining f, due to Wasscher and reprinted in Wieder (1979). First calculate α from

$$Q = \frac{\ln(\frac{1}{2} - \alpha)}{\ln(\frac{1}{2} + \alpha)} \qquad (1.1.12a)$$

and then calculate f from

$$f = \frac{\ln(\frac{1}{4})}{\ln(\frac{1}{2} + \alpha) + \ln(\frac{1}{2} - \alpha)} \qquad (1.1.12b)$$

Here it is of course required that $-\frac{1}{2} < \alpha < \frac{1}{2}$, but this range of α covers $Q = 0$ to ∞. For example, a ratio $Q \simeq 4.8$ gives a value $\alpha \simeq 0.25$, and then $f \simeq 0.83$. Thus, the ratio must be fairly large before ρ is appreciably reduced.

It is useful to further average ρ by including the remaining two contact permutations, and also reversing current for all four permutations. Then ρ becomes

$$\rho = \frac{\pi d}{\ln 2}\tfrac{1}{8}[(R_{21,34} - R_{12,34} + R_{32,41} - R_{23,41})f_A + (R_{43,12} - R_{34,12} + R_{14,23} - R_{41,23})f_B] \qquad (1.1.13)$$

where f_A and f_B are determined from Q_A and Q_B respectively, by applying either Eq. (1.1.11) or Eq. (1.1.12). Here,

$$Q_A = \frac{R_{21,34} - R_{12,34}}{R_{32,41} - R_{23,41}} \qquad (1.1.14a)$$

$$Q_B = \frac{R_{43,12} - R_{34,12}}{R_{14,23} - R_{41,23}} \qquad (1.1.14b)$$

The Hall mobility is determined by using the configuration of Fig. 1.1.7(b), in which the current and voltage contacts are crossed. The Jones–Zener expansion of the mobility tensor in the presence of a magnetic field leads to the following equation for isotropic semiconductors (DeMey, 1983):

$$\mathbf{E} = \rho\mathbf{j} + \rho\mu_H(\mathbf{j} \times \mathbf{B}) \qquad (1.1.15)$$

Equation (1.1.15) is correct to order $\mu_H B$, and neglects magnetoresistive $(\mu_H^2 B^2)$ terms. Now, for $\mathbf{B} = 0$, the voltage difference between contacts 2 and 4 is

$$(V_4 - V_2)_{B=0} = \int_{r_2}^{r_4} \mathbf{E} \cdot d\mathbf{r} = \rho \int_{r_2}^{r_4} \mathbf{j} \cdot d\mathbf{r} \qquad (1.1.16)$$

In the presence of the field,

$$(V_4 - V_2)_B = \rho \int_{r_2}^{r_4} \mathbf{j}' \cdot d\mathbf{r} + \rho\mu_H \int_{r_2}^{r_4} (\mathbf{j}' \times \mathbf{B}) \cdot d\mathbf{r} \qquad (1.1.17)$$

for point contacts, and our assumption of negligible magnetoresistivity, current density field **j** must remain invariant in the magnetic field, i.e., **j**, so that

$$V_{H42} = (V_4 - V_2)_B - (V_4 - V_2)_0 = \rho\mu_H \int_{r_2}^{r_4} (\mathbf{j} \times \mathbf{B}) \cdot d\mathbf{r} \qquad (1.1.18)$$

e **B** is perpendicular to the sample, $\mathbf{B} = B\mathbf{z}$, Eq. (1.1.18) simple omes

$$V_{H42} = \rho\mu_H BI/d \qquad (1.1.19)$$

Hall coefficient is obtained by averaging V_{H42} and V_{H31}:

$$R_H = \frac{d}{B}\left[\frac{R_{31,42} + R_{42,13}}{2}\right] \qquad (1.1.20)$$

general, to minimize magnetoresistive and other effects, as discussed ier, it is useful to average over current and magnetic-field polarities. n

$$R_H = \frac{d}{B}\tfrac{1}{8}[R_{31,42}(+B) - R_{13,42}(+B) + R_{42,13}(+B) - R_{24,13}(+B)$$
$$+ R_{13,42}(-B) - R_{31,42}(-B) + R_{24,13}(-B) - R_{42,13}(-B)] \qquad (1.1.21)$$

5 Geomerical effects: van der Pauw structures

hough the van der Pauw scheme is applicable to specimens of arbitrary pe, subject to the conditions described earlier, in practice a symmetrical pe is nearly always used. Some of the more common examples are shown Fig. 1.1.9, with the square (a) undoubtedly being the most common of

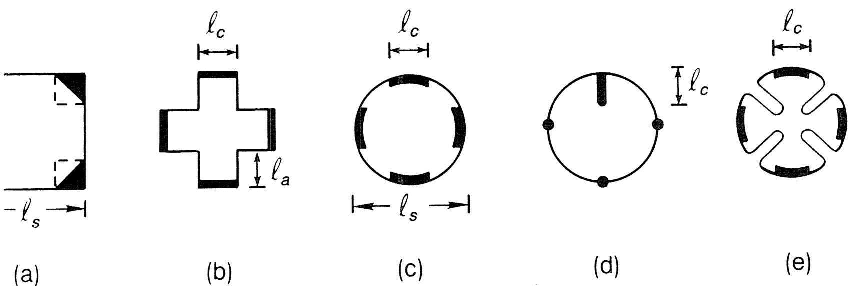

1.1.9 Various common sample geometries, with finite contact sizes, used for der Pauw measurements: (a) square; (b) Greek cross; (c) and (d) circles; (e) er-leaf

because of the ease of fabrication and the fact that the whole sample stitutes 'active' area (as opposed to the (b) and (e) structures). fortunately, the square is also somewhat more susceptible than the

others to the finite-contact-size problem, mentioned earlier. Consider the configuration of Fig. 1.1.9(a), with square of triangular contacts at the corners of the square. This system, perhaps the most common in use today, has been analyzed both theoretically, by solving Laplace's equation, and experimentally, by determining the potential distributions in an electrolytic tank. To put the results (Fig. 1.1.10, Chwang *et al.*, 1974) in perspective, we

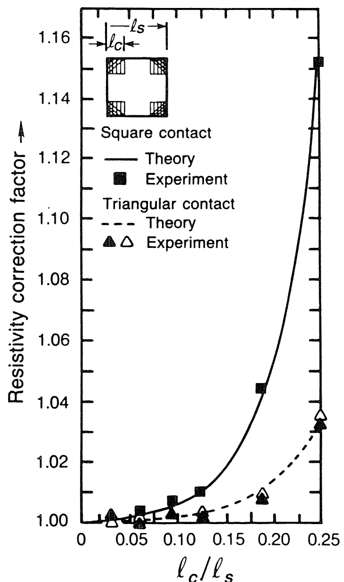

Fig. 1.1.10 Contact-size correction factors for the resistivity of a square pattern. (After Chwang *et al* (1974). Reproduced by permission of Pergamon Press)

may note that typical samples used in our laboratory are about 6 mm × 6 mm, with contact size l_c as large as 1 mm. Then, $l_c/l_s \simeq 0.16$, and the decrease in resistivity will be less than 2%, which is certainly quite acceptable. The situation for Hall voltage is, unfortunately, much worse. With triangular contacts of the same dimensions, the Hall-voltage correction is about 15%, as shown in Fig. 1.1.11 (Chwang *et al.*, 1974), with some dependence on $\tan\theta \simeq \mu B$. Clearly, 15% would be at or beyond the limits of acceptability, so that contact dimensions become very important.

To mitigate the effects of contact size, sample shapes with a longer periphery may be employed. A slight gain can be realized by going to a circular or disk shape (Fig. 1.1.9c), for which van der Pauw (1958) has given a correction:

$$\frac{\Delta\rho}{\rho} \simeq -\frac{1}{16\ln 2}\frac{l_c^2}{l_s^2} \quad \text{(per contact)} \qquad (1.1.22)$$

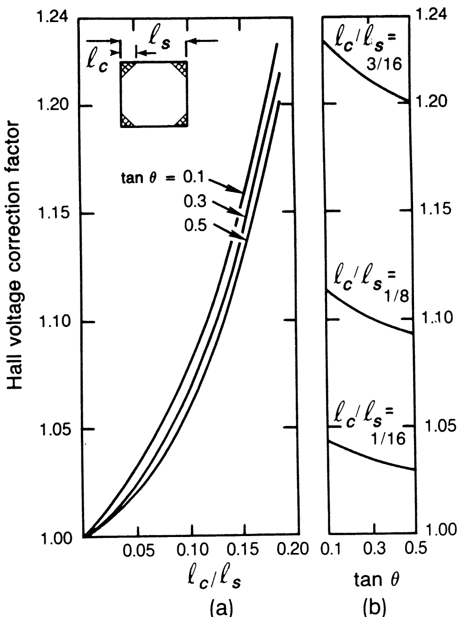

Fig. 1.1.11 Contact-size correction factors for the Hall voltage of a square pattern. Here θ is the Hall angle, defined as $\tan\theta = -E_y/E_x \simeq -\mu B$. (After Chwang *et al.* (1974). Reproduced by permission of Pergamon Press)

:re l_s is the diameter of the disk. Thus, if $l_c/l_s \simeq \frac{1}{6}$, as in our earlier mple, then $\Delta\rho/\rho \simeq -1\%$ for four non-ideal contacts, according to the nula. Some experimental results for p-type Ge disks are shown in Fig. 12 (van Daal, 1965), for which sample A_2 seems to obey Eq. (1.1.22) sonably well. For thinner samples (A_1) the error increases appreciably. wever, the error nearly vanishes for both thicknesses by going to a ver-leaf' pattern (samples B_1 and B_2), also shown in Fig. 1.1.9(e). :ause of this advantage, the clover-leaf configuration is also used quite en on photolithographically defined test patterns. However, there is a le-off in the sense that the large 'lobes', which diminish the contact ors, take up valuable space on the test pattern.

'he effects of non-ideal contacts on the *Hall voltage* of a circle or disk has) been studied by van der Pauw. For small l_c he found that

$$\frac{\Delta\mu_H}{\mu_H} = \frac{\Delta R_H}{R_H} \simeq \frac{2}{\pi^2}\frac{l_c}{l_s} \quad \text{(per contact)} \tag{1.1.23}$$

ere the lengths are defined in Fig. 1.1.9(c). Thus, if $l_c/l_s = \frac{1}{6}$, $\Delta\mu_H/\mu_H \simeq$ % for four contacts. The mobility errors for p-type Ge disks, shown in

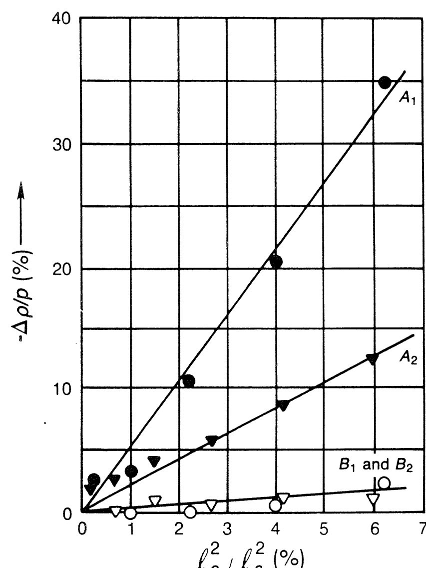

Fig. 1.1.12 Contact-size errors for the resistivity of a Ge disk, Fig. 1.1.9(c). Sample A_1 has a diameter l_s of 20 mm, and a thickness δ of 0.2 mm, while sample A_2 has $l_s = 24.5$ mm and $\delta =$ 1.3 mm. Curves B_1 and B_2 show the results after the samples were converted to clover-leaf patterns (Fig. 1.1.9e) by cutting slots. (After van Daal (1965). Reproduced by permission of Philips Research Laboratories)

Fig. 1.1.13 (van Daal, 1965), are even somewhat higher than would be predicted by Eq. (1.1.23). However, by cutting slots to make the sample into a clover-leaf pattern (Fig. 1.1.9e), the errors are reduced considerably.

One of the most accurate van der Pauw structures, from the aspect of finite-contact-size corrections, is the symmetrical Greek cross, shown in Fig. 1.1.9(b). Note that the contact size l_c is as large as the arm width in this version of the structure. Let ρ be the *ideal* van der Pauw resistivity, i.e., $\rho = \pi dRf/\ln 2$, where R is defined by the bracketed quantity in Eq. (1.1.10), and let ρ_m be the *measured* resistivity, which is different from the ideal value due to the finite contact size. Then, David and Buehler (1977) have shown that, as long as $l_a/l_c \gtrsim 0.1$, where l_a is the arm length, the resulting error can be approximated by

$$E = (0.59 \pm 0.006)\exp\left[-(6.23 \pm 0.02)l_a/l_c\right] \tag{1.1.24}$$

where $E = 1 - \rho/\rho_m \simeq \Delta\rho/\rho_m$. This relationship is shown in Fig. 1.1.14 (David and Buehler, 1977), and it is seen that the typical errors are very

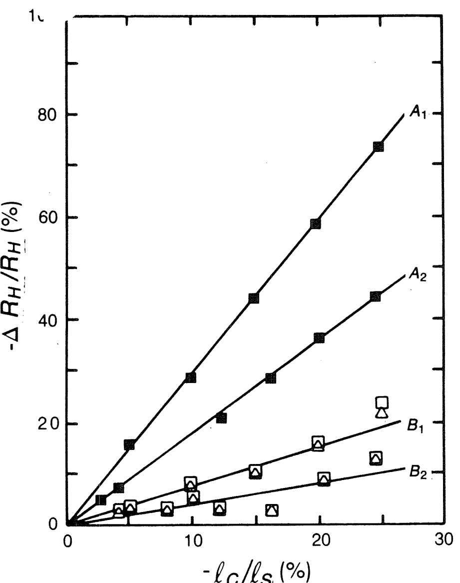

Fig. 1.1.13 Contact-size errors for the Hall effect in a Ge disk. See Fig. 1.1.12 for the sample descriptions. (After van Daal (1965). Reproduced by permission of Philips Research Laboratories)

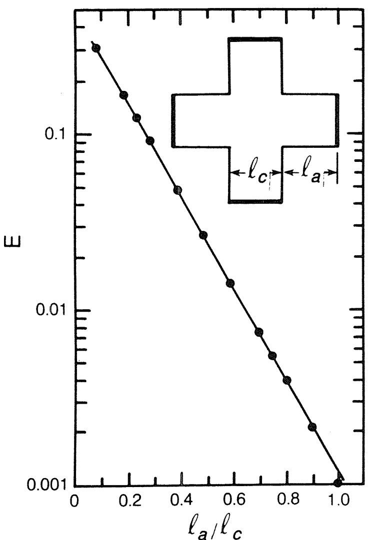

Fig. 1.1.14 Contact-size errors for the resistivity of a Greek-cross pattern. (After David and Buehler (1977). Reproduced by permission of Pergamon Press)

small. For example, to compare with the other structures, we assume that $l_c/(l_c+2l_a)=\frac{1}{6}$, where l_c+2l_a corresponds to the total dimension of the structure, i.e., is analogous to l_s in the other structures. Then, $l_a/l_c=\frac{5}{2}$, and $E \simeq 10^{-7}$, a totally negligible error. However, the main advantage of the Greek cross over the other structures comes in the Hall-effect measurements, for which De Mey (1973, 1983) has shown that

$$\frac{\mu_H-\mu_{Hm}}{\mu_H}=\frac{\Delta\mu_H}{\mu_H}\simeq 1.045\mathrm{e}^{-\pi l_a/l_c} \qquad \text{(four contacts)} \qquad (1.1.25)$$

which gives $\Delta\mu_H/\mu_H=0.04\%$ for our example. Even if $l_a=l_c$, the error is only 4.5%, which is certainly more tolerable than the contact-size errors found in all the other structures, except for the clover-leaf pattern.

It is of interest to know what the effect of *unequal* arm lengths would be. An application of this idea, to be discussed later, is shown in Fig. 1.1.15,

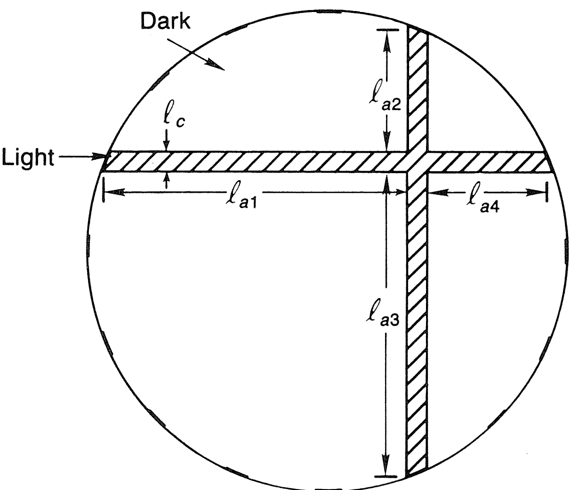

Fig. 1.1.15 A Greek-cross pattern formed by two intersecting light slits on an otherwise dark semi-insulating wafer. The possible errors due to finite slit size l_c are given by Eq. (1.1.26)

which depicts a means of mapping the photo-Hall effect on a semi-insulating GaAs wafer (Look and Pimentel, 1987). The relevant expression for the mobility error can be obtained from Eq. (1.1.25), which was derived under the approximation that the errors in the individual arms are additive to produce the total error. Then, since Eq. (1.1.25) includes four *equal* arms, the formula for four *unequal* arms would be

$$\frac{\Delta\mu_H}{\mu_H}\simeq\frac{1.045}{4}\left[\mathrm{e}^{-\pi l_1/l_c}+\mathrm{e}^{-\pi l_2/l_c}+\mathrm{e}^{-\pi l_3/l_c}+\mathrm{e}^{-\pi l_4/l_c}\right] \qquad (1.1.26)$$

in, there is little error as long as $l_i \gtrsim l_c$. To bring the intersection of the s close to the periphery, and still get accurate results, either the arm ths or the contact sizes can be reduced. In practice, only point contacts ıld normally be used in this application anyway.

6 A comparison of various strucures

deciding what kind of geometrical structure to use for a particular lication, several factors should be considered, including:

available size
available fabrication techniques
limitations of measurement time
necessary accuracy
need for magnetoresistance data.

onsidering these factors, we will refer to Fig. 1.1.16, which depicts six of most popular structures.

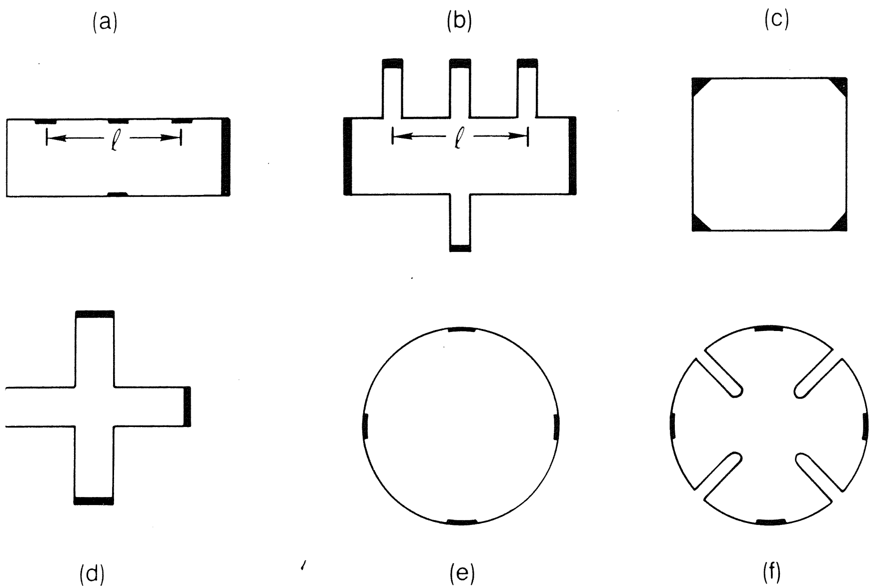

1.1.16 Various patterns commonly used for resistivity and Hall-effect ısurements

irst of all, the available size can be a severe constraint. In our ɔratory, we have often measured bulk samples of dimension 2 mm or , which virtually rules out any complicated shapes, such as (b), (d), or in fact, it is sometimes not possible to modify an existing sample shape ıll. Thus, the best procedure for small samples is simply to put four very small contacts around the periphery and apply the standard van der Pauw analysis. Contact-size errors can be estimated if the shape is somewhat symmetrical. The simple Hall-bar structure (a) is not recommended for a very small bulk sample, unless the sample is already in that form, because it is then necessary to measure l and w, which can introduce large errors.

For larger bulk samples, there is a greater choice among the various structures. The availability of an ultrasonic cutting tool opens up the possibility of using (b), (d), (e), or (f), if desired. Here, it might be noted that (b) is rather fragile compared to the others. If the samples must be cleaved from a wafer, which is quite typical for GaAs characterization, then the shapes are basically limited to (a) and (c). In our laboratory, for example, it is common to use a square (c) of about 6 mm × 6 mm, and then put contacts of dimension 1 mm or less on the corners. It was these sample and contact dimensions that were considered in some of the numerical contact-size-effect examples discussed earlier.

If photolithographic capabilities are available, then one of the more complex test structures (b), (d), or (f) should be used, because of the advantages they offer. Most manufacturers of discrete semiconductor devices or circuits include Hall-bar or van der Pauw structures at several points on the wafer, sometimes one in every reticle (repeated unit). An example is shown in Fig. 1.1.17 (Ezis, 1988) which includes (b) and a variation of (c), along with various other test devices, transistors, and circuits.

Another possible constraint is that of measurement time. By comparing Eq. (1.1.7) with (1.1.13), and Eq. (1.1.8) with (1.1.21), it appears that a typical van der Pauw experiment should take about 2–3 times as long as a Hall-bar experiment, and indeed, this is experimentally the case. Thus, in an experiment which involves many measurements on the same sample, such as a temperature-dependence study, it may well be a distinct advantage to use a Hall-bar instead of a van der Pauw pattern. Also, if a contact-switching network is not part of the available apparatus, then a van der Pauw structure cannot be conveniently used.

If high accuracy is necessary for the Hall-effect measurements, then structures (b), (d), and (e) are the best, because, as we have seen, contact-size effects are much stronger for Hall-effect data than for resistivity data. The same structures, along with (a), should be used if μB must be made large, since structures (c) and (e) do not have as good a V_H vs B linearity. From a heat-dissipation point of view, structures (a) and (b) are the worst, since they are required to be long and narrow, and thus the Hall voltage is relatively small for a given current, since $V_H \propto w$. A high heat dissipation can lead to large temperature gradients, and thus stronger thermomagnetic effects, or may simply raise the sample temperature an unacceptable amount.

Finally, it is important to ask whether or not the same sample is going to be used for magnetoresistance measurements, because, if so, structures (a)

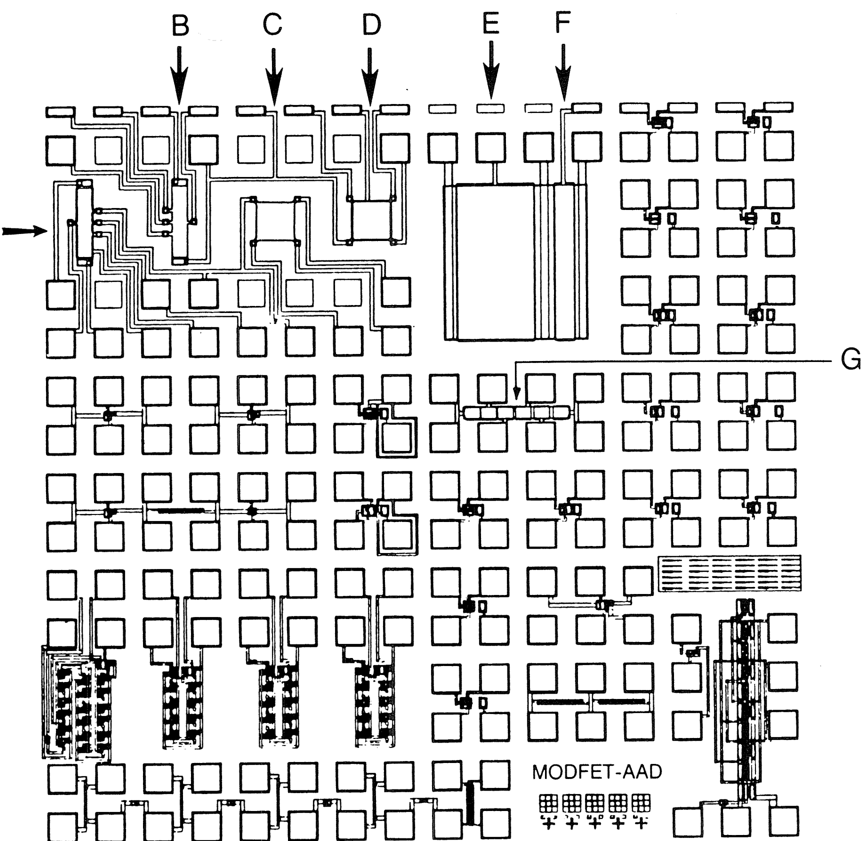

g. 1.1.17 A 2 mm × 2 mm reticle with several test structures, devices, and simple ·cuits: (A) 40 μm × 100 μm gated Hall bar; (B) ungated Hall bar; (C) 100 μm × 0 μm ungated van der Pauw square; (D) gated van der Pauw square; (E) 0 μm × 400 μm FATFET; (F) 50 μm × 400 μm FATFET; (G) TLM contact-sistance pattern. (After Ezis (1988). Reproduced by permission of the U.S. Air orce)

ıd (b) are undoubtedly the best. The reason is that the analysis of agnetoresistance is more complicated in van der Pauw structures than in all-bar structures, and, in general, a simple formula cannot be found. It ay be noted that in Shubnikov–de Haas and quantum-Hall measurements, which magnetic-field dependence is critical, the Hall bar is nearly always sed.

As a final note in the comparison of Hall-effect structures it is of interest inquire whether or not any systematic differences are observed between ıe various geometries *in practice.* Recently the National Bureau of tandards has conducted a round-robin investigation of Hall-effect meas-rements among laboratories. The structures investigated were squares and

Greek crosses, cut from the same wafer ($d \simeq 0.56$ mm, $n \simeq 3 \times$ ^{7} cm^{-3}), as shown in Fig. 1.1.18 (Seabaugh and Bell, 1988). One set of these

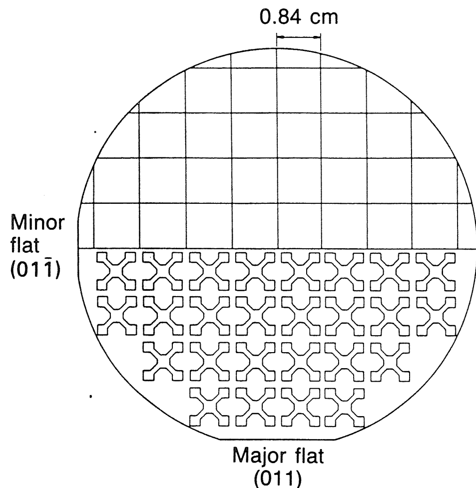

Fig. 1.1.18 A 3-inch, Si-doped, LEC GaAs wafer cut into square and cross patterns, as shown, for a round-robin investigation. (After Seabaugh and Bell (1988). Reproduced by permission of the National Bureau of Standards)

configurations was sent to each participating laboratory, with instructions to put on contacts according to the usual procedure used by that laboratory. As might be expected, some of the contacts were small and well defined, while others covered a rather significant portion of the sample. Each set of samples, with contacts, was then measured by the laboratory that put them on, and then was sent to several other laboratories. The results showed some systematic differences between the two structures, but fortunately they were small and not significant for most purposes. Thus, for GaAs samples in this thickness (~0.1 μm) and concentration range, it appears that the square shape can be used with confidence. However, results may be different for other thicknesses and concentrations. A full report on the round-robin study will be published later (Seabaugh and Bell, 1988).

1.1.7 Contacts

What should be the simplest part of a Hall-effect measurement, namely, putting on the contacts, is often the most troublesome. One would think that after more than 25 years of electrical measurements in GaAs, there would be a standard recipe or recipes which would produce good ohmic

contacts on any kind of GaAs. Unfortunately that is not the case, for several reasons: (1) requirements are changing, as contact dimensions are necessarily reduced for smaller devices, and as different materials and device structures are introduced; (2) the recipes cannot be made complete because unknown factors, e.g., polish damage, are variable and/or poorly understood; and (3) what is 'ohmic' for one application may not be ohmic for another application; in fact, even a reduction in temperature can sometimes change an ohmic contact into a non-ohmic contact. For GaAs Hall-effect measurements, the necessary currents range from about 10^{-12} to 10^{-1} A. But the resistance of a Hall device remains constant as the lateral dimensions are scaled down equally, and thus the current requirements should be the same. This means that the contact-current *density* in a small device is correspondingly larger than that in a large device, and thus the contact itself must have a lower 'specific contact resistivity' in order to be acceptable. Because of such problems, it is worthwhile to discuss ohmic contacts in some detail.

1.1.7.1 Definition of ohmic contact

There are many definitions of an ohmic contact, including the following:

(A) a perfect source and sink of both carrier types and having no tendency to inject or collect either electrons or holes;
(B) a source of carriers with an internal resistance R_c which is totally negligible compared with the semiconductor resistance;
(C) a source of carriers with a non-negligible internal resistance R_c, but one which obeys Ohm's law for current densities of interest.

Definition (A) has only academic significance since no actual contacts ever fulfill this condition. For purposes of this book, we will basically adopt either (B) or (C) as our definition. That is, if the total circuit resistance R_T is given as $R_T = 2R_c + r_s l/w$, where r_s is the sheet resistance, l the length, and w the width of the semiconductor material between the two contacts, then the contacts will be considered ohmic if R_T is independent of current magnitude and polarity. This condition could be satisfied in either of two ways: (1) $R_c \ll r_s l/w$, which is equivalent to definition (B); or (2) R_c itself is independent of current magnitude and polarity, which is definition (C). One ambiguity with our definition is that if R_T turns out to be non-ohmic, then we really don't know whether the problem is with R_c or r_s. That is, suppose an n-type semiconductor had an n–p–n junction somewhere between two ohmic contacts. Then r_s would probably not be ohmic, so that R_T would not be ohmic either, even though the contacts were. However, for Hall-effect measurements, we are not interested in the contacts themselves, only in ensuring that they not interfere with the measurements of V_c and V_H. In a few cases, definition (C) is not sufficient to give an *acceptable* contact even if

R_c is ohmic. That is, if R_c is so high that sufficient current cannot be passed to get good measurements of V_c and V_H, then the contact is not acceptable.

1.1.7.2 Theory of ohmic contacts

To quantify an ohmic contact, it is usual to employ one of the following 'figures of merit':

(1) the *specific contact resistance* $\rho_c(\Omega\text{-cm}^2)$, also known as the *specific contact resistivity*, the *contact resistivity*, or the *contact resistance*, in various sources; and
(2) the *normalized contact resistance*, or *specific transfer resistance*, which we will designate by $r_c(\Omega\text{-mm})$.

The first of these (ρ_c) has both theoretical and practical significance, while the second (r_c) has only a practical significance.

To illustrate the concept of specific contact resistance, consider the structure shown in Fig. 1.1.19(a), which consists of a semiconductor slab of

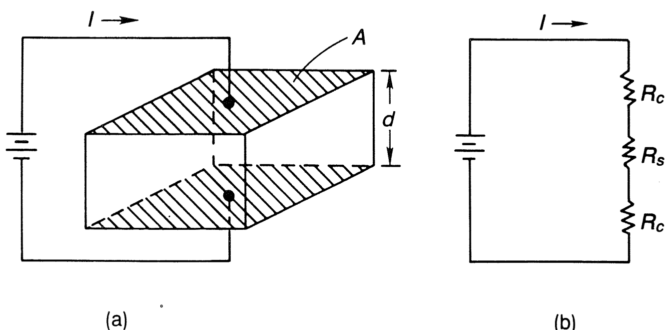

Fig. 1.1.19 (a) A simple structure and (b) equivalent circuit, for contact-resistance measurements

thickness d and area A, covered on top and bottom by the contacting metal. The simple equivalent circuit is shown in Fig. 1.1.19(b). It is clear that both the contact and bulk resistances will scale inversely with A, but only the bulk resistance will scale with a thickness (d, in this case), since the effective contact thickness is not even known. Thus, it seems natural to define $R_c = \text{constant}/A$, and the constant is called ρ_c, normally written in units of $\Omega\text{-cm}^2$. A formal definition of ρ_c is usually given as

$$\rho_c = \left\{ \frac{\partial j}{\partial V} \bigg|_{V=0} \right\} \Omega\text{-cm}^2 \qquad (1.1.27)$$

which will be discussed in more detail below.

The other figure of merit has application to planar contacts on a thin layer, as illustrated in Fig. 1.1.20. Here each contact has a defi[illegible] area,

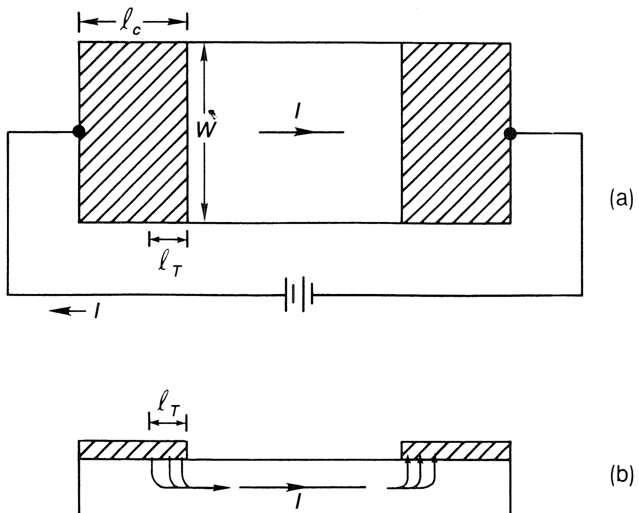

Fig. 1.1.20 An illustration of 'current crowding' in planar contacts. Here l_T is the *transfer length*: (a) planar view; (b) cross-sectional view

wl_c, but this area is not relevant under most circumstances. The reason is that the current does not flow uniformly out of the *whole* length of the contact l_c, but only from a length l_T, known as the *transfer length*. It is well known, and will be shown later, that $l_T = \sqrt{(\rho_c/R_s)}$, where R_s is the sheet resistance of the material under the contact, and thus the contact resistance is roughly given by $R_c = \rho_c/wl_T = \sqrt{(\rho_c/R_s)}/w$, as long as $l_T \lesssim 0.5l_c$. Usually, $l_T \ll l_c$, so that R_c is independent of l_c. Under these circumstances the area wl_c does not have much significance, but w itself still does, of course. Thus, a meaningful figure of merit would be given by $R_c =$ constant$/w \equiv r_c/w$, where the most common unit for r_c is Ω-mm. It must be noted that r_c is purely an operational figure of merit, which cannot be related to the barrier resistance or any other intrinsic property of the contact. However, it can be applied to any planar contact and is the quantity of interest to device and circuit designers.

We will now return to the specific contact resistivity ρ_c, as defined by Eq. (1.1.27). As will be discussed in more detail later, a metal–semiconductor junction can be described by a conduction-band diagram such as that shown for an n-type semiconductor in Fig. 1.1.21. Basically, an electron going from the metal to the semiconductor must go over an energy barrier $e\phi_B$, whereas an electron going the other way must traverse a barrier eV_{bi}, where V_{bi} is known as the *built-in* or *diffusion potential*; here, both ϕ_B and V_{bi} are defined as positive quantities. (For now we will ignore electrons going *through* the barrier). At equilibrium, Fig. 1.1.21(a), the electron currents j_{1e}

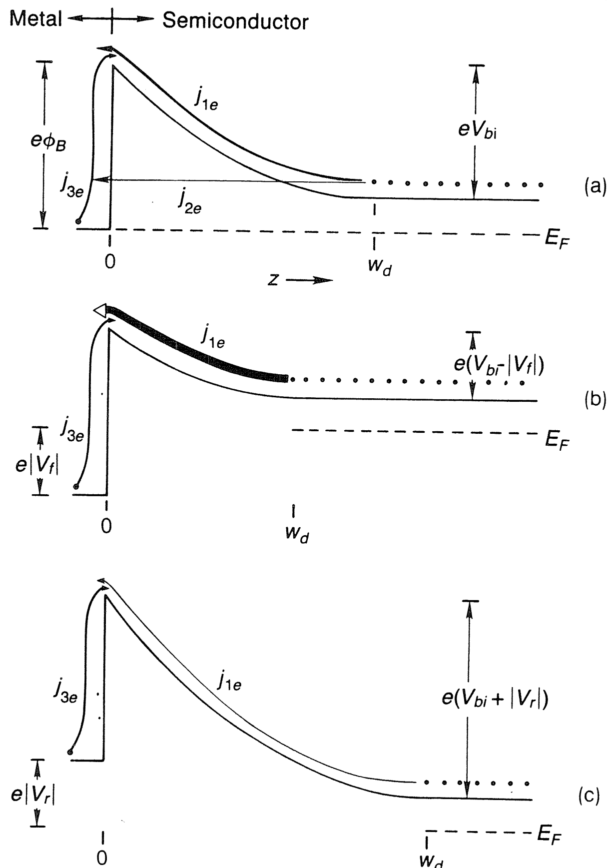

Fig. 1.1.21 The various electron-current components in a Schottky barrier under unbiased and biased conditions: j_{1e} and j_{3e} are injection currents and j_{2e} is a tunneling current. (a) No bias; (b) forward bias; (c) reverse bias

and j_{3e} will be of equal and opposite magnitudes because the net current must vanish. The currents j_{1e} and j_{3e} are known as thermionic currents, since it is the few electrons which have high thermal energies which can traverse the barriers. Let the Fermi energy in the neutral semiconductor region ($z \to \infty$) be defined as the zero of energy. Then when a positive voltage V_f is applied to the metal (a *forward* bias for an n-type semiconductor), its Fermi level will be lowered by $e|V_f|$ with respect to the semiconductor (Fig. 1.1.21b) and the $S \to M$ barrier will decrease to $e(V_{bi} - |V_f|)$, thereby raising j_{1e} by a factor $\exp(e|V_f|/kT)$. The $M \to S$ electron current j_{3e} remains the same, since its barrier does not change. Conversely, when a negative (*reverse*) bias is applied to the metal, the $S \to M$ barrier is raised by $e|V_r|$,

ıd the current j_{1e} is *decreased* by $\exp(e|V_r|/kT)$. Again, j_{3e} is unchanged ı first order. The total situation can be described by the well-known diode ɿuation

$$j(\text{ther.}) = j_{rs}[\exp(eV/kT) - 1]$$
$$= K_{rs}\exp(-e\phi_B/kT)[\exp(eV/kT) - 1] \qquad (1.1.28)$$

'here j(ther.) is the conventional (positive) thermionic current density owing from semiconductor to metal. Here j_{rs} is the *reverse-saturation ırrent,* which is approximately constant for reverse bias (negative V) until reakdown begins to occur. It is clear that Eq. (1.1.28) does not represent n 'ohmic' contact except at very low voltages, for which

$$j = j_{rs}\frac{eV}{kT}, \qquad V \ll kT/e \qquad (1.1.29)$$

Iowever, the magnitude of j(ther.) is mainly limited by the $\exp(-e\phi_B/kT)$ ɜrm, since $e\phi_B \gg kT$ for GaAs at normal temperatures. Thus, if ϕ_B can be ıade small, then a high current density can be supported by a very small oltage drop across the contact, and that is what we really want in a contact.

The problem in GaAs is that ϕ_B cannot be made small by the proper hoice of metal, evidently because of a high surface-state density. The lternative then is to make the barrier as *thin* as possible, in which case the ınneling current j_2, which was ignored before, can become appreciable. 'he $S \to M$ tunneling probability for electrons at the depletion edge is given y the familiar WKB approximation:

$$T(w_d) = \exp\left[-2\int_{w_d}^{0}\left\{\frac{2m}{\hbar^2}[\mathscr{E}(z) - \mathscr{E}(w_d)]\right\}^{1/2} dz\right] \qquad (1.1.30)$$

ʼhere $\mathscr{E}(z)$ describes the shape of the barrier. As a fairly good approxima- :on, the barrier is parabolic so that

$$\mathscr{E}(z) - \mathscr{E}(w_d) = e^2N(z - w_d)^2/2\epsilon$$

ʼhere N is the net donor concentration, ϵ is the dielectric constant, and w_d ; the depletion depth, given by $w_d = [2\epsilon(V_{bi} - V)/eN]^{1/2}$. The integration herefore results in

$$T \simeq \exp\frac{e(V - V_{bi})}{\frac{he}{4\pi}\left(\frac{N}{\epsilon m^*}\right)^{1/2}} \propto \exp\frac{e(V - V_{bi})}{\mathscr{E}_{00}} \qquad (1.1.31)$$

ʋhere $\mathscr{E}_{00}$ is a standard designation in the literature. To compare the ıagnitudes of the tunneling and thermionic currents, note from Eq. 1.1.28) that

$$j(\text{ther.}) \propto j_{rs}\exp(eV/kT) \propto \exp[e(V - \phi_B)/kT]$$

for $eV \gg kT$, and note also that

$$j(\text{tun.}) \propto \exp[e(V - V_{bi})/\mathscr{E}_{00}].$$

Now V_{bi} and ϕ_B are not too different, and both $V - V_{bi}$ and $V - \phi_B$ are negative for all realistic values of V. Therefore, if $\mathscr{E}_{00} \gg kT$, then tunneling current will dominate, as illustrated in Fig. 1.1.22(b). For GaAs, $\mathscr{E}_{00} \simeq$

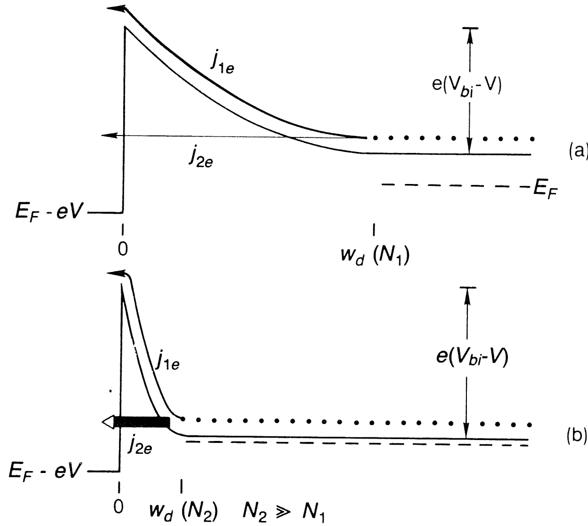

Fig. 1.1.22 The reduction of the depletion width w_d, and consequent increase of electron tunneling current j_{2e}, due to a much higher doping density, $N_2 \gg N_1$

$2.0 \times 10^{-11} N^{1/2}$ eV, where N is in cm^{-3}. Therefore, $\mathscr{E}_{00} \gtrsim kT$ at $T = 300$ K when $N \gtrsim 1.6 \times 10^{18}$ cm^{-3}. For even higher N we would expect that $\ln j(\text{tun.}) \propto \mathscr{E}_{00}^{-1} \propto N^{-1/2}$. This relationship is illustrated in Fig. 1.1.23 (Mead, 1969) for highly doped GaAs, showing that the theory has at least reasonable validity. Again, the tunneling phenomenon does not lead to an ohmic contact in the sense $j \propto V$, except for $eV \ll \mathscr{E}_{00}$. However, the important thing for most purposes is that a large current density be produced by a small voltage drop across the contact, and that will be true if N is large enough.

The tunneling current is commonly known as *field-emission current,* just as the 'over-the-barrier' current was known as *thermionic-emission current.* However, it is also possible to have a mixture, *thermionic-field-emission current,* which requires electrons to be thermally excited part way up the barrier, where they can then tunnel through the barrier, which is thinner at that point. These ideas are illustrated in Fig. 1.1.24 (Rideout, 1975), showing the regions of dominance of these three current modes as a function of T and N.

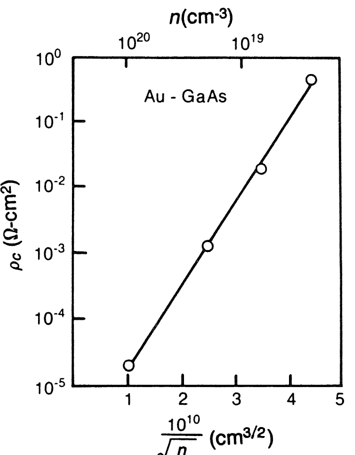

Fig. 1.1.23 Specific contact resistivity ρ_c of Au–Schottky barriers on n-type GaAs as a function of n for field-emission dominated conduction. (After Mead (1969). Reprinted by permission of the publisher, The Electrochemical Society, Inc)

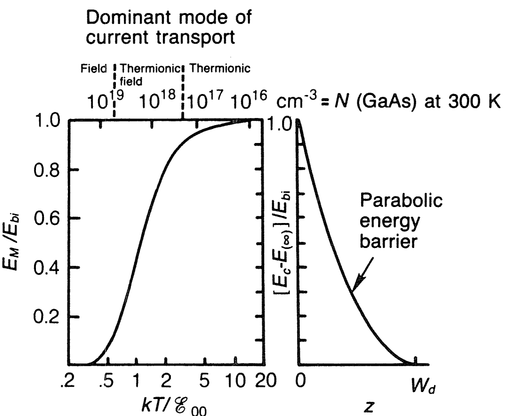

Fig. 1.1.24 Relative position of maximum transmission through or over a Schottky barrier vs the parameter $kT/\mathscr{E}_{00}$ (or n at 300 K). Note that field emission dominates for $n \gtrsim 5 \times 10^{18}\,\text{cm}^{-3}$ at 300 K. (After Rideout, (1975). Reproduced by permission of Pergamon Press)

The recipe for an ohmic contact would then seemingly require either a small ϕ_B or a large N. Generally the latter option is more viable, and is usually implemented by using a thin n^+–GaAs region between the contact metal and the *active layer*. For example, a MESFET active layer would normally have $N \simeq 2 \times 10^{17}\,\text{cm}^{-3}$, which by itself would not lead to a thin enough barrier. Thus, an n^+ layer with $N \simeq 3 \times 10^{18}\,\text{cm}^{-3}$ is placed between the metal and the active layer. The working of such an ohmic contact is illustrated schematically in Fig. 1.1.25 for (b) forward bias (metal positive),

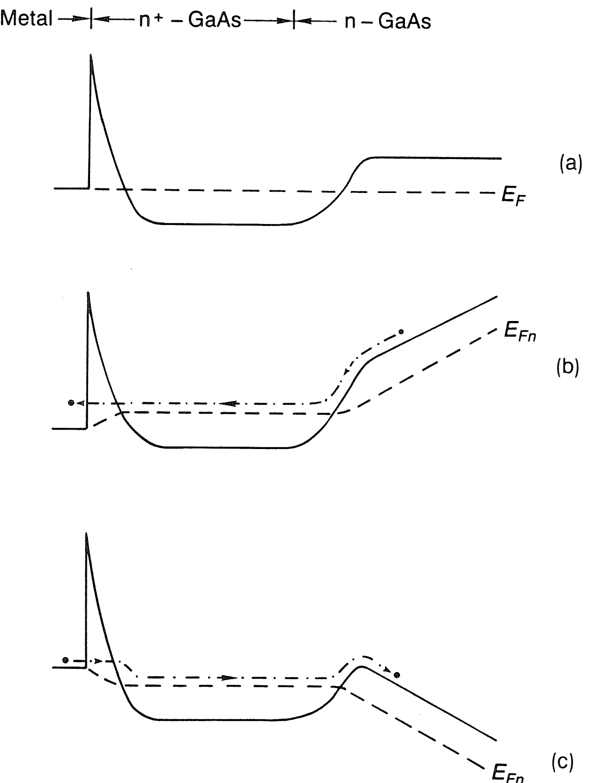

Fig. 1.1.25. Electron flow in a metal/n^+-semiconductor junction under forward bias (b), and reverse bias (c). In either case the current flows freely and thus the contact is ohmic

and (c) reverse bias (metal negative). In either case, the 0.8 eV barrier, $e\phi_B$, presents little resistance if N is large enough, and the n^+–n barrier (<0.3 eV) is not high enough to appreciably affect the reverse transport, except perhaps at very low temperatures.

Unfortunately, however, the tunneling model is not sufficient to explain the low values of contact resistivity being observed for present-day

ıetal/semiconductor junctions in GaAs, probably because most of these unctions are alloyed, and thus not strictly planar. The most popular ıetallization is composed of Au, Ge, and Ni, and will be described in more letail later. However, Fig. 1.1.26 (Braslau, 1981) shows that typical values

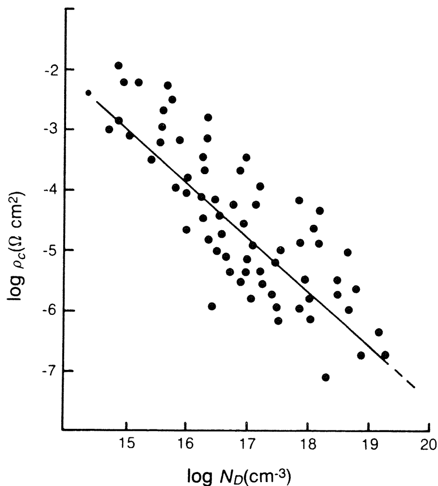

Fig. 1.1.26 The relationship of ρ_c to N_D for contact results from many different laboratories. The results appear to follow Eq. (1.1.32). (After Braslau (1981). Reproduced by permission of The American Institute of Physics)

ıf ρ_c for this material are much lower for a given N than would have been ıredicted by the tunneling model (see Fig. 1.1.23). Also, it appears that $\rho_c \sim N^{-1}$, rather than $\log \rho_c \sim N^{-1/2}$. It is perhaps not surprising that the unneling model fails here when the interface in such a contact is examined. 'or example, in Fig. 1.1.27 (Shih *et al.*, 1987) it is seen that the metal

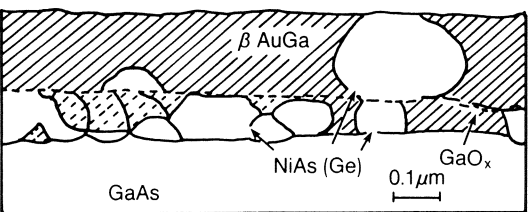

Fig. 1.1.27 The various material phases present after annealing an AuGeNi contact at 440°C for 2 min. (After Shih *et al.*, (1987). Reproduced by perr-'-sion of The American Institute of Physics)

elements have mixed with the Ga and As in a very complicated way, and have formed several new compounds in the process. In fact, it sometimes appears that spikes of highly doped material are protruding into the GaAs, and that the current mainly transfers through these spikes. Braslau (1981) has formulated a model to take account of these spikes, as illustrated in Fig. 1.1.28. Here it is assumed that the metal makes contact with the protrusions, which are modeled as hemispheres of average radius $\langle r \rangle$, and have an average density $1/\langle A \rangle^2$. Then the barrier resistance per hemisphere is given by $R_c \simeq \rho_c / 2\pi \langle r \rangle^2 f$, where f is a field-enhancement factor ($f \gtrsim 1$) to take account of the non-uniform field distribution of the protrusion. To the barrier resistance we must add a spreading resistance per hemisphere of $\rho / \pi \langle r \rangle$, where ρ is the resistivity of the GaAs underneath. The total

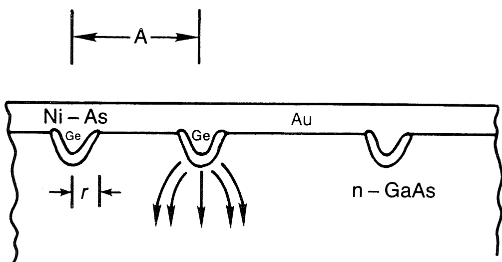

Fig. 1.1.28 A model for ohmic contacts in which conduction takes place through a parallel array of Ge-rich protrusions. (After Braslau (1981). Reproduced by permission of The American Institute of Physics)

effective specific contact resistivity is then

$$\rho_c^{\text{eff}} = \langle A \rangle^2 \left\{ \frac{\rho}{\pi \langle r \rangle} + \frac{r_c}{2\pi \langle r \rangle f} \right\} \tag{1.1.32}$$

The second term is considered negligible if $\rho > 10^{-3}\ \Omega$-cm, so that $\rho_c^{\text{eff}} \propto \rho \propto (\mu N)^{-1}$ in that case. Thus, this model can explain the dependence of ρ_c on N, and also predicts that ρ_c can be decreased by decreasing $\langle A \rangle$, i.e., by producing more protrusions per unit area. However, that is a difficult task since it is not even known what produces the protrusions, and furthermore, there are cases (cf. Fig. 1.1.27) where they do not seem to be necessary to form a good ohmic contact. Further work will be necessary to understand this problem completely.

A final method of making ohmic contacts in GaAs should be discussed. Although we previously discounted the possibility of making $e\phi_B$ much less than 0.8 eV (see, however, Section 1.1.7.3.1 and Iliadis (1987)), there is a way of getting a lower 'effective' ϕ_B which is becoming increasingly popular.

'his novel methoc akes use of a different semiconductor material, such as nAs, which either has an electron affinity $e\chi$ *greater* than the metal work unction $e\phi_m$, or has surface states which pin the Fermi level *near* the onduction band. The barrier $e\phi_B$ is then small, as illustrated in Fig. .1.29(b) (Woodall *et al.*, 1981), unlike the GaAs case (Fig. 1.1.29a) for

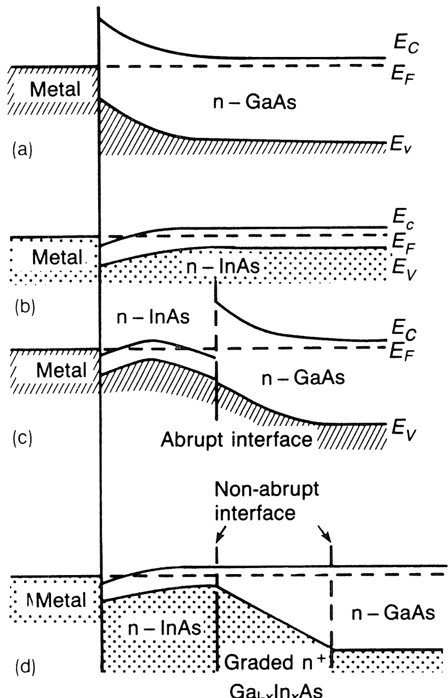

Fig. 1.1.29 Band diagrams for various semiconductor interfaces: (a) metal on n-GaAs; (b) metal on n-InAs; (c) metal on n-InAs on n-GaAs; (d) metal on n^+-InAs on graded n^+-$Ga_{1-x}In_xAs$ on n-GaAs. (After Woodall *et al.* (1981). Reproduced by permission of The American Institute of Physics)

vhich $e\phi_B$ is large. Thus, electrons can move easily between the metal and nAs. When the InAs is put between the metal and GaAs (Fig. 1.1.29c) hen a conduction-band discontinuity exists and impedes the electron flow. f, however, the InAs is graded from InAs$\rightarrow In_xGa_{1-x}As \rightarrow$GaAs, then the electrons can once again flow freely. This model may offer an explanation of vhy pure In has always proved to be a good contact for n-type GaAs Lakhani, 1984; Allen *et al.*, 1987), even though it is isoelectronic with Ga, and thus not a donor. If the In metal alloys with the GaAs, and forms a

graded heterojunction, then it might make an ohmic contact in the way depicted in Fig. 1.1.29. However, the major interest in the heterojunction method at present is to make *non-alloyed* contacts, in which case the InAs or $In_xGa_{1-x}As$ is epitaxially grown onto the GaAs, and then the metal is evaporated on, without heating. The major advantage here is for small-dimension devices in which neither vertical nor lateral diffusion due to the alloying process can be tolerated.

1.1.7.3 Practical ohmic contacts for GaAs

So far we have discussed the definition and theory of ohmic contacts. However, it is probably even more important for the purposes of this book to give some practical methods for making such contacts. As stated earlier, the total current necessary for a given signal strength in a Hall-effect measurement is approximately constant as the Hall-pattern dimensions are scaled down. Thus, the current *density* that the contacts must handle is much higher for the small pattern, and better ohmic contacts are necessary. It is reasonable, therefore, to discuss the large-area and small-area cases separately.

1.1.7.3.1 Contacts for small devices. Contact fabrication procedures for small devices are continually changing as the device dimensions decrease. However, the 'work-horse' metallization for GaAs, and for other III–V compounds such as $Al_xGa_{1-x}As$, is the AuGe eutectic (88% Au, 12% Ge) which melts at about 360°C. Up until recent times, it has been believed that this metal produces an ohmic contact by means of Ge diffusion into the GaAs, and subsequent Ge_{Ga} donor formation, which then makes the required n^+ layer, as discussed in the last section. It has also been believed that placing a Ni overlay on the AuGe is helpful because it inhibits the 'balling-up' of the AuGe. However, it is now realized that the situation is much more complex than this. For example, there is evidence (Iliadis, 1987), to suggest that the Ge indeed produces n^+ doping, but also that it induces disorder, even below the Au–Ge eutectic temperature, and through this process reduces ϕ_B. Thus, both enhanced tunneling and barrier-lowering are serving to reduce the contact resistance. At higher temperatures, several new compounds, such as NiAs:Ge, are formed and play important roles. Furthermore, 'protrusions' of the NiAs or other compounds may be necessary for the best results. Thus, it is clear that this system is still not completely understood; however, it is the one most commonly used today; and perhaps for the foreseeable future. One fairly convenient 'recipe' for such contacts, due to Braslau, is reproduced in Shur (1987), p. 151. A somewhat more complicated recipe, involving sputter cleaning (Callegari *et al.*, 1985), produces more stable and reliable contacts; the details are given in Table 1.1.3. Other recipes may be found in the literature cited in Table 1.1.4.

Table 1.1.3 Fabrication of reliable AuGeNi ohmic contacts to n-type GaAs by sputter cleaning before deposition. (After Callegari *et al.* 1985. Reproduced by permission of the American Institute of Physics.)

(1) Evacuate evaporation system to 2×10^{-5} Pa; then fill with O_2 to 5.3 Pa
(2) Sputter clean with O_2 gas for about 5 min at about 100 V d.c.
(3) Pump out O_2 and fill with Ar at 1.3 Pa.
(4) Sputter clean with Ar for about 5 min at about 250 V d.c.; then pump system below 10^{-5} Pa.
(5) Deposit, sequentially, 5 nm of Ni, 100 nm of eutectic AuGe, 30 nm of Ni, and 50 or 100 nm of Au.
(6) Alloy in furnace for about 3 min at about 420°C, in an $Ar/H_2(H_2 10\%)$ gas mixture.

A problem with the AuGe:Ni system is that high-temperature (>400°C) alloying is usually necessary, thus producing an inhomogeneous interface, and some lateral spreading, which can be detrimental in many cases. Thus, some lower-temperature furnace and surface-heater processes have been investigated (Kuzuhara *et al.*, 1985), as well as laser annealing (Imanaga *et al.*, 1987), and some other processes that require no annealing at all (Kalkur *et al.*, 1985). Furthermore, many other metal systems besides AuGe:Ni have been studied. It is beyond the scope of this book to discuss these new processes and metals in great detail, but we do list a large number of the recent (mostly 1986 and 1987) literature results in Table 1.1.4. Earlier reviews (Rideout, 1975; Piotrowska *et al.*, 1983) cover much of the previous time period. Results for p-type GaAs and a few ternary III–V compounds involving Ga and/or As are also included in Table 1.1.4. It should be noted that most workers have used the same contacting procedures for the important ternary $Al_xGa_{1-x}As$ as for GaAs. Also, as discussed earlier, much progress has been made with In compounds, probably due to the formation of a graded $In_xGa_{1-x}As$ layer, which avoids the formation of high barriers in the interface region. For example, Allen *et al.* (1987) have achieved specific contact resistivities of less than 1×10^{-6} Ω-cm² with In/Pd metallization by using rapid thermal annealing (RTA) at 500°C for 20 s. A further advantage of In contacts is their high-temperature (up to 900°C) stability (Otsuki *et al.*, 1988).

1.1.7.3.2 Contacts for larger structures. For typical bulk Hall-effect patterns, with mm or even cm dimensions, the contacts can be made large enough that the current densities are not high. For such cases it is not necessary to have specific contact resistivities of 10^{-6} Ω-cm², although some workers still prefer the use of AuGe, which requires evaporation. An old method, which we have found very useful, and still use routinely in our laboratory, is to solder pure In onto the sample, say at the corners of a van der Pauw square, and then anneal at about 425°C for 2–3 min in a flowing inert gas (Ar or N For semi-insulating GaAs, it is not necessary to anneal

the contact at all. It has been our experience that soldered In will wet any clean, polished GaAs surface, without use of an ultrasonic iron. Some workers prefer In/Sn, of mixtures from 5 to 50% Sn, for n-type GaAs, and In/Au or In/Zn, with about 5% Au or Zn for p-type GaAs; such alloys are also easily soldered. A reasonable procedure for this type of contact is outlined below:

(1) Clean sample surface, if necessary, with a trichloroethylene, acetone, methanol, and DI water sequence, or other standard procedure.
(2) Apply In or In/Sn, for n-type samples, and In or In/Au, for p-type samples, with a small soldering iron. Generally the surfaces are wetted immediately.
(3) Anneal at 425°C for 2 min in flowing Ar or N_2. This step is usually not necessary for semi-insulating GaAs.

In our laboratory, we have found that if this technique does not produce a low-resistance contact on a particular sample, then neither will evaporated AuGe or any other metal. That is, if In fails as a contact, then the material itself is probably inhomogeneous and non-ohmic.

For semi-insulating GaAs, it is sometimes possible to get by with very crude contacts, since the current densities will normally be very low. For example, unalloyed In, silver paste, and even a conductive rubber (Kuhnel *et al.*, 1987) have been used. However, the ohmic nature of the contacts should always be tested by reversing the current and magnetic-field polarities, and by varying the current magnitude.

1.1.8 Apparatus

1.1.8.1 General considerations

Hall-effect measurements in conductive GaAs may be performed with very simple and inexpensive apparatus. For example, reasonably good values may be obtained for 1 Ω-cm, bulk, n-type material with a battery, 500 G bar magnet, and a common multimeter, which can all be purchased for less than $100. In contrast, a large, fully automated apparatus, which can handle semi-insulating samples (say, 10^{10} Ω), and which is interfaced with a closed-cycle He cryogenic system, can cost as much as $100 000. The basic instruments needed for all Hall-effect experiments are a current (or voltage) source, ammeter, voltmeter, magnet, and also a switchbox if van der Pauw measurements are to be performed. Beyond that, however, several factors need to be considered:

1.1.8.1.1 sample size
1.1.8.1.2 measurement temperature and pressure
1.1.8.1.3 impedance levels
1.1.8.1.4 magnetic-field strength
1.1.8.1.5 requirements for photo-excited measurements
1.1.8.1.6 automation.

Table 1.1.4 Ohmic-contact properties for GaAs and other III–V compounds

Semiconductor	Carrier concentration (10^{18} cm^{-3})	Contact metal*	Preparation	ρ_c (10^{-6} Ω-cm^2)	Reference
n-GaAs	2.2	Au/Pd/Ge	evap., surf. heater, 450°C, 30 s	0.5	Chen *et al.* (1986)
	2.2	Au/Ge/Ni	evap., surf. heater, 450°C, 30 s	0.4	Chen *et al.* (1986)
	5	Ni/AuGe	evap., laser, 40 ns	56	Sircar (1986)
	5	Ni/AgGe	evap., laser, 40 ns	95	Sircar (1986)
	1	Au/Ni/AuGe	evap., surf. heater, 320°C, 60 s	15	Patrick *et al.* (1986)
	10	Ni/Au/Ge	evap., no alloying	0.2	Shenai (1987)
	1.8	AuGe/Ni	evap., laser, 20 ns	1.5	Imanaga *et al.* (1987)
	2	Au/Pd	electroless dep., furnace, 350°C, 2 min	8	Lamouche *et al.* (1986)
	100	Au/Cr	evap., no alloying	2.5	Schubert *et al.* (1986)
	0.5	WSi_x	evap., RTA, 800°C, few s	1	Wright *et al.* (1986)
	0.3	In	evap., surf. heater, 350°C, 15 s	12	Lakhani (1984)
	0.15	In/Pt	evap., surf. heater, 400°C	2	Marvin *et al.* (1985)
	2	Au/In	electroless dep., furnace, 350°C, 2 min	15	Lamouche *et al.* (1987)
	2	In/Pd	evap., RTA, 500°C, 20 s	0.8	Allen *et al.* (1987)
	0.3	In	evap., furnace, 700°C, 10 min	10	Otsuki *et al.* (1988)
p-GaAs	4	Au/Pd	electroless dep., furnace, 250°C, 2 min	200	Lamouche *et al.* (1986)
	2	Ag/TiN/Pt/Mg	evap., furnace, 450°C, 30 min	100	Kattelus *et al.* (1986)
	1	Ag/W/Pt	evap., furnace, 400°C, 30 min	300	So *et al.* (1987)
	100	Ni/AuZn	evap., furnace, 450°C, 2.5 min	10	Bose and Henderson (1987)
n-InGaAs		Au/Cr	evap., no alloying	2.2	Huelsman and Fonstad (1986)
	15	Au/Pt/Ti	evap., no alloying	0.05	Nittono *et al.* (1986)
	1.8	Al	evap., no alloying	0.5	Kuroda *et al.* (1987)
p-InGaAs		Au/Cr	evap., no alloying	82	Heulsman and Fonstad (1986)
	1	Ni/AgZn/Ti	evap., furnace, 400°C, 2 min	11	Allevato *et al.* (1987)
n-InAlAs/InGaAs	1	Au/Ag/Au/Ge/Ni	evap., furnace, 480°C, 60 s	0.8	Zwicknagl *et al.* (1986)
n-AlGaAs/GaAs	3	Au/Ni/AuGe	evap., 500°C, 50 s	0.1	Ketterson *et al.* (1985)

* Top metal is on left if order is known.

.1.8.1.1 *Sample size.* Very large samples will require a correspondingly ırge sample holder, low-temperature dewar (if needed), and magnet ole-piece area. Very small samples will require special means of attaching ıe lead-in wires to the samples, perhaps by thermal or ultrasonic binding.

.1.8.1.2 *Measurement temperature and pressure.* If temperatures other ıan room temperature are of interest, then a special sample-isolation ystem is needed. For high temperatures, components must be chosen arefully to avoid melting and burning. However, a relatively simple system onsisting of an open quartz tube, resistive-wire heater around the tube, lass-wool insulation, aluminum sample holder, and platinum thermometer an be set up, with an inert flowing gas to cool the system quickly, if esired. For low temperatures, a vacuum dewar is needed for isolation, and are must be taken to avoid large thermal gradients in the sample area. A ariety of cooling options are available, ranging from liquid cryogens to losed-cycle He or N_2 refrigerators. The latter are commercially available in ery small sizes. Thermometers must be chosen with magnetic-field effects ı mind. Unfortunately, those with the least magnetic-field dependence sually also have the poorest reproductibility. For example, both capacitnce thermometers and thermocouples are quite independent of B, but are lso not very reproducible. In contrast, pure Pt as a resistance thermometer ; very reproducible, but also highly B-dependent at low temperatures. One ood compromise is carbon-glass as a resistance thermometer, but it is not ery sensitive above liquid-nitrogen temperatures. Another good comıromise is a GaAs diode, which has a much larger useful range (1–400 K) han the carbon resistor, and yet is not unacceptably B-dependent. Some vorkers have solved the magnetic-field problem by taking a different pproach, i.e. by using separate thermometers for measurement and ontrol. The control thermometer is kept outside of the magnetic field, vhile the measurement thermometer is read only when the field is off.

Pressure-dependent studies of the Hall effect are now more viable than in ıe past, with the advent of the diamond-anvil cell (Patel *et al.*, 1986; Patel nd Spain, 1987; van Straaten and Silvera, 1987). Such cells have achieved ressures of over 100 GPa (1000 kbar), but semiconductor applications have enerally required pressures of only about 10 GPa or less. Some of the ngineering problems in high-pressure work, such as bringing out the urrent and voltage leads, are formidable, but can be solved. Another ecurring problem in high-pressure work is choosing the proper pressureransmitting medium to make sure that the pressure is hydrostatic. An xample of two-band effects, induced by high pressure, will be given later Patel *et al.*, 1986).

.1.8.1.3 *Impedance levels.* The measured resistivities of GaAs range rom 10^{-4} to 10^{9} Ω-cm, so for a 1 mm thick sample, the resistances would ange from 10^{-3} tc [illegible]^{0} Ω. For the 10^{-3} Ω sample, the current must typically

be kept below 100 mA to avoid sample heating, thus giving a conductivity voltage $V_c \lesssim 10^{-4}$ V = 100 μV. If $\mu \simeq 1000$ cm^2/V-s, and $B \simeq 5$ kG, then the Hall voltage will be about 5 μV. Thus, a nanovoltmeter will probably be required for acceptable voltage resolution, and since the input impedance of such an instrument is typically 10^{9} Ω or less, it cannot be used for a 10^{10} Ω sample. On the other hand, electrometers or high-impedance buffer amplifiers, which are necessary for the 10^{10} Ω sample, will typically have internal noise levels of about 10 μV, and thus may be unacceptable for the 10^{-3} Ω sample. Also, the connections between a 10^{10} Ω sample and the electrometers must be well shielded, to avoid microphonics and noise pick-up. However, such shielded cables may have capacitances of 100 pf/ft or more, so that a 10 ft cable would lead to an RC time constant of 10 s. One way to reduce the time constants is to drive the shields with a low-impedance, unity-gain output of the electrometer or buffer amplifier. Another precaution with high-impedance measurements is to make sure the current is read on the low-impedance side of the sample, so that any leakage currents (which would probably occur on the high-impedance side) are not counted as part of the sample current. Thus, it is clear that the impedance levels of the samples to be measured must be considered in the design of the apparatus. Examples will be given later.

1.1.8.1.4 *Magnetic-field strength.* The Hall voltage will be approximately given by $V_H \simeq \mu BIR$ in MKS units, or $\mu BIR/10^8$ in laboratory units (μ in cm^2/V-s, B in gauss, I in amperes, and R in ohms). For low-resistivity GaAs, say 10^{-3} Ω-cm material ($R \simeq 10^{-2}$ Ω), μ is about 10^{3} cm^2/V-s, and if the current is limited to 10 mA to avoid heating, then $V_H \simeq 10^{-9} B(G)$. In such a case, it may be very helpful to have a magnetic-field strength as high as 10 kG (giving $V_H \simeq 10\,\mu$V) instead of only 1 kG (giving $V_H \simeq 1\,\mu$V). In contrast, if $\mu B > 10^{8}$, in laboratory units, then some nonlinear effects begin to enter the relevant equations, so that if $\mu \simeq 10^{5}$ cm^2/V-s, for example, then B should be kept below 1 kG.

Another point to consider is the size of the pole pieces. For example, it is grossly unnecessary to have 12 in pole pieces, with uniformity of 100 μG/cm, for Hall-effect measurements. Basically, the field inhomogeneity errors are less than other errors in the problem if B changes by 5% or less over the largest sample dimension. Thus, for example, one of the commercially available Hall-effect apparatuses uses a permanent magnet with only 1 in × 1 in pole pieces, and a 0.8 in gap. Perhaps the most widely used all-purpose magnet is an electromagnet with 4 in pole pieces and adjustable gap, and operating at a power of 1–2 kW.

1.1.8.1.5 *Photo-excited measurements.* With the simple addition of a laser or monochromator, it is possible to increase the variety of investigations considerably, including photoconductivity, photo-Hall, and photomagnetoelectric measurements. Also, the use of light is sometimes n[illegible]ssary to

)

eate enough carriers in a semi-insulating sample to be able to make a easurement at all. This is a problem that can occur in thin films of very ıre GaAs. Each of these applications will be discussed in more detail later, ıt the requirement for photo-excitation should be considered early in the esign of an apparatus. For example, a low-temperature dewar may need to e designed with flat windows, which are transparent to the wavelengths of iterest. A good general-purpose light source is a $\frac{1}{4}$ m, high-intensity ionochromator with a tungsten-halide lamp. Gratings are usually available ır wavelength ranges from 0.5 to 3.5 μm, which covers most of the spectral ınge of interest in GaAs.

1.8.1.6 Automation. Since the advent of relatively low-cost computers, has become increasingly desirable to automate experiments such as those iscussed here. Most commercial instruments available these days can be urchased with computer interfaces, and virtually every aspect of a [all-effect experiment can be controlled with a computer. It is often esirable to use a standard interface I/O bus, e.g. the IEEE-488 standard us, which is now available for use with a wide variety of computers and igh-level languages. With a standard such as this, hardware problems are irtually eliminated. In regard to software, there are good reasons for riting one's own programs, because modifications are often necessary. A ompiled language, such as FORTRAN, is generally not as desirable as an iterpreted language, such as BASIC, since in the former case, the program ıust be recompiled and linked every time a change is made, no matter how nall. However, if a fast enough computer is dedicated to the experiment, ıen the compiling and linking times may not be appreciable. Examples of ommercially available automated apparatuses are given below and in ppendix D.

.1.8.2 High-impedance van der Pauw apparatus

basic design for a high-impedance, automated van der Pauw–Hall pparatus, which can accommodate samples of up to $10^{12}\,\Omega$, is given in Fig. .1.30. All components are commercially available (e.g., from Keithley, ıc.; see Appendix D), and the electrometers can, of course, be replaced by igh-impedance, unity-gain buffer amplifiers, although at some sacrifice in ıput impedance. The inputs and outputs of the high-impedance scanner, nd the inputs to the ammeter and electrometers, are of triaxial design, hich has the advantage that the inner shields can be driven by the nity-gain output of the electrometers, which effectively reduces cable-harging effects. The outer shields are all grounded at a common point, lthough in practice the grounding may not be critical. The current source hould have an effective output impedance of about $10^{12}\,\Omega$ and be able to egulate currents of 10^{-10} A. At higher resistance levels, the current egulation will cross over to voltage regulation, and the currents will

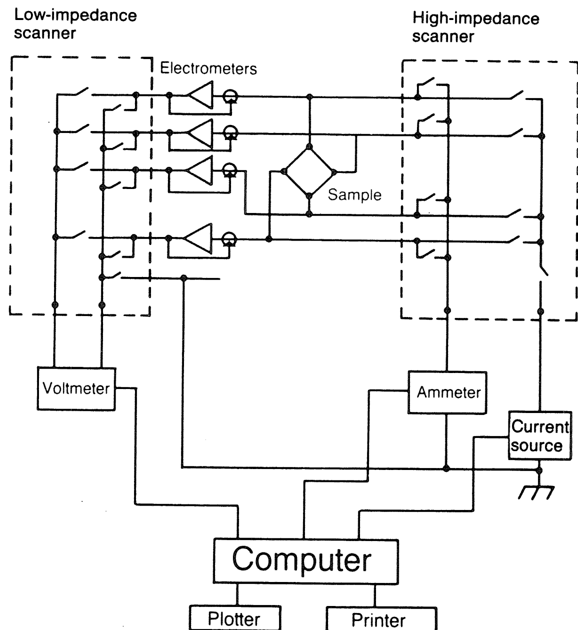

Fig. 1.1.30 A schematic diagram of an automated, high-impedance Hall-effect apparatus. All components are commercially available

diminish; however, the data will still be accurate as long as the actual current and voltage are both measured. The low-impedance scanner should be mainly designed for low thermal offsets (say, a few microvolts) since current leakage is not a problem on this side of the electrometers. Note that although the ammeter needs to be of electrometer design, to be able to measure the very low currents, the voltmeter does not, since the electrometer *output* impedances are only a few kilohms.

The wiring to the high-impedance scanner in this design allows the current source and current sink to be individually applied to any desired sample contact. Also, the high input and low input on the voltmeter can be connected to any electrometer unity-gain output through the low-impedance scanner. Figure 1.1.30 does not represent the most efficient design in terms of the minimum number of scanner switches, but does illustrate the main ideas quite well. Although not shown here, for very low-resistance samples it is desirable, and sometimes necessary, to be able to bypass the electrometers, since their typical noise levels of 10 μV peak to peak may be unacceptably high.

We will not discuss the computer and peripherals in any detail here, because so many variations available today will work well. However, we would recommend that the system be designed around the standard

EE-488 interface bus, which allows new instruments to be added at will, d effectively eliminates serious hardware problems. For the worker who shes to personally build the major parts of the data-acquisition system, ere are designs available, usually employing high-impedance operational nplifiers instead of electrometers (Weissfloch *et al.*, 1987). However, it ould be noted that the input impedances of commercially available erational amplifiers are about a factor 10 below those available with pical commercial electrometers.

'.8.3 *Commercial instruments*

r those who wish to purchase a complete Hall-effect apparatus, there are ; of early 1988) at least five companies who build and market such uipment. These are listed in Table D.1, in Appendix D, as a service to e reader; however, no special endorsement or disclaimer is given with gard to any particular unit or company. Some of the companies offer egrated systems, including magnet, cryogenics, and software; examples of ch units are given in Fig. 1.1.31. Before making a final decision, the ospective purchaser should make sure that the apparatus being considered l be suitable for all the samples of interest, especially if those samples are ghly conductive or resistive. The major consideration here is 'resistance', t 'resistivity'. For example, a highly conductive sample of 10^{-4} Ω-cm sistivity, has a very accessible resistance of 10 Ω if it is only 0.1 μm thick.

.9 **Measurements in thin films**

principle, there are few fundamental differences between bulk measure-ents and measurements in thin films. (One of them is the possible portance of surface scattering in a thin film, but this effect is rarely servable and will not even be considered here.) However, there are many *actical* differences, the two most important being substrate conduction and face (and interface) depletion. These effects will be considered in some tail here because of the special interest in epitaxial growth technology ese days, and also because they are often ignored or poorly understood. o other problems, depth inhomogeneity and electron transfer in hetero-uctures, will be considered in later chapters.

.9.1 *Substrate conduction*

general, thin layers are grown onto (or implanted into) a 'platform' of ne sort, usually a substrate of the same material as the layer. The most nmon substrate used these days for GaAs layer growth is 'semi-ulating' (SI) GaAs, with resistivities ranging from 10^7 to 10^9 Ω-cm. The ter value is near the 'maximum' resistivity for GaAs (about 2×10^9 Ω-cm, normal electron and hole mobilities), so that virtually any layer that is

Fig. 1.1.31 Examples of complete Hall-effect systems which are commercially available. (a) A compact system for 296 and 77 K measurements. (Reproduced by permission of DCL Semiconductor Co.) (b) A typical laboratory set-up for sophisticated measurements. (Reproduced by permission of Systems for Science, Inc., and Electronic Decisions, Inc.) (See Appendix D for further information on these and other manufacturers)

on SI GaAs has a lower resistivity than the substrate. Thus, it is natural assume that the substrate will not conduct any significant amount of rent, but this assumption is not always true because of the relative :knesses. The sheet resistance of the substrate is $r_s = \rho_s/d_s$ where d_s is the strate thickness, and the sheet resistance of the layer is $r_l = \rho_l/d_l$. Then, $_l = \rho_s d_l/\rho_l d_s$, and for typical values of these parameters, say, $\rho_s = 10\ \Omega$-, $d_l \simeq 0.1\ \mu$m, and $d_s = 500\ \mu$m, we will have $r_s/r_l \simeq 2\times 10^3/\rho_l$. Thus, ρ_l st be less than 20 Ω-cm in order for the substrate to carry less than 1% of current, whereas even pure, p-type MBE GaAs can have a resistivity as h as 200 Ω-cm. (Depletion effects will also occur in this case, as discussed the next section.) From another point of view, if $\rho_l \simeq 10^5\ \Omega$-cm, which is en observed (deep acceptor or donor center), then the necessary layer :kness to hold the substrate current to less than 1% is 500 μm! The ects are more pronounced at higher temperatures. For example, at 400 K 7°C), the SI GaAs resistivity will have dropped to $10^5\ \Omega$-cm, and even a -cm layer would have to be at least 0.5 μm thick to limit the substrate rent to 1%.

For mobility and carrier concentration determinations, the substrate iduction effects are even more severe. As is well known (Petritz, 1958), d will be discussed in detail later, the *two-layer* resistivity and Hall bility are given by:

$$\rho^{-1} = \sigma = \frac{\sigma_s d_s + \sigma_l d_l}{d_s + d_l} = \frac{d_s/\rho_s + d_l/\rho_l}{d_s + d_l} \tag{1.1.33}$$

d

$$\mu_H = |R_H \sigma| = \left| \frac{R_{Hl}\sigma_l^2 d_l + R_{Hs}\sigma_s^2 d_s}{\sigma_l d_l + \sigma_s d_s} \right| \tag{1.1.34}$$

ost of the present-day SI GaAs has $\rho_s < 5\times 10^8\ \Omega$-cm, and therefore xed-conductivity effects are absent (Look, 1980) and the material may be ssified as n-type. If, now, the epitaxial layer is p-type, then Eq. (1.1.34) comes

$$\mu_H = \left| \frac{p_l \mu_{pl}^2 d_l - n_s \mu_{ns}^2 d_s}{p_l \mu_{pl} d_l + n_s \mu_{ns} d_s} \right| \tag{1.1.35}$$

nsider the following example: $n_s \simeq 10^7\ \mathrm{cm}^{-3}$, $p_l \simeq 10^{13}\ \mathrm{cm}^{-3}$, $\mu_{ns} \simeq$)0 cm²/V-s, $\mu_{pl} \simeq 400\ \mathrm{cm^2/V\text{-}s}$, and $d_s \simeq 500\ \mu$m. Then the sample is type' only if $d_l > 0.2\ \mu$m, and 'n-type' otherwise. It is even possible to serve homogeneous layers 'change type' as a function of temperature, e to this effect. A more common observation is for the mobility of a ype layer to begin to fall rapidly as temperature is increased, say above) K. The reason for this phenomenon is that n_s increases rapidly with nperature [approximately as $\exp(-0.75/kT)$], and thus μ_H begins to proach zero.

It might be argued that substrate conduction should never affect a p-type

layer because the resulting p–n junction should isolate the substrate and layer. However, there are two points to be made in this regard: (1) for a layer of 0.2 μm or less, alloyed contacts will probably penetrate through the layer and allow current to flow through the substrate in spite of the junction; and (2) the junction barrier will not be high enough for effective isolation unless the layer is quite conductive, in which case the substrate will not matter anyway. These warnings are not meant to imply that junction isolation is never effective, because it has been successfully used on many occasions. However, it is not a panacea for all substrate conduction problems and the resulting electrical-measurement data should be critically examined to make sure that such problems do not exist.

1.1.9.2 Surface and interface depletion

As already discussed (cf. Fig. 1.1.21), a metal–semiconductor junction in GaAs produces a barrier, either due to the difference in electron affinities between the two materials, or due to surface states in the semiconductor. In the latter case, which seems to be more important for GaAs, the metal is somewhat incidental, and a barrier, denoted by $e\phi_s$, exists simply due to the presence of the free surface. Another barrier exists due to charge transfer in the interface region, i.e. in the junction formed by the conductive layer and the SI substrate. These effects are illustrated in Fig. 1.1.32. In the

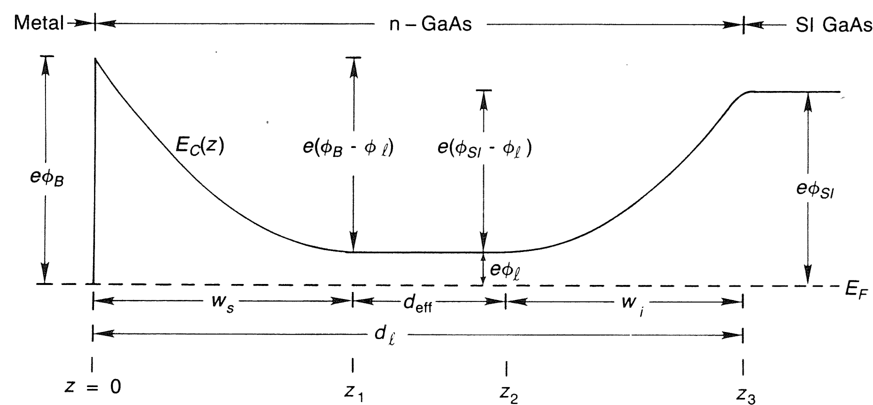

Fig. 1.1.32 A band diagram for a conducting layer of thickness d_l on a semi-insulating substrate. Current (parallel to the layer plane) is carried only in the region denoted by d_{eff}, the 'electrical' thickness

'depletion' or 'abrupt' approximation, which is certainly good enough for these purposes, the layer is considered to be totally devoid of free carriers in the regions $0 \le z < z_1$ and $z_2 < z \le z_3$, and has the usual free carrier concentration n_l in the region $z_1 \le z \le z_2$, where $n_l = N_D - N_A$ if the donors are shallow. Thus, the only region in the layer which can carry current is the

utral region, of thickness $d_{\text{eff}} = d_l - w_s - w_i$, where d_l is the total layer ickness. As will be derived later, w_s and w_i are given by

$$w_s = \left[\frac{2\epsilon(\phi_{sn} - \phi_l - kT/e)}{e(N_D - N_A)}\right]^{1/2} \tag{1.1.36}$$

$$w_i = \left[\frac{2\epsilon(\phi_{SI} - \phi_l - kT/e)}{e(N_D - N_A)}\right]^{1/2} \tag{1.1.37}$$

ıere

$$\phi_{SI} \simeq (kT/e)\ln(N_c/n_{SI}) \tag{1.1.38}$$

$$\phi_l \simeq (kT/e)[\ln(N_c/n_l) - n_l/\sqrt{8}\,N_c] \tag{1.1.39}$$

$$N_C \simeq 8.63 \times 10^{13} T^{3/2}\{1 - 1.93 \times 10^{-4}\,T - 4.19 \times 10^{-8}\,T^2\} \tag{1.1.40}$$

ere the effective density of states N_C is for the lowest Γ conduction band ılakemore, 1982), and is quite accurate for $T > 100$ K. (However, we will ıply it down to 77 K without significant loss of accuracy.) At 296 K $_C \simeq 4.12 \times 10^{17}\,\text{cm}^{-3}$, and at 77 K $N_C \simeq 5.74 \times 10^{16}\,\text{cm}^{-3}$. The formula for , Eq. (1.1.39), is fairly accurate for $n_l \ll 10N_C$ (Kroemer, 1981); more curate approximations can be found elsewhere (Joyce and Dixon, 1977; ilsson, 1978), but this term is not that important anyway. The kT/e terms Eqs. (1.1.36) and (1.1.37) essentially give a correction to the depletion ıproximation in the sense that they account for free-electron *leakage* of a w Debye lengths (λ_D) into the depletion region where

$$\lambda_D = \left[\frac{\epsilon kT/e}{e(N_D - N_A)}\right] \tag{1.1.41}$$

ıe final values of w_s and w_i have little meaning, of course, unless w_s and $\gg l_D$, i.e. unless $(\phi_s - \phi_l)$ and $(\phi_{SI} - \phi_l) \gg kT/e$. The value of ϕ_{sn} is ımewhat uncertain, but is approximately 0.7 V for oxidized material ıpicer *et al.*, 1980; Lindau and Kendelewicz, 1986).

For p-type material we would simply replace ϕ_{sn} with ϕ_{sp}, where $_p \simeq 0.5$ eV (with respect to the valence band), n_l with p_l, n_{SI} with p_{SI}, $_D - N_A)$ with $(N_A - N_D)$, and N_C with N_V, where (Blakemore, 1982)

$$N_V \simeq 1.83 \times 10^{15}\,T^{3/2} \tag{1.1.42}$$

Some depletion corrections for both n-type and p-type material of various ıncentrations, at 296 and 77 K, are listed in Table 1.1.5. Note that the *total* ırrections for n-type and p-type samples are not too different, since they ade off somewhat between surface and interface contributions. As can be en, the corrections can be quite large for low-concentration material; for ample a 5 μm layer with n (or p) $\simeq 10^{14}\,\text{cm}^{-3}$ would be almost fully pleted. Even a 10 μm uniform layer with $n \simeq 10^{14}\,\text{cm}^{-3}$ would have a true rrier concentration of nearly twice the value determined by using the etallurgical thickness. For $10^{17}\,\text{cm}^{-3}$ material, typical for FET structures, e correction is mı smaller; however, actual FET layers are usually only

Table 1.1.5 Depletion-depth corrections in GaAs (assumptions: $n_{SI} = 5 \times 10^7\,\text{cm}^{-3}$, $\phi_{Bn} = 0.7$ V, $\phi_{Bp} = 0.5$ V, $n = N_D - N_A$, $p = N_A - N_D$)

Type	Temperature (K)	Concentration (cm^{-3})	$w_s(\mu m)$	$w_i(\mu m)$	$w_{tot}(\mu m)$
n	296	10^{14}	2.56	2.22	4.78
		10^{15}	0.862	0.759	1.62
		10^{16}	0.288	0.257	0.544
		10^{17}	0.0956	0.0864	0.182
		10^{18}	0.0310	0.0282	0.0592
		10^{19}	0.00981	0.00891	0.0187
	77.2	10^{14}	3.05	3.03	6.08
		10^{15}	0.975	0.970	1.94
		10^{16}	0.312	0.310	0.622
		10^{17}	0.0995	0.0990	0.198
		10^{18}	0.0314	0.0313	0.0627
		10^{19}	0.00995	0.00990	0.0198
p	296	10^{14}	1.61	2.74	4.35
		10^{15}	0.587	0.912	1.499
		10^{16}	0.207	0.303	0.510
		10^{17}	0.0716	0.100	0.171
		10^{18}	0.0244	0.0329	0.0574
		10^{19}	0.00823	0.0108	0.0190
	77.2	10^{14}	2.48	3.26	5.74
		10^{15}	0.798	1.04	1.84
		10^{16}	0.256	0.333	0.589
		10^{17}	0.0825	0.106	0.189
		10^{18}	0.0265	0.0340	0.0605
		10^{19}	0.00839	0.0107	0.0191

0.1–0.2 μm thick anyway, so the correction can still be very important. Plots of the corrections for n-type material are given in Fig. 1.1.33.

Another way to determine the depletion correction, rather than using the formulas given here, is to deposit a metal on another piece of the material (or use an Hg probe on the same material) and carry out a capacitance–voltage (C–V) measurement, which can actually map n_l as a function of depth. The reason that this method can reasonably determine the depletion correction in bare GaAs is that the presence of the metal does not affect the surface barrier too much, since the surface states are so dense. The C–V profiling method is discussed in detail later.

The necessity of proper depletion corrections has recently been demonstrated in the interpretation of temperature-dependent Hall-effect measurements in thin layers of pure, n-type GaAs (Lepkowski *et al.*, 1987). For a 5.5 μm sample with $n \simeq 1.8 \times 10^{14}\,\text{cm}^{-3}$, it was found that the neutral (undepleted) region was about 2 μm at 296 K, and only about 1 μm at 77 K. Thus, the uncorrected Hall concentration appeared to increase rapidly at higher temperatures, which would traditionally have been inte· ·eted as

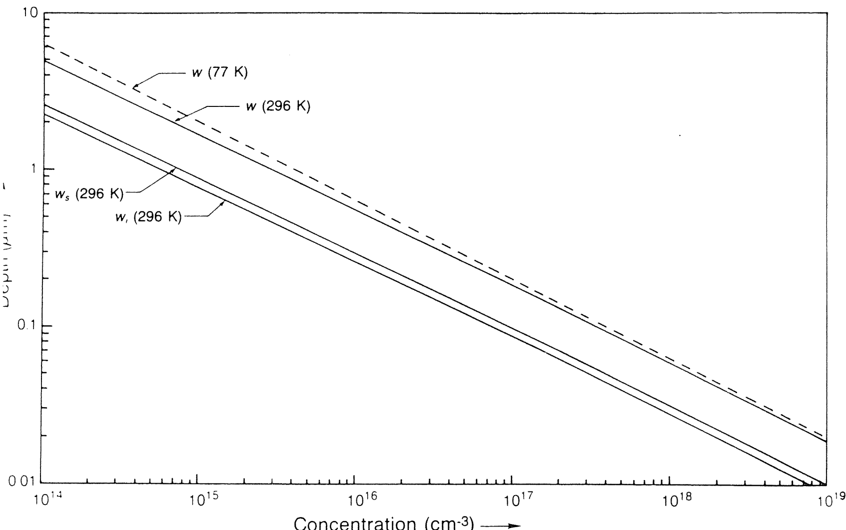

ig. 1.1.33 Surface, interface, and total depletion widths in GaAs as functions f electron concentration and temperature

ıuiring the existence of a deeper donor center. However, a much thicker nple of nearly the same concentration did not show the strong up-turn, as :n in Fig. 1.1.34 (Lepkowski *et al.*, 1987). It is apparent, therefore, that : up-turn was not caused by a deeper donor in this case and that great ·e must be exercised in fitting T-dependent Hall data for thin samples. ıte that the dip in n vs. T which appears even in the thick sample is ›bably due to the temperature dependence of r_H, the Hall factor.

1.2 CONDUCTIVITY AND HALL COEFFICIENT

far we have discussed some of the practical aspects of carrying out ıll-effect measurements. However, it is also of value to explore the more ›tle aspects of the relationship between the Hall effect and the major rameter it determines, carrier concentration. Furthermore, it is important define and discuss the various kinds of mobility, and then to relate both ›bility and carrier concentration to the relevant materials properties. The pendence of mobility on physical parameters is the subject of scattering :ory, which has been covered thoroughly in other works and thus will not covered in as much detail here. Other subjects, however, such as the nperature dependence of the carrier concentration for multi-charge ıters, and the use of proper degeneracy factors, will be covered in greater tail in this work, since they tend to not be as thoroughly discussed in ıer references. Also, we will develop multi-band conductivity theory to a :ater than usual extent, since it is important for semi-insulating GaAs,

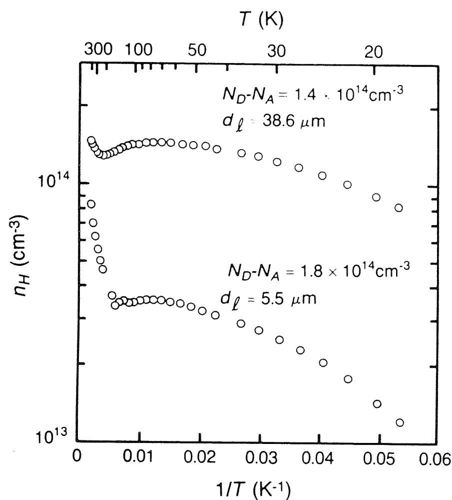

Fig. 1.1.34 The electron Hall concentration n_H vs. inverse temperature T^{-1} for two similarly doped GaAs epitaxial layers of different thickness. The strong upturn at high temperature in the 5.5 μm sample is primarily due to a changing electrical thickness (d_{eff}) rather than deep-level electron excitation. (After Lepkowski *et al.* (1987). Reproduced by permission of The American Institute of Physics)

GaAs at high temperatures or under high pressures, some of the ternaries such as $Al_xGa_{1-x}As$, and heterostructures which contain quantum subbands.

1.2.1 The current equations

In this section we will derive the current equations for electrons in a non-degenerate band which has spherical equal-energy surfaces, a situation which quite well describes the lowest (Γ_6) conduction band of GaAs, especially near its minimum at $\mathbf{k} = 0$. The electrons are assumed to exist and move in a six-dimensional phase space $(\mathbf{r}, \mathbf{k})$, with the average occupancy of the phase space described by a distribution function $f(\mathbf{r}, \mathbf{k}, t)$, which is both an implicit and explicit function of time. The time evolution of the distribution function can be written in a rather straightforward manner:

$$\frac{\partial f}{\partial t} + \dot{\mathbf{r}} \cdot \boldsymbol{\nabla}_r f + \dot{\mathbf{k}} \cdot \boldsymbol{\nabla}_k f - \left(\frac{\partial f}{\partial t}\right)_{\text{coll}} = 0 \qquad (1.2.1)$$

where the last term (*collision* term) represents changes in f due to electrons

hich have been scattered and have moved 'instantaneously' to another oint in phase space. Equation (1.2.1) is the well-known Boltzmann ansport equation, which has been solved for many different kinds of stems. The usual approach is to assume that in the presence of external elds **E** and **B** the equilibrium distribution f_0 is shifted by a small amount f_1, hich of course is a function of **E** and **B**. The collision term is then related the transition probabilities of the specific scattering mechanisms involved, nd an equation for f_1 can be developed for the steady-state situation, i.e., $f/\partial t = 0$. When all the scattering mechanisms are elastic, i.e. involve no nergy gained or lost as a result of the collision, then the collision term can e reduced to the form

$$\left(\frac{\partial f}{\partial t}\right)_{\text{coll}} = -\frac{f - f_0}{\tau(\mathscr{E})} = -\frac{f_1}{\tau(\mathscr{E})} \qquad (1.2.2)$$

here $\tau(\mathscr{E})$ is a *relaxation* time, dependent only on energy. For inelastic attering, however, $(\partial f/\partial t)_{\text{coll}}$ cannot be written in so simple a form, since oth the initial and final energies are involved, and it is necessary to solve q. (1.2.1) by numerical methods. Even if Eq. (1.2.2) is valid, it is still ecessary to use good judgment in guessing at the proper form for f_1, pecially when magnetic fields are involved. Thus, although the oltzmann-equation approach is very useful, and gives quite rigorous sults, the physics is somewhat obscured, especially when the scattering is elastic and the mobilities or magnetic fields are high enough that $\mu B \gtrsim 1$. herefore, we will begin with a less rigorous approach here, which gives the me results for elastic scattering. For the inelastic scattering case, we will mply outline one method of solving the Boltzmann equation.

The equations of motion for an electron in the band of interest are

$$\dot{\mathbf{r}} = \mathbf{v} = \frac{1}{\hbar}\nabla_k \mathscr{E}(\mathbf{k}) \qquad (1.2.3)$$

$$\hbar\dot{\mathbf{k}} = -e(\mathbf{E} + \mathbf{v} \times \mathbf{B}) \qquad (1.2.4)$$

here **k** is the wave vector and $\mathscr{E}(\mathbf{k})$ the energy of the electron. For our sumption of a parabolic band (spherical equal-energy surfaces) the energy beys

$$\mathscr{E}(\mathbf{k}) = \frac{\hbar^2 k^2}{2m^*} \qquad (1.2.5)$$

here m^* is the effective mass. Then

$$\mathbf{v} = \frac{1}{\hbar}\nabla_k \mathscr{E}(k) = \frac{\hbar\mathbf{k}}{m^*} \qquad (1.2.6)$$

nd from Eq. (1.2.4),

$$m^*\dot{\mathbf{v}} = -e(\mathbf{E} + \mathbf{v} \times \mathbf{B}) \qquad (1.2.7)$$

which is just the classical equation for an electron of mass m^* experiencing the Lorenz force. Since the only velocity-dependent force (i.e., $\mathbf{v} \times \mathbf{B}$) is perpendicular to the motion, Eq. (1.2.7) will contain an oscillatory component of motion which will never die down. However, we know that collisions will eventually destroy, or 'dephase' the oscillatory motion; i.e. after a certain time τ (again, the *relaxation* time) the phase of the precession about the magnetic field will bear no relationship to the initial phase. If it is assumed that the phase loss is exponential with time, then the collisional force can be represented by

$$\mathbf{F}_{\text{coll}} = -m^* \frac{\mathbf{v} - \mathbf{v}}{\tau} \qquad (1.2.8)$$

where $\bar{\mathbf{v}}$ is the equilibrium velocity, i.e., an average velocity which would hold in the absence of all external forces. The total balance of forces now gives

$$m^*\dot{\mathbf{v}} = -e(\mathbf{E} + \mathbf{v} \times \mathbf{B}) - m^* \frac{\mathbf{v} - \bar{\mathbf{v}}}{\tau} \qquad (1.2.9)$$

It is assumed here that the *magnitudes* of **v** and $\bar{\mathbf{v}}$ are not too different at any time; otherwise, τ would probably be a function of v, as well as $\bar{v}$, and the equation could not be solved, in general. That is, we require that $\tau = \tau(\bar{v}) = \tau(\bar{\mathscr{E}})$, which implies that $\mathscr{E} \simeq \bar{\mathscr{E}}$, so that only elastic collisions are allowed in this formulation. For inelastic scattering, there is no guarantee that the approach to equilibrium will be exponential at all, even for small perturbations of **v**, and thus Eq. (1.2.9), with constant τ, is not applicable. Unfortunately, the dominant scattering mechanism is in pure GaAs for $T > 100$ K, polar optical-mode phonon scattering, is not elastic, because a high-energy ($>kT$) optical phonon is exchanged in the scattering process. At temperatures well above the polar-optical temperature, $T_{po} \simeq 419$ K, the scattering is again 'effectively' elastic, so that Eq. (1.2.9) is applicable for $T < 100$ K or $T \gg 420$ K, but not in between. The situation is better for *impure* GaAs, since impurity scattering is elastic. For example, if there are 10^{19} ionized-impurities/cm^3, then impurity scattering will dominate from low temperatures to well above T_{po}, and thus, the major scattering will be elastic or effectively elastic over the whole range. In spite of all these caveats, we will apply Eq. (1.2.9) anyway, because all of the galvanomagnetic phenomena of interest can be illustrated by its solution, even though there will be some sacrifice of accuracy in certain cases.

If the external magnetic field **B** is in the z-direction, then the x- and y-components of Eq. (1.2.9) give

$$\frac{dv_y}{dt} = -\frac{e}{m^*}E_x - \omega_c v_y - \frac{v_x - \bar{v}_x}{\tau} \qquad (1.2.10)$$

$$\frac{dv_y}{dt} = -\frac{e}{m^*}E_y + \omega_c v_x - \frac{v_y - \bar{v}_y}{\tau} \qquad (1.2.11)$$

ıere $\omega_c \equiv eB/m^*$, the cyclotron frequency. The z-component of Eq. .2.9) is of no interest because there is no z-component of **E** applied, and ıne is generated. Equations (1.2.10) and (1.2.11) form a pair of coupled, ıear differential equations which can be solved, e.g. by the Laplace-ınsform method, as shown in Appendix A. The results are:

$$v_x(t) = e^{-t/\tau}\Big\{\cos\omega_c t\Big[v_x(0) - \frac{1}{1+\omega_c^2\tau^2}\Big[\Big(\bar{v}_x - \frac{eE_x\tau}{m^*}\Big) - \omega_c\tau\Big(\bar{v}_y - \frac{eE_y\tau}{m^*}\Big)\Big]\Big]$$
$$+\frac{\sin\omega_c t}{\omega_c t}\Big[\Big[\Big(\bar{v}_x - \frac{eE_x\tau}{m^*}\Big) - \omega_x\tau v_y(0)\Big]$$
$$-\frac{(\bar{v}_x - eE_x\tau/m^*) - \omega_c\tau(\bar{v}_y - eE_y\tau/m^*)}{1+\omega_c^2\tau^2}\Big]\Big\}$$
$$+\frac{1}{1+\omega_c^2\tau^2}\Big[\Big(\bar{v}_x - \frac{eE_x\tau}{m^*}\Big) - \omega_c\tau\Big(\bar{v}_y - \frac{eE_y\tau}{m^*}\Big)\Big] \quad (1.2.12)$$

th a similar equation for $v_y(t)$:

$$v_y(t) = e^{-t/\tau}\{v_x \leftrightarrow v_y,\ E_x \leftrightarrow E_y,\ \omega_c \to -\omega_c \text{ in Eq. (1.2.12)}\}$$
$$+\frac{1}{1+\omega_c^2\tau^2}\Big[\Big(\bar{v}_y - \frac{eE_y\tau}{m^*}\Big) + \omega_c\tau\Big(\bar{v}_x - \frac{eE_x\tau}{m^*}\Big)\Big] \quad (1.2.13)$$

fter a long time, $t/\tau \gg 1$, the system will reach steady state, and neither e initial values of velocity, $v_x(0)$ and $v_y(0)$ nor the initial phase (zero in is case) will matter, since the terms multiplied by $\exp(-t/\tau)$ will vanish. ıe cyclotronic motion, given by the $\sin\omega_c t$ and $\cos\omega_c t$ terms, will also ısappear, not actually, but in an average sense, since the phase information ll be lost. An equivalent picture would be that a *group* of electrons, which ıre subjected to **E** and **B** forces at $t = 0$, would exhibit cyclotronic motion, phase, for a time up to $t \simeq \tau$, but at much later times $t \gg \tau$, would have ı *net* cyclotronic motion.

The fact that the average electron velocities have changed from $\bar{v}_x$ and $\bar{v}_y$ the expressions given by $v_x(\infty)$ and $v_y(\infty)$, respectively, can be repre-nted by a change in the distribution function, $f(\mathbf{k})$, which is no longer herically symmetrical about $\mathbf{k} = 0$. The expansion of $f(\mathbf{k})$ in a Taylor ries gives, to first order,

$$f(\mathbf{k}) = f_0(\mathscr{E}) + [\bar{v}_x - v_x(\infty)]\frac{\partial f_0}{\partial \bar{v}_x} + [\bar{v}_y - v_y(\infty)]\frac{\partial f_0}{\partial \bar{v}_y} + [\bar{v}_z - v_z(\infty)]\frac{\partial f_0}{\partial \bar{v}_z} \quad (1.2.14)$$

ıce $|\bar{v}_x| \gg |\bar{v}_x - v_x(\infty)|$, etc., we can approximate the energy as

$$\mathscr{E} \simeq \tfrac{1}{2}m^*(\bar{v}_x^2 + \bar{v}_y^2 + \bar{v}_z^2) \simeq \tfrac{3}{2}m^*\bar{v}_x^2 \simeq \tfrac{3}{2}m^*\bar{v}_y^2 \simeq \tfrac{3}{2}m^*\bar{v}_z^2 \quad (1.2.15)$$

and therefore

$$\frac{\partial f_0}{\partial \bar{v}_x} = \frac{\partial f}{\partial \mathscr{E}}\frac{\partial \mathscr{E}}{\partial \bar{v}_x} \simeq 3m^*\bar{v}_x\frac{\partial f_0}{\partial \mathscr{E}} \quad (1.2.16)$$

with similar expressions for the y- and z-components.

The x-component of current can be represented by

$$j_x = -\frac{e}{4\pi^3}\int_{\mathscr{E}_{\min}}^{\mathscr{E}_{\max}} f(\mathbf{k})\bar{v}_x\,d\mathbf{k} = -ne\frac{\int_{\mathscr{E}_{\min}}^{\mathscr{E}_{\max}} f(\mathbf{k})\bar{v}_x\,d\mathbf{k}}{\int_{\mathscr{E}_{\min}}^{\mathscr{E}_{\max}} f_0(\mathbf{k})\,d\mathbf{k}} \quad (1.2.17)$$

where $\mathscr{E}_{\min}$ and $\mathscr{E}_{\max}$ are the minimum and maximum energies, respectively, in the band. The integration is over $d\mathbf{k} = dk_x\,dk_y\,dk_z = (m^*/\hbar)^3\,d\bar{v}_x\,d\bar{v}_y\,d\bar{v}_z$ for a parabolic band. We note that $\bar{v}_x$, $\bar{v}_y$ and $\bar{v}_z$ are odd functions in their respective velocity spaces and f_0, $\partial f_0/\partial\mathscr{E}$, and $\tau(\mathscr{E})$ are even functions. Thus, by substituting Eqs. (1.2.14) and (1.2.16) into Eq. (1.2.17), and gathering all the even terms (the odd terms vanish), Eq. (1.2.17) becomes

$$j_x = -ne\frac{\int_{\mathscr{E}_{\min}}^{\mathscr{E}_{\max}} \bar{v}_x^2 \frac{1}{1+\omega_c^2\tau^2}\Big\{\frac{eE_x\tau}{m^*} - \omega_c\tau\frac{eE_x\tau}{m^*}\Big\}\frac{\partial f_0}{\partial \mathscr{E}}\,d\mathbf{k}}{\int_{\mathscr{E}_{\min}}^{\mathscr{E}_{\max}} f_0(\mathbf{k})\,d\mathbf{k}} \quad (1.2.18)$$

To get Eq. (1.2.18) in terms of $\mathscr{E}$ only, we let $\mathscr{E}_{\min} = 0$, and then note that $d\mathbf{k} \propto k^2\,dk \propto \mathscr{E}^{1/2}\,d\mathscr{E}$ and $\bar{v}_x^2 \simeq 2\mathscr{E}/3m^*$. Also, from the functional form of f_0, i.e.,

$$f_0 = 1/[1 + \exp(\mathscr{E} - \mathscr{E}_F)/kT]$$

the denominator of Eq. (1.2.18) becomes

$$\int_0^{\mathscr{E}_{\max}} f_0(\mathbf{k})\,d\mathbf{k} \propto \int_0^{\mathscr{E}_{\max}} f_0\mathscr{E}^{1/2}\,d\mathscr{E}$$
$$= \tfrac{2}{3}\Big\{\mathscr{E}^{3/2}f_0\Big|_0^{\mathscr{E}_{\max}} - \int_0^{\mathscr{E}_{\max}} \mathscr{E}^{3/2}\frac{\partial f_0}{\partial \mathscr{E}}\,d\mathscr{E}\Big\}$$
$$= -\tfrac{2}{3}\int_0^{\mathscr{E}_{\max}} \mathscr{E}^{3/2}\frac{\partial f_0}{\partial \mathscr{E}}\,d\mathscr{E} \quad (1.2.19)$$

since $f_0 \simeq 0$ at $\mathscr{E} = \mathscr{E}_{\max}$. Thus, Eq. (1.2.18) becomes

$$j_x = \frac{ne^2}{m^*}\Big\{\Big\langle\frac{\tau}{1+\omega_c^2\tau^2}\Big\rangle E_x - \Big\langle\frac{\omega_c\tau^2}{1+\omega_c^2\tau^2}\Big\rangle E_y\Big\}$$
$$\equiv \sigma_{xx}E_x + \sigma_{xy}E_y \quad (1.2.20)$$

ıd similarly, j_y can be written

$$j_y = \frac{ne^2}{m^*}\left\{\left\langle\frac{\omega_c\tau^2}{1+\omega_c^2\tau^2}\right\rangle E_x + \left\langle\frac{\tau}{1+\omega_c^2\tau^2}\right\rangle E_y\right\}$$
$$= \sigma_{yx}E_x + \sigma_{yy}E_y \qquad (1.2.21)$$

here the brackets denote an energy average; i.e., for some function $f(\tau)$

$$\langle f(\tau)\rangle = \frac{\int_0^\infty f(\tau)\mathscr{E}^{3/2}\frac{\partial f_0}{\partial \mathscr{E}}\,\mathrm{d}\mathscr{E}}{\int_0^\infty \mathscr{E}^{3/2}\frac{\partial f_0}{\partial \mathscr{E}}\,\mathrm{d}\mathscr{E}} \qquad (1.2.22)$$

Iere we have extended the upper integation limit to ∞, since $\partial f_0/\partial\mathscr{E}$ falls off ɾell before the band maximum in all practical cases. Note that $\partial f_0/\partial\mathscr{E}$ can e written as $f_0(1-f_0)/kT$, since

$$f_0 = 1/[1+\exp(\mathscr{E}-\mathscr{E}_F)/kT]$$

'hus, for nondegenerate electrons (Boltzmann statistics), $\partial f_0/\partial\mathscr{E} \simeq$ $kT)^{-1}\exp(\mathscr{E}_F-\mathscr{E})/kT$, since $\exp(\mathscr{E}_F-\mathscr{E})/kT \gg 1$. For degenerate elec-rons (Fermi–Dirac statistics), on the other hand, $f_0(1-f_0)$ is a sharply ›eaked function, having a value of unity at $\mathscr{E}=\mathscr{E}_F$, and zero otherwise [like $\delta(\mathscr{E}-\mathscr{E}_F)$]. Thus, for degenerate electrons, $\langle f(\tau)\rangle = f(\tau(\mathscr{E}_F))$, and for ıondegenerate electrons, $\langle f(\tau)\rangle$ becomes

$$\langle f(\tau)\rangle = \frac{\int_0^\infty f(\tau)\mathscr{E}^{3/2}\mathrm{e}^{-\mathscr{E}/kT}\,\mathrm{d}\mathscr{E}}{\int_0^\infty \mathscr{E}^{3/2}\mathrm{e}^{-\mathscr{E}/kT}\,\mathrm{d}\mathscr{E}} \qquad (1.2.23)$$

As will be shown later, it is often possible to write τ in the form, $\tau = a\mathscr{E}^{-s}$ where a and s are constants. In such a case, $\langle f(\tau)\rangle$ can be expressed in terms of the gamma function, $\Gamma(p)$:

$$\Gamma(p) \equiv \int_0^\infty x^{p-1}\mathrm{e}^{-x}\,\mathrm{d}x \qquad (1.2.24)$$

Some useful properties of the Γ function include the following: $\Gamma(p) = (p-1)\Gamma(p-1)$, for any value of p; $\Gamma(p) = (p-1)!$, if p is an integer; and $\Gamma(1/2) = \pi^{1/2}$. Thus, the commonly encountered functions $\langle\tau\rangle$ and $\langle\tau^2\rangle$ become

$$\langle\tau\rangle = \frac{\int_0^\infty \tau\mathscr{E}^{3/2}\mathrm{e}^{-\mathscr{E}/kT}\,\mathrm{d}\mathscr{E}}{\int_0^\infty \mathscr{E}^{3/2}\mathrm{e}^{-\mathscr{E}/kT}\,\mathrm{d}\mathscr{E}} = \frac{\int_0^\infty a\mathscr{E}^{3/2-s}\mathrm{e}^{-\mathscr{E}/kT}\,\mathrm{d}\mathscr{E}}{\int_0^\infty \mathscr{E}^{3/2}\mathrm{e}^{-\mathscr{E}/kT}\,\mathrm{d}\mathscr{E}}$$
$$= a(kT)^{-s}\frac{\Gamma(5/2-s)}{\quad} \qquad (1.2.25)$$

$$\langle\tau^2\rangle = \frac{\int_0^\infty \tau^2\mathscr{E}^{3/2}\mathrm{e}^{-\mathscr{E}/kT}\,\mathrm{d}\mathscr{E}}{\int_0^\infty \mathscr{E}^{3/2}\mathrm{e}^{-\mathscr{E}/kT}\,\mathrm{d}\mathscr{E}} = a^2(kT)^{-2s}\frac{\Gamma(5/2-2s)}{\Gamma(5/2)} \qquad (1.2.26)$$

Note that an energy dependence of $\tau(\tau\propto\mathscr{E}^{-s})$ translates directly to a temperature dependence of τ $(\tau\propto T^{-s})$. This fact is important in determining the temperature dependence of mobility.

For multiple scattering mechanisms, each of which can be described by a relaxation time, the inverse relaxation times (i.e. scattering rates) simply add. Thus,

$$\frac{1}{\tau(\mathscr{E})} = \frac{1}{\tau_1(\mathscr{E})} + \frac{1}{\tau_2(\mathscr{E})} + \frac{1}{\tau_3(\mathscr{E})} + \cdots \qquad (1.2.27)$$

and it is this total $\tau(\mathscr{E})$ which is used in Eqs. (1.2.25) and (1.2.26). As explained before, one of the important mechanisms in GaAs for $T > 100$ K, polar optical-phonon scattering, cannot be described in terms of a true relaxation time. However, as we will show later, there are approximations for the polar optical-phonon term which work sufficiently well in most situations.

1.2.2 Hall effect, physical magnetoresistance

The sample geometry for a Hall-effect experiment was illustrated in Fig. 1.1.1, in which it is apparent that no current can flow in the y direction, since only high-impedance voltmeters contact the sides perpendicular to that direction. Thus, $j_y = 0$, and, from Eq. (1.2.21), $E_y = -\sigma_{yx}E_x/\sigma_{yy} = \sigma_{xy}E_x/\sigma_{yy}$. Then, Eq. (1.2.20) gives

$$j_x\big|_{j_y=0} = \sigma_{xx}E_x + \sigma_{xy}\frac{\sigma_{xy}}{\sigma_{yy}}E_x = \frac{\sigma_{xx}^2+\sigma_{xy}^2}{\sigma_{xx}}E_x \qquad (1.2.28)$$

The Hall coefficient is defined as in Eq. (1.1.1):

$$R_H = \frac{E_y}{j_xB}\bigg|_{j_y=0} = \frac{1}{B}\frac{\sigma_{xy}/\sigma_{yy}}{(\sigma_{xx}^2+\sigma_{xy}^2)/\sigma_{xx}} = \frac{1}{B}\frac{\sigma_{xy}}{\sigma_{xx}^2+\sigma_{xy}^2} \qquad (1.2.29)$$

We will now evaluate Eqs. (1.2.28) and (1.2.29) for several cases, including the dependences of j_x and R_H on energy and magnetic-field strength as outlined in Table 1.2.1.

Table 1.2.1 Various cases for τ and B

	τ		B		
Case	dep. on $\mathscr{E}$	indep. of $\mathscr{E}$	0	low $(\omega_c\tau \ll 1)$	high $(\omega_c\tau \gg 1)$
1.2.2.1		×	×	×	×
1.2.2.2	×		×		
1.2.2.3	×			×	
1.2.2.4	×				

.2.2.1 Energy-independent τ; arbitrary B

'or this case

$$\sigma_{xx} = \frac{ne^2}{m^*}\left\langle\frac{\tau}{1+\omega_c^2\tau^2}\right\rangle \rightarrow \frac{ne^2}{m^*}\frac{\tau}{1+\omega_c^2\tau^2} \qquad (1.2.30)$$

$$\sigma_{xy} = -\frac{ne^2}{m^*}\left\langle\frac{\omega_c\tau^2}{1+\omega_c^2\tau^2}\right\rangle \rightarrow -\frac{ne^2}{m^*}\frac{\omega_c\tau^2}{1+\omega_c^2\tau^2} \qquad (1.2.31)$$

'hen, j_x and R_H are given by Eqs. (1.2.20) and (1.2.21) respectively:

$$j_x = \frac{\sigma_{xx}^2+\sigma_{xy}^2}{\sigma_{xx}}E_x = \frac{ne^2}{m^*}\frac{\tau^2+\omega_c^2\tau^4}{\tau(1+\omega_c^2\tau^2)}E_x = \frac{ne^2\tau}{m^*}E_x$$

$$= \sigma E_x = ne\mu E_x \qquad (1.2.32)$$

$$R_H = \frac{1}{B}\frac{\sigma_{xy}}{\sigma_{xx}^2+\sigma_{xy}^2} = -\frac{1}{B}\frac{m^*}{ne^2}\frac{\omega_c\tau^2(1+\omega_c^2\tau^2)}{\tau^2+\omega_c^2\tau^4} = -\frac{1}{B}\frac{m^*\omega_c}{ne^2}$$

$$= -\frac{1}{ne} \qquad (1.2.33)$$

Equation (1.2.32) shows that there is no magnetoresistance (i.e. j_x is ndependent of B) no matter how large B is, if τ is independent of energy. This result is well known, and easily understood in terms of the Lorenz 'orce acting on electrons which all have the same velocity ($v_x = (e\tau/m^*)E_x$). n that case, the Hall field E_y can exactly balance the $\mathbf{v}\times\mathbf{B}$ force on each of he electrons and maintain their motion straight across the sample (dis-egarding the helical motion, of course). Therefore, there is no extra ength of travel, and so no extra resistance due to the magnetic field. The Hall coefficient, given by Eq. (1.2.33), also has a very simple form, $R_H = -1/ne$, which is independent of magnetic-field strength.

Before going on, it is instructive to consider the expected magnitudes of he various quantites in Eqs. (1.2.32) and (1.2.33). Here we will employ aboratory units, which are related to the more standard MKS units by the elationships given in Table 1.1.1. As an example, very pure, n-type, epitaxial GaAs will typically have values $n \simeq 10^{14}\,\mathrm{cm}^{-3}$ and $\mu \simeq 8\times 10^3\,\mathrm{cm}^2/\mathrm{V\text{-}s}$, at 300 K, giving $\sigma \simeq 0.13\,\Omega^{-1}\,\mathrm{cm}^{-1}$. For such samples, it is usual to use an electric field E_x of about 0.1 V/cm, so that $j_x \simeq 13\,\mathrm{mA/cm}^2$. (At very low temperatures, say $T < 20$ K, the field must be kept much lower o avoid impact ionization of the shallow donors.) The Hall coefficient R_H 'or this example is $R_H \simeq -6\times 10^4\,\mathrm{cm}^3$/coulomb. As a second example, at he high end of the concentration range, we consider a sample having $n \simeq 10^{20}\,\mathrm{cm}^{-3}$, with a corresponding mobility, $\mu \simeq 10^3\,\mathrm{cm}^2/\mathrm{V\text{-}s}$. In this case, $\sigma \simeq 1.6\times 10^4\,\Omega^{-1}\,\mathrm{cm}^{-1}$, $R_H \simeq 6\times 10^{-2}\,\mathrm{cm}^3$/coulomb, and $j_x \simeq 1.6\,\mathrm{A/cm}^2$ for $E_x \simeq 0.1$ V/cm, which may cause sample heating. At the other end of the concentration range, we consider Cr-doped GaAs, which has $n \simeq 10^6\,\mathrm{cm}^{-3}$ and $\mu \simeq 4\times 10^3\,\mathrm{cm}^2/\mathrm{V\text{-}s}$, giving $\sigma \simeq 6\times 10^{-10}\,\Omega^{-1}\,\mathrm{cm}^{-1}$, $R_H \simeq 6\times$

$10^{12}\,\mathrm{cm}^3$/coulomb, and $j_x \simeq 6\times 10^{-11}\,\mathrm{A/cm}^2$ for $E_x = 0.1$ V/cm. Clearly, there is a wide range of possible σ and R_H values for n-type GaAs. For p-type material, a similar range exists, except that the mobilities are typically less by an order of magnitude.

The drift velocity is given by $v_x \simeq \mu E_x$, or $v_x \simeq 8\times 10^2$ cm/s, for $\mu \simeq 8000\,\mathrm{cm}^2/\mathrm{V\text{-}s}$ and $E_x \simeq 0.1$ V/cm. This velocity is much less than the mean thermal velocity, $v_{th} \simeq \sqrt{(8kT/\pi m^*)} \simeq 4\times 10^7$ cm/s, since $m^* \simeq 0.066 m_e$ for electrons in GaAs. However, if E_x approaches 10^3–10^4 V/cm, then $v_x \simeq v_{th}$, and the whole theory will break down since the energy, relaxation time, and other quantites will depend upon E_x. The validity of the theory also depends on the magnitude of $\omega_c\tau$. For $\mu \simeq 8000\,\mathrm{cm}^2/\mathrm{V\text{-}s}$, $\tau \simeq m^*\mu/e \simeq 3\times 10^{-13}$ s, and for $B \simeq 10^4 G$, $\omega_c \simeq 2.6\times 10^{12}$/s, so that $\omega_c\tau \simeq 0.8$. When $\omega_c\tau \gtrsim 1$, the transport will require a full quantum-mechanical treatment, at least for low temperatures. At higher temperatures the present theory is evidently valid for nondegenerate electrons as long as $kT \gg \hbar\omega_c$, or $T > 20$ K in GaAs, if $B = 10^4$ G. For highly degenerate electrons the condition for validity would be $(\mathscr{E}_F - \mathscr{E}_C) \gg \hbar\omega_c$ (Beer, 1963).

1.2.2.2 Energy-dependent τ; $B = 0$

For this case, i.e., $\omega_c = 0$, the definitions of σ_{xx} and σ_{xy} in Eqs. (1.2.20) and (1.2.21) give $\sigma_{xx} = ne^2\langle\tau\rangle/m^*$ and $\sigma_{xy} = -ne^2\omega_c\langle\tau^2\rangle/m^*$; here we cannot let $\omega_c = eB/m^* = 0$, because the Hall coefficient includes division by B. With these values of σ_{xx} and σ_{xy}, Eqs. (1.2.32) and (1.2.33) yield

$$j_x = \left.\frac{\sigma_{xx}^2+\sigma_{xy}^2}{\sigma_{xx}}E_x\right|_{B\to 0} = \sigma_{xx}E_x = \frac{ne^2\langle\tau\rangle}{m^*}E_x \qquad (1.2.34)$$

$$R_H = \left.\frac{1}{B}\frac{\sigma_{xy}}{\sigma_{xx}^2+\sigma_{xy}^2}\right|_{B\to 0} = -\frac{1}{ne}\frac{\langle\tau^2\rangle}{\langle\tau\rangle^2} \equiv -\frac{r}{ne} \qquad (1.2.35)$$

Equation (1.2.34) leads to the 'standard' definition of μ for cases in which a relaxation time can be defined; i.e. since $\sigma = ne\mu$, μ must be given by

$$\mu = \frac{e\langle\tau\rangle}{m^*} \qquad (1.2.36)$$

Furthermore, Eq. (1.2.35) gives the 'standard' definition of r, the Hall factor; i.e. $r = \langle\tau^2\rangle/\langle\tau\rangle^2$. If $\tau \propto \mathscr{E}^{-s}$, then for non-degenerate electrons, as shown in Eqs. (1.2.25) and (1.2.26), r can be written

$$r = \frac{\langle\tau^2\rangle}{\langle\tau\rangle^2} = \frac{\Gamma(\frac{5}{2})\Gamma(\frac{5}{2}-2s)}{[\Gamma(\frac{5}{2}-s)]^2} \qquad (1.2.37)$$

As an example, consider acoustic-mode deformation-potential scattering, for which $s = \frac{1}{2}$; then $r = 3\pi/8 = 1.18$. The largest possible value of r would occur for ionized-impurity scattering, for which $s = \frac{3}{2}$; in that case, $r = 315\pi/512 = 1.93$. In practice, however, there is always a mixture of

cattering mechanisms, and r is almost always much less than 1.93. This fact s illustrated in Fig. 1.2.1, which shows r as a function of temperature for a

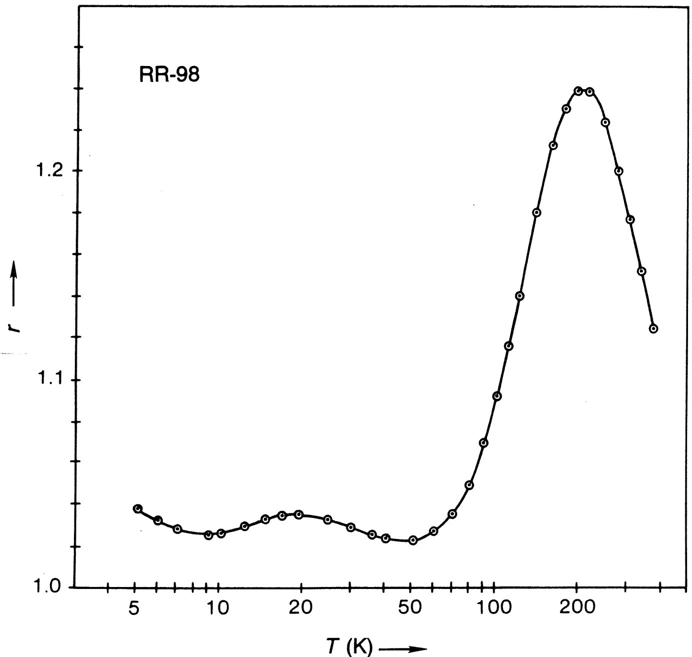

Fig. 1.2.1 The electron Hall r-factor vs. temperature T for a relatively pure, epitaxial, GaAs layer. (Sample RR-98, also shown in Figs. 1.4.6 and 1.4.7)

ure, epitaxial GaAs layer. Here r was calculated by a numerical technique Rode, 1970; Nag, 1980) in order to properly take account of polar ptical-mode phonon scattering, for which a relaxation time cannot be lefined in the usual sense. Impurity scattering dominates the mobility below bout 70 K for this sample, and yet r varies only between 1.02 and 1.23 over he whole range of temperature. In the case of highly doped samples, for vhich impurity scattering may dominate at much higher temperatures, the lectrons will probably be degenerate, in which case

$$r = \langle \tau^2(\mathscr{E}_F) \rangle / \langle \tau(\mathscr{E}_F) \rangle^2 = \tau^2(\mathscr{E}_F)/\tau^2(\mathscr{E}_F) = 1.$$

n Fig. 1.2.2 (Sizelove and Look, 1988), r is plotted as a function of n_H and compensation factor, N_I/n_H, at 77.2 K, an important temperature for haracterization purposes. Indeed, $r \to 1$ at high n_H for all compensation actors, and never exceeds 1.42. In fact, over this same range of $n_H(1 \times 10^{12}$ o $1 \times 10^{18}\ \mathrm{cm}^{-3})$ and N_I/n_H (1 to 10), the theoretical r varies only from 1.02 o 1.26 at 300 K, from 1.00 to 1.42 at 77 K, and from 1.00 to 1.74 at 10 K Sizelove and Lo 1988). Thus, the assumption that $r = 1.2 \pm 0.2$ will

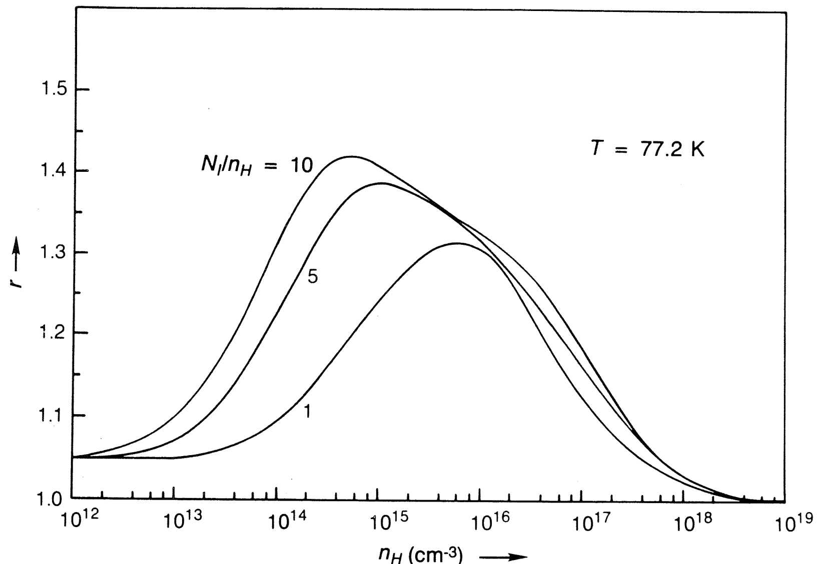

Fig. 1.2.2 The 77.2 K, low-field, electron Hall r-factor vs. Hall concentration n_H at different compensation ratios N_I/n_H. (After Sizelove and Look (1988). Reproduced by permission of the American Institute of Physics)

cover most cases of interest in GaAs, at least for $T \gtrsim 77$ K, and even the assumption $r = 1$ will not give grossly inaccurate results.

For holes, the situation is not quite as clear, since the degenerate valence bands make accurate calculations much more difficult. A first-order approximation can be obtained by treating the two bands (light-hole and heavy-hole bands) as decoupled, each with an isotropic effective mass, and then combining their individual conductivities and Hall coefficients by using the two-band mixed-conductivity formulas (Appendix B, Eqs. (B.2.3) and (B.2.4)). Such a calculation gives r factors at 300 K which can be greater than 2 for relatively pure materials, as displayed in Fig. 1.2.3 (Lee and Look, 1983). A more accurate calculation, taking into account the energy-band structure in the $\mathbf{k} \cdot \mathbf{p}$ approximation, also predicts that $r \simeq 2$ for pure material at 300 K (Takeda *et al.*, 1985). Thus, it appears that the usual assumption $r = 1$ can lead to greater errors for hole conduction than electron conduction.

1.2.2.3 *Energy-dependent τ; low B*

We define 'low B' by the inequality $\omega_c \tau \ll 1$. Then the quantities σ_{xx} and σ_{yy} can be expanded to first order in $\omega_c^2\tau^2$ or $\omega_c^3\tau^3$:

$$\sigma_{xx} = \frac{ne^2}{m^*}\left\langle \frac{\tau}{1+\omega_c^2\tau^2} \right\rangle \to \frac{ne^2}{m^*}\{\langle\tau\rangle - \omega_c^2\langle\tau^3\rangle\} \qquad (1.2.38)$$

$$\sigma_{xy} = -\frac{ne^2}{m^*}\left\langle \frac{\omega_c\tau^2}{1+\omega_c^2\tau^2} \right\rangle \to -\frac{ne^2\omega_c}{m^*}\{\langle\tau^2\rangle - \omega_c^2\langle\tau^4\rangle\} \qquad (1.2.39)$$

ourse, as mentioned before, polar optical-mode scattering cannot be ncluded here since a relaxation time cannot be defined in a simple way. ince this mechanism is important in GaAs at 300 K, the experimental alues given in the table are not necessarily expected to be near any of the heoretical values.

We should mention here that most references (e.g., Putley, 1960) state hat, to order $\omega_c^2\tau^2$, the quantity $\Delta R/R_0$ vanishes, in contrast to the result in Eq. (1.2.45). While technically correct, this statement is somewhat misleading, because R has a factor B in the denominator, and thus should be xpanded to order $\omega_c^3\tau^3 \propto B^3$, as we have done, in order to get B^2 terms in he final answer. In fact, the coefficient $(\beta - 2\xi)$ does not vanish and can be elatively large, as seen in Table 1.2.2.

It should also be noted that, for *degenerate* materials, the coefficients ξ nd β do vanish, since $\langle\tau^n\rangle = \tau^n(\mathscr{E}_F)$, a constant, in this case. Thus, for $n \gtrsim 10^{17}\,\mathrm{cm}^{-3}$ or so, there should be no magnetoresistance or magneto-Hall ffect, in the low-field limit. If such effects are not small, experimentally, hen the sample is probably inhomogeneous.

1.2.2.4 *Energy-dependent τ; high B*

High B is defined by the relationship $\omega_c\tau \gg 1$, although the inequality $\hbar\omega_c \ll kT$ also must hold. In this case, σ_{xx} and σ_{xy} become

$$\sigma_{xx} = \frac{ne^2}{m^*}\left\langle\frac{\tau}{1+\omega_c^2\tau^2}\right\rangle \to \frac{ne^2}{m^*}\frac{\langle\tau^{-1}\rangle}{\omega_c^2} \tag{1.2.48}$$

$$\sigma_{xy} = -\frac{ne^2}{m^*}\left\langle\frac{\omega_c\tau^2}{1+\omega_c^2\tau^2}\right\rangle \to -\frac{ne^2}{m^*}\frac{1}{\omega_c} \tag{1.2.49}$$

so that

$$\sigma = \frac{\sigma_{xx}^2+\sigma_{xy}^2}{\sigma_{xx}} \to \frac{ne^2}{m^*}\frac{\langle\tau^{-1}\rangle^2/\omega_c^4 + 1/\omega_c^2}{\langle\tau^{-1}\rangle/\omega_c^2} \to \frac{ne^2}{m^*}\frac{1}{\langle\tau^{-1}\rangle} \tag{1.2.50}$$

$$R = \frac{1}{B}\frac{\sigma_{xy}}{\sigma_{xx}^2+\sigma_{xy}^2} \to -\frac{1}{B}\frac{m^*}{ne^2}\frac{1/\omega_c}{\langle\tau^{-1}\rangle^2/\omega_c^4 + 1/\omega_c^2} \to -\frac{1}{B}\frac{m^*\omega_c}{ne^2} = -\frac{1}{ne} \tag{1.2.51}$$

Thus, σ approaches a constant σ_∞ in high magnetic fields, and the ratio σ_0/σ_∞ is given by

$$\frac{\sigma_0}{\sigma_\infty} = \frac{\rho_\infty}{\rho_0} = \langle\tau\rangle\langle\tau^{-1}\rangle \equiv \gamma = \frac{\Gamma(\frac{5}{2}+s)\Gamma(\frac{5}{2}-s)}{[\Gamma(\frac{5}{2})]^2} \tag{1.2.52}$$

Representative values of γ are given in Table 1.2.2. This *saturation* of σ at high B is seldom observed in practice, although the initial decrease of σ with B at low fields, predicted by Eq. (1.2.44), is nearly always seen.

The value of $R = -1/ne$ at high fields is independent of any energy averaging, a result which is in fact quite general, and holds for arbitary band structure, scattering mechanisms, and degeneracy as long as the material is isotropic and spin-dependent scattering is excluded (Rode *et al.*, 1983). Thus, very accurate values of n can be determined by making $\omega_c\tau = \mu B \gg 1$ (MKS units). For pure GaAs at 77 K, it is possible to have $\mu > 2\times 10^5\,\mathrm{cm^2/V\text{-}s} = 20\,\mathrm{m^2/V\text{-}s}$, so that a moderate field of $10\,\mathrm{kG} = 1\,\mathrm{T}$ gives $\mu B > 20$ (MKS units). However, it would take a much larger magnetic field to make $\mu B \gg 1$ for holes, since the mobilities are an order of magnitude lower.

1.2.3 Geometric magnetoresistance (GMR)

The normal Hall-bar configuration is long and narrow (Fig. 1.1.2a), in order to maximize the Hall field (E_y) in the middle of the sample, and the boundary condition for analysis is $j_y = 0$. However, it is also advantageous at times to use a configuration which is short and wide (Fig. 1.1.2b), which has a nearly vanishing Hall field, i.e. $E_y \simeq 0$, because of the shorting effects of the large-area contacts. For such a case, the current analysis is particularly simple:

$$j_x = \sigma_{xx}E_x = \frac{ne^2}{m^*}\left\langle\frac{\tau}{1+\omega_c^2\tau^2}\right\rangle E_x \tag{1.2.53}$$

Here $R_H = 0$, of course, but we can examine σ under the same conditions as before:

1.2.3.1 *Energy-independent τ*

If $\tau \neq \tau(\mathscr{E})$, then

$$\sigma_{\mathrm{GMR}} = \frac{ne^2}{m^*}\left\langle\frac{\tau}{1+\omega_c^2\tau^2}\right\rangle \to \frac{ne^2}{m^*}\frac{\tau}{1+\omega_c^2\tau^2} = \frac{ne\mu}{1+\mu^2B^2} = \frac{\sigma_0}{1+\mu^2B^2} \tag{1.2.54}$$

From Eq. (1.2.54) we get an extremely useful relationship, which will be discussed later:

$$\mu = \frac{1}{B}\left[\frac{\sigma_0}{\sigma} - 1\right]^{1/2} \tag{1.2.55}$$

1.2.3.2 *Energy-dependent τ; $B = 0$*

For this case

$$\sigma_{\mathrm{GMR}} = \frac{ne^2}{m^*}\left\langle\frac{\tau}{1+\omega_c^2\tau^2}\right\rangle \to \frac{ne^2\langle\tau\rangle}{m^*} = ne\mu$$

Note here that if n is known from another experiment, e.g., capacitance–voltage, then the *conductivity* mobility can be determined by a simple

measurement of current and parallel voltage. However, if the voltage is measured at the terminals, then contact resistance must also be considered in the analysis.

1.2.3.3 Energy-dependent τ; low B

Here we let $\omega_c\tau \ll 1$ so that

$$\begin{aligned}\sigma_{GMR} &= \frac{ne^2}{m^*}\left\langle\frac{\tau}{1+\omega_c^2\tau^2}\right\rangle \to \frac{ne^2}{m^*}\{\langle\tau\rangle - \omega_c^2\langle\tau^3\rangle\} \\ &= \frac{ne^2}{m^*}\langle\tau\rangle\left\{1 - \frac{e^2B^2\langle\tau\rangle^2}{(m^*)^2}\frac{\langle\tau^3\rangle}{\langle\tau\rangle^3}\right\} \\ &= ne\mu\{1-\xi_{GMR}\mu^2B^2\} \\ &= \sigma_0\{1-\xi_{GMR}\mu^2B^2\} \end{aligned} \tag{1.2.56}$$

where the *geometric* magnetoresistance coefficient ξ_{GMR} is given by

$$\xi_{GMR} = \frac{\langle\tau^3\rangle}{\langle\tau\rangle^3} = \frac{\Gamma(\frac{5}{2}-3s)[\Gamma(\frac{5}{2})]^2}{[\Gamma(\frac{5}{2}-s)]^3} \tag{1.2.57}$$

(Note that in some references ξ_{GMR} is defined as $\xi_{GMR} = \langle\tau^3\rangle/\langle\tau\rangle^3 - 1$.) The name for this phenomenon is derived from the fact that its difference from the 'usual' magnetoresistance is due to the 'geometry' of the situation, i.e., Fig. 1.1.2(b) as opposed to Fig. 1.1.2(a); the former case is generally called the 'physical' magnetoresistance (PMR). However, the GMR is usually a much larger effect; as an extreme example, for degenerate electrons, $\xi_{GMR} = 1$ while $\xi_{PMR} = 0$. In analogy to Eq. (1.2.44), $\Delta\rho/\rho_0$ for this case becomes

$$\left(\frac{\Delta\rho}{\rho_0}\right) \simeq \xi_{GMR}\mu^2B^2 \tag{1.2.58}$$

1.2.3.4 Energy-dependent τ; high B

If $\omega_c\tau \gg 1$, then

$$\sigma_{GMR} = \frac{ne^2}{m^*}\left\langle\frac{\tau}{1+\omega_c^2\tau^2}\right\rangle \to \frac{ne^2\langle\tau^{-1}\rangle}{m^*} = \frac{\sigma_0}{\mu^2B^2}\langle\tau\rangle\langle\tau^{-1}\rangle$$

which suggests that $\sigma_{GMR} \to 0$ as $B \to \infty$. Thus, σ_{GMR} is not a very useful quantity at high B.

1.2.3.5 Structures for GMR measurements

A commonly used structure of the past which satisfies the GMR boundary condition of a vanishing Hall field is the Corbino disk, in which current is passed from a po[illegible] contact in the center to a concentric contact on the periphery (see, e.g., Wieder, 1979). In this case, the boundary condition is $E_\phi = 0$, where ϕ is the azimuthal coordinate. A presently popular structure, however, is the field-effect transistor, which has the shape of Fig. 1.1.2(b). The utility of this latter structure is that mobility can be measured in an actual device. Chapter 2 will discuss this phenomenon in greater detail.

1.2.4 Definitions of various mobilities

Up to now, in this chapter, we have introduced four different 'mobilities', and it is perhaps useful to review and compare them. They are: the conductivity mobility (Eq. (1.2.36)); the Hall mobility (from Eq. (1.2.37)); the physical-magnetoresistance mobility (from Eqs. (1.2.41) and (1.2.42)); and the geometric-magnetoresistance mobility (from Eqs. (1.2.56) and (1.2.57)). The definitions are:

$$\mu = \frac{e\langle\tau\rangle}{m^*} \tag{1.2.59}$$

$$\mu_H = \frac{e\langle\tau\rangle}{m^*}\frac{\langle\tau^2\rangle}{\langle\tau\rangle^2} = r\mu \tag{1.2.60}$$

$$\mu_{PMR} = \frac{e\langle\tau\rangle}{m^*}\frac{\langle\tau^2\rangle}{\langle\tau\rangle^2}\left\{\frac{\langle\tau^3\rangle\langle\tau\rangle}{\langle\tau^2\rangle^2} - 1\right\}^{1/2} = \xi^{1/2}r\mu = \xi^{1/2}\mu_H \tag{1.2.61}$$

$$\mu_{GMR} = \frac{e\langle\tau\rangle}{m^*}\left\{\frac{\langle\tau^3\rangle}{\langle\tau\rangle^3}\right\}^{1/2} = \xi_{GMR}^{1/2}\mu \tag{1.2.62}$$

Each of these mobilities is measured by a totally different experiment, but they are related to each other in clearly defined ways, as shown above. For degenerate materials, i.e. $\tau = \tau(\mathscr{E}_F)$, a constant, it is the easily seen that $\mu_H = \mu_{GMR} = \mu$, but that $\mu_{PMR} = 0$. Thus, μ_{PMR} is not a very useful quantity for characterization purposes. The most widely measured mobility, by far, is μ_H, and thus the magnitude of the Hall factor r is of great interest. It is typically calculated, but sometimes can be measured, by the relationship $r = R_0/R_\infty$. Fortunately, r as well as ξ_{GMR} are usually close to unity in GaAs, even for nondegenerate materials, so that both μ_H and μ_{GMR} are quite useful as definitions of mobility.

1.2.5 Mixed conductivity: multi-band effects

Our discussion thus far has assumed that the electrical current is carried by electrons (or holes) in only one band. However, this is often not the case, and effects due to at least three conduction bands and two valence bands have been seen in GaAs. For example, multi-band effects must always be considered in GaAs at high temperatures, $T \gtrsim 600$ K (Nichols *et al.*, 1980; Saxena *et al.*, 1984; Hunter *et al.*, 1984) and high pressures, P [illegible] GPa =

) kbars (Patel *et al.*, 1986), but also, at all temperatures in semi-insulating aAs with $\rho \gtrsim 5 \times 10^8$ Ω-cm (Look, 1980). The latter problem has been udied in great detail: Inoue and Ohyama (1970), Philadelpheus and uthymiou (1974), Look (1975), Lindquist (1977), Zucca (1977), Betko and Ierinsky (1979), Haloulos *et al.* (1980), Martin (1980), Look (1980), Vinter *et al.* (1982), Hrivnak *et al.* (1982), Look (1983), Betko and Ierinsky (1986), Fornari (1986), Hrivnak (1987), and Pistoulet and Iamamdjian (1987). Because of the significance of multi-band conduction ı GaAs, most of the relevant formulas are derived here; however, only a w of the more important ones will be covered in this section, with the rest iscussed in Appendix B.

.2.5.1 *Two-band conduction: electrons and holes*

t moderate temperatures, pressures, and electric fields, usually only two ands carry the current in GaAs. Electrons are mainly situated in the lowest Γ_{6c}) conduction band, and holes in the highest (Γ_{8v}) degenerate valence ands. The electrons can be well represented by a single, isotropic effective ıass, and we will also assume that the holes can be thus represented, in pite of the fact that the two degenerate valence bands have different ıasses. The total currents are then given by

$$j_x = j_{nx} + j_{px} = (\sigma_{nxx} + \sigma_{pxx})E_x + (\sigma_{nxy} + \sigma_{pxy})E_y \qquad (1.2.63)$$

$$j_y = j_{ny} + j_{py} = (\sigma_{nyx} + \sigma_{pyx})E_x + (\sigma_{nyy} + \sigma_{pyy})E_y \qquad (1.2.64)$$

here the σ_{nij} are given by Eqs. (1.2.20)–(1.2.21) and the σ_{pij} are found by tting $e \to -e$ and $n \to p$. The total conductivity and Hall coefficient are ıen determined by the same boundary conditions as before:

$$\sigma|_{\text{Hall-bar}} = \frac{j_x}{E_x}\bigg|_{j_y=0} = \frac{(\sigma_{nxx} + \sigma_{pxx})^2 + (\sigma_{nxy} + \sigma_{pxy})^2}{(\sigma_{nxx} + \sigma_{pxx})} \qquad (1.2.65)$$

$$R|_{\text{Hall-bar}} = \frac{E_y}{j_x B}\bigg|_{j_y=0} = \frac{1}{B}\frac{(\sigma_{nxy} + \sigma_{pxy})}{(\sigma_{nxx} + \sigma_{pxx})^2 + (\sigma_{nxy} + \sigma_{pxy})^2} \qquad (1.2.66)$$

$$\sigma_{\text{GMR}} = \frac{j_x}{E_x}\bigg|_{E_y=0} = (\sigma_{nxx} + \sigma_{pxx}) \qquad (1.2.67)$$

Ve consider these quantities for various τ and B conditions below.

.2.5.1.1 *Energy-independent τ; arbitrary B.* In Appendix B it is shown hat if $\tau \neq \tau(\mathscr{E})$, then Eqs. (1.2.65) and (1.2.66) yield, respectively,

$$\sigma = \frac{(\sigma_n + \sigma_p)^2 + \sigma_n^2\sigma_p^2(R_n + R_p)^2B^2}{(\sigma_n + \sigma_p) + \sigma_n\sigma_p(\sigma_n R_n^2 + \sigma_p R_p^2)B^2} \qquad (1.2.68)$$

$$R = \frac{\sigma_n^2 R_n + \sigma_p^2 R_p + \sigma_n^2\sigma_p^2 R_n R_p(R_n + R_p)B^2}{(\sigma_n + \sigma_p)^2 + \sigma_n^2\sigma_p^2(R_n + R_p)^2B^2} \qquad (1.2.69)$$

where $\sigma_n = ne\mu_n$, $\sigma_p = pe\mu_p$, $R_n = -1/ne$, and $R_p = 1/pe$. (Note that, for convenience, we have dropped the subscript '0' on σ_n, σ_p, R_n and R_p.) These equations can be put into the form

$$\frac{1}{B^2} + \mu_n^2 Y = S_{\rho m}\frac{\rho_0}{\Delta\rho} = -S_{Rm}\frac{R_0}{\Delta R} \qquad (1.2.70)$$

where

$$\mu_n^2 Y = \frac{\sigma_n^2\sigma_p^2(R_n + R_p)^2}{(\sigma_n + \sigma_p)^2} = \frac{\mu_n^2(c-1)^2}{(1+bc)^2} \qquad (1.2.71)$$

Here, $b = \mu_n/\mu_p$ and $c = n/p$. The quantities $S_{\rho m}$ and S_{Rm} are found experimentally from the slopes of $1/B^2$ vs. $\rho_0/\Delta\rho$ and $1/B^2$ vs. $-R_0/\Delta R$ plots, respectively; they are related to the σ_i and R_i by Eqs. (B.1.21) and (B.1.23) in Appendix B. The 'm' in the subscripts stands for 'mixed' because the fact that the magnetoresistance and magneto-Hall effect exist at all when τ is independent of energy is due to the simultaneous presence of electrons and holes. That is, the Hall field E_y cannot *simultaneously* balance the magnetic-field forces ($\mathbf{v} \times \mathbf{B}$) on both electrons and holes. Thus, the path lengths from contact to contact are increased, which increases the resistance.

Note that we have four experimental quantities, R_0, σ_0, $S_{\rho m}$, and S_{Rm}, and four unknowns, n, p, μ_n, and μ_p. By algebraic manipulation, it is possible to exactly invert the equations to get n, p, μ_n and μ_p in terms of R_0, σ_0, $S_{\rho m}$, and S_{Rm}. The final results are listed in Eqs. (B.1.43)–(B.1.50) of Appendix B. For example,

$$\mu_n = \frac{1 + \beta^{-1}}{1 - b^{-1}}(-R_0\sigma_0) \qquad (1.2.72)$$

where $\beta = S_{\rho m}/S_{Rm}$. The assumption here, namely that all of the magnetic-field dependence is due to mixed-conductivity effects, is most accurate for SI GaAs with ρ near the maximum resistivity, i.e., $\rho \gtrsim 10^9$ Ω-cm. For lower resistivities, single-carrier magnetic-field effects become quite important (Betko and Merinsky, 1979; Look, 1980).

When $B = 0$ Eqs. (1.2.68) and (1.2.69) reduce to the familiar equations:

$$\sigma = \sigma_n + \sigma_p = e(n\mu_n + p\mu_p) \qquad (1.2.73)$$

$$R = \frac{\sigma_n^2 R_n + \sigma_p^2 R_p}{(\sigma_n + \sigma_p)^2} = \frac{-n\mu_n^2 + p\mu_p^2}{e(n\mu_n + p\mu_p)^2} \qquad (1.2.74)$$

where it is seen that R can vanish when $n\mu_n^2 = p\mu_p^2$. This phenomenon is illustrated in Fig. 1.2.4 (Look, 1975), in which the relative values of n, p, μ_n, and μ_p in Cr-doped GaAs are varied as a function of temperature. Since $\mu_n^2/\mu_p^2 \simeq 100$, the zero should occur when $p \simeq 100n$. Changes in the sign of R are much more commonly observed in low-bandgap semiconductors, such as InSb and $Hg_xCd_{1-x}Te$.

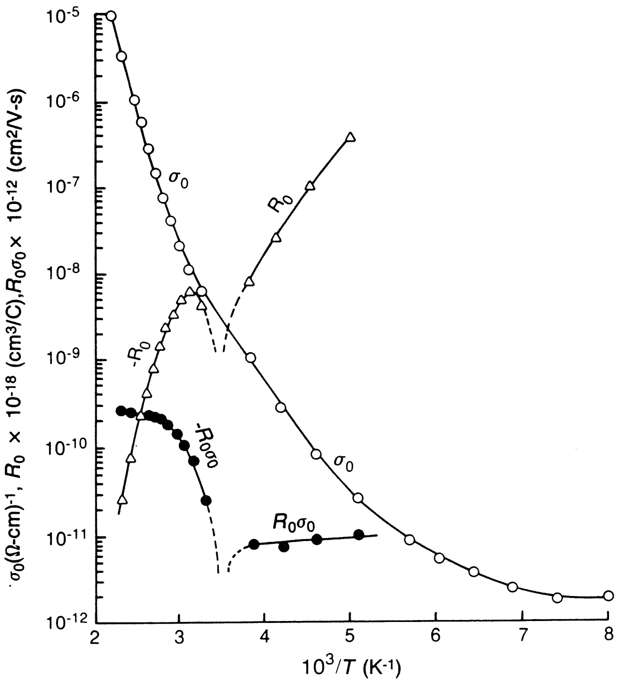

Fig. 1.2.4 The zero-field Hall coefficient R_0 and conductivity σ_0 and their product $R_0\sigma_0 \equiv \mu_H$, as a function of inverse temperature T^{-1}, for a Cr-doped, semi-insulating GaAs sample. The effects of mixed conductivity are clearly seen in the sign change of R_0. (After Look (1975). Reproduced by permission of Pergamon Press)

1.2.5.1.2 Energy-dependent τ; low B. For this case, the σ_{ixx} terms are expanded to order $\omega_{ci}^2\tau_i^2$, and the σ_{ixy} terms to order $\omega_{ci}^3\tau_i^3$. Then, it is shown in Appendix B that $\Delta\rho/\rho_0$ and $\Delta R/R_0$ are given by

$$\frac{\Delta\rho}{\rho_0} = \left[\frac{\sigma_n\sigma_p(R_n\sigma_n - R_p\sigma_p)^2}{(\sigma_n+\sigma_p)^2} + \frac{\xi_n R_n^2\sigma_n^3 + \xi_p R_p^2\sigma_p^3}{(\sigma_n+\sigma_p)}\right]_0 B^2$$
$$= \left[\frac{c(\alpha b+1)^2}{\alpha^2 b(1+bc)^2} + \frac{\xi_n bc}{(1+bc)} + \frac{\xi_p}{\alpha^2 b^2(1+bc)}\right]_0 r_{n0}^2\mu_n^2 B^2 \qquad (1.2.75)$$

$$-\frac{\Delta R}{R_0} = \left[\frac{\sigma_n^2\sigma_p^2(R_n+R_p)(R_n\sigma_n - R_p\sigma_p)^2}{(\sigma_n+\sigma_p)^2(R_n\sigma_n^2 + R_p\sigma_p^2)} + \frac{\beta_n R_n^3\sigma_n^4 + \beta_p R_p^3\sigma_p^4}{R_n\sigma_n^2 + R_p\sigma_p^2}\right.$$
$$\left. - \frac{2\xi_n R_n^2\sigma_n^3 + 2\xi_p R_p^2\sigma_p^3}{(\sigma_n+\sigma_p)}\right]_0 B^2$$
$$= \left[\frac{c(1-\alpha c)(1+\alpha b)^2}{\alpha^2(1+bc)^2(\alpha b^2 c - 1)} + \frac{\beta_n \alpha b^2 c}{(\alpha b^2 c - 1)} - \frac{\beta_p}{\alpha^2 b^2(\alpha b^2 c - 1)}\right.$$
$$\left. - \frac{[illegible]bc}{(1+bc)} - \frac{2\xi_p}{\alpha^2 b^2(1+bc)}\right]_0 r_{n0}^2\mu_n^2 B^2 \qquad (1.2.76)$$

where $\alpha = r_n/r_p$, and the subscript '0' means that the quantity inside the brackets is to be evaluated at $B = 0$. It is clear that these equations split cleanly into single-carrier and mixed conductivity terms, the former being those with ξs and βs which were defined before (Eqs. (1.2.42) and (1.2.43) respectively). Again, we can arrange Eqs. (1.2.75) and (1.2.76) in the form:

$$\frac{1}{B^2} = (S_{pm} + S_{ps})\frac{\rho_0}{\Delta\rho} = -(S_{Rm} + S_{Rs})\frac{R_0}{\Delta R} \qquad (1.2.77)$$

where S_{pm}, S_{ps}, S_{Rm}, and S_{Rs} are given in terms of the eight unknowns: n, p, μ_n, μ_p, ξ_n, ξ_p, β_n, and β_p in Eqs. (B.1.21)–(B.1.24). The problem now is that there are four experimental quantities, σ_0, R_0, $S_{pm} + S_{ps}$, and $S_{Rm} + S_{Rs}$, and eight unknowns. Thus, this problem cannot be solved, in general, unless some of the parameters are already known. Other ways of approaching the mixed-conductivity problem are discussed in Appendix B.

1.2.5.1.3 Energy-dependent τ; high B. In this case, $\omega_{cn}\tau_n$ and $\omega_{cp}\tau_p \gg 1$, and we will only quote the $B = \infty$ results, which are derived in Appendix B:

$$\sigma_\infty = \frac{e\mu_n\mu_p(p-n)^2}{n\mu_p\gamma_n + p\mu_n\gamma_p} \qquad (1.2.78)$$

$$R_\infty = \frac{1}{e(p-n)} \qquad (1.2.79)$$

where $\gamma_i = \langle\tau_i\rangle\langle\tau_i^{-1}\rangle$. The result for R_∞ is particularly simple, and has no energy dependence. Since we also know that $n_i^2 = np$, where n_i is the intrinsic carrier concentration, it is always possible to determine n and p separately, if the high-field experiment can be carried out. Furthermore, Eqs. (1.2.73) and (1.2.74) would also give us μ_n and μ_p (to within r_n and r_p factors). Unfortunately, however, the $\omega_{cp}\tau_p \gg 1$ condition is difficult to satisfy, since it requires $B \gg 250$ kG (because $\mu_p \simeq 400$ cm^2/V-s in GaAs).

1.3 SCATTERING THEORY: MOBILITY

In the previous sections, we have discussed ways of determining the mobility from experimental parameters, especially the conducivity and Hall coefficient. We now want to relate the experimental mobility to materials parameters, such as effective mass, dielectric constant, etc. To do this, it is necessary to know what mechanisms cause electron and hole scattering in GaAs and how to calculate scattering rates from the various mechanisms. The general elements of the theory are well covered in many excellent reference works and textbooks (see e.g., Beer, 1963; Putley, 1960; Rode, 1975; Wiley, 1975; Nag, 1980). More recent works have critically examined some of the standard approximations (Meyer and Bartoli, 1985) or offered different approaches (Beck and Anderson, 1987). We will, of course, concentrate on the particular scattering mechanisms of interest i[illegible] As.

The probability of an electron making a transition from wave vector $\mathbf{k}$ to , due to a perturbing potential ΔV, is given by the familiar 'golden rule':

$$T_{\mathbf{kk}'} = \frac{2\pi}{\hbar} |M(\mathbf{k}, \mathbf{k}')|^2 \, \delta(\mathscr{E}_{\mathbf{k}} - \mathscr{E}_{\mathbf{k}'}) \qquad (1.3.1)$$

ıere $\delta(x - x')$ is the Dirac delta function, and M is a matrix element:

$$M(\mathbf{k}, \mathbf{k}') = \int_{\substack{\text{unit}\\ \text{cell}}} \psi^*_{\mathbf{k}'}(\mathbf{r}) \, \Delta V \psi_{\mathbf{k}}(\mathbf{r}) \, \mathrm{d}\mathbf{r} \qquad (1.3.2)$$

which the wave functions are normalized over a unit cell. For defects in a ystal, the scattering event mainly affects the wave function of the electron ɜing scattered, and only insignificantly changes the wave functions of the ttice atoms in the vicinity of the defect. Thus, only the electronic wave nction, given by

$$\psi_{\mathbf{k}}(\mathbf{r}) = U_{\mathbf{k}}(\mathbf{r}) \mathrm{e}^{\mathrm{i}\mathbf{k}\cdot\mathbf{r}} \qquad (1.3.3)$$

ɜed be considered in the expression for $M(\mathbf{k}, \mathbf{k}')$. The perturbing potential ın be expanded in a Fourier series

$$\Delta V = \sum_{\mathbf{q}} A(\mathbf{q}) \mathrm{e}^{\mathrm{i}\mathbf{q}\cdot\mathbf{r}} \qquad (1.3.4)$$

ınce both exp $(\mathrm{i}\mathbf{k} \cdot \mathbf{k})$ and exp $(\mathrm{i}\mathbf{q} \cdot \mathbf{r})$ are periodic functions, the integral in q. (1.3.2) vanishes when $\mathbf{q} = \mathbf{k}' - \mathbf{k}$. Thus,

$$M(\mathbf{k}, \mathbf{k}') = A(\mathbf{k}' - \mathbf{k}) \int U^*_{\mathbf{k}'}(\mathbf{r}) U_{\mathbf{k}}(\mathbf{r}) \, \mathrm{d}\mathbf{r}$$

$$= A(\mathbf{k}' - \mathbf{k}) I(\mathbf{k}, \mathbf{k}') \qquad (1.3.5)$$

here $|I(\mathbf{k}, \mathbf{k}')|$ is often known as the overlap integral.

On the other hand, for lattice scattering the situation is somewhat more ɔmplicated. Here the lattice-atom wave functions will change in the ɔllision process, and must be included in $M(\mathbf{k}, \mathbf{k}')$. The total wave function

$$\chi_{\mathbf{k},n} = \psi_{\mathbf{k}} \prod_{\mathbf{q}} \phi_{\mathbf{q},n} \qquad (1.3.6)$$

'here the $\phi_{\mathbf{q},n}$ are Hermite polynomials, indexed according to the wave ector $\mathbf{q}$ and excitation state n. The perturbing potential in this case can be 'ritten in the form

$$\Delta V = \sum_{\mathbf{q}} A(\mathbf{q}) [a_{\mathbf{q}} \mathrm{e}^{\mathrm{i}\mathbf{q}\cdot\mathbf{r}} + a^{\dagger}_{\mathbf{q}} \mathrm{e}^{-\mathrm{i}\mathbf{q}\cdot\mathbf{r}}] \qquad (1.3.7)$$

'here the $a^{\dagger}_{\mathbf{q}}$ and $a_{\mathbf{q}}$ are the usual creation and annihilation operators, espectively, which change the $\phi_{\mathbf{q},n}$ as follows:

$$a_{\mathbf{q}} \phi_{\mathbf{q},n} = \sqrt{n_{\mathbf{q}}} \, \phi_{\mathbf{q},n-1} \qquad (1.3.8\text{a})$$

$$a^{\dagger}_{\mathbf{q}} \phi_{\mathbf{q},n} = \sqrt{(n_{\mathbf{q}} + 1)} \, \phi_{\mathbf{q},n+1} \qquad (1.3.8\text{b})$$

By substituting Eqs. (1.3.6) and (1.3.7) into Eq. (1.3.2) (where the wave functions are now the $\chi_{\mathbf{k},n}$), and using the rules given by Eq. (1.3.8), the matrix element for lattice scattering becomes

$$M(\mathbf{k}, \mathbf{k}') = A(\mathbf{q}) [n_{\mathbf{q}} + \tfrac{1}{2} \pm \tfrac{1}{2}]^{1/2} I(\mathbf{k}, \mathbf{k}') \qquad (1.3.9)$$

where '+' corresponds to emission of a phonon, and '−' to absorption. Thus, a difference between defect scattering and lattice scattering is the $n_{\mathbf{q}}$ term in the matrix element of the latter. Another difference is that energy conservation requires that $\mathscr{E}_{\mathbf{k}'} \simeq \mathscr{E}_{\mathbf{k}}$ for defect scattering, while the condition is $\mathscr{E}_{\mathbf{k}'} \simeq \mathscr{E}_{\mathbf{k}} \pm \hbar\omega_{\mathbf{q}}$ for lattice scattering, where $\hbar\omega_{\mathbf{q}}$ is the energy of the relevant lattice photon.

So far we have considered only the effects of the perturbing potential ΔV on the free electrons, but the electrons themselves will also affect ΔV by rearranging their local densities to 'screen out' ΔV at large distances. It is possible to show (Section 1.3.1.1) that the effect of this screening is to reduce each Fourier coefficient $A(\mathbf{q})$ by a factor $q^2/(q^2 + 1/\lambda_D^2)$, where $\lambda_D^2 \simeq e^2 n/\epsilon kT$ is the Debye length for free electrons (Nag, 1980). Screening is very important for ionized-impurity scattering, but can largely be neglected for lattice scattering.

The probability $S(\mathbf{k})$ of an electron being scattered from wave vector $\mathbf{k}$ can now be calculated:

$$S(\mathbf{k}) = \frac{V_c}{8\pi^3} \int \frac{2\pi}{\hbar} |M(\mathbf{k}, \mathbf{k}')|^2 \, \delta(\mathscr{E}_{\mathbf{k}} - \mathscr{E}_{\mathbf{k}'}) \, \mathrm{d}\mathbf{k}' \qquad (1.3.10)$$

where V_c is the crystal volume, and $1/(8\pi^3)$ is the density of states in $\mathbf{k}'$ space. (Only half of the *total* density in $\mathbf{k}'$ space is included here since spin must be conserved by all of the scattering mechanisms that we will consider.) Equation (1.3.10) is strictly valid only for nondegenerate electrons since the probability of state $\mathbf{k}'$ being empty is not included in the integral. Note that

$$|M(\mathbf{k}, \mathbf{k}')|^2 \propto |I(\mathbf{k}, \mathbf{k}')|^2 \equiv G(\mathbf{k}, \mathbf{k}') \qquad (1.3.11)$$

where $G(\mathbf{k}, \mathbf{k}')$ is known as the *overlap function*. For parabolic bands, $U_{\mathbf{k}'} \simeq U_{\mathbf{k}}$, so that $G(\mathbf{k}, \mathbf{k}') \simeq 1$, whereas for nonparabolic bands, $G(\mathbf{k}, \mathbf{k}')$ can be rather complicated, as discussed in detail by Nag (1980). For example, the heavy-hole band has an overlap function given by

$$G_{hh}(\mathbf{k}, \mathbf{k}') = \frac{1 + 3\cos^2\theta_k}{4} \qquad (1.3.12)$$

where θ_k is the angle between $\mathbf{k}$ and $\mathbf{k}'$, while the light-hole and split-off-hole bands are significantly more complex. It is this overlap function, among other things, that makes the calculation of scattering rates for holes much more complicated than those for electrons (Costato *et al.*, 1972; Wiley, 1975; Takeda *et al.*, 1985).

Equation (1.3.10) for $S(\mathbf{k})$ is the probability of an electron being scattered ut of a small region $d\mathbf{k}$ around $\mathbf{k}$, whereas there also will be electrons attered *into* $d\mathbf{k}$, from other regions $d\mathbf{k}'$ around $\mathbf{k}'$. The scattering-*out* rate

$$\left[\frac{V_c}{4\pi^3} f(\mathbf{k},\mathbf{r},t)\, d\mathbf{k}\right]\left[\frac{V_c}{8\pi^3}[1-f(\mathbf{k}',\mathbf{r},t)]\, d\mathbf{k}'\right] S(\mathbf{k},\mathbf{k}') \qquad (1.3.13)$$

hereas the scattering-*in* rate is

$$\left[\frac{V_c}{4\pi^3} f(\mathbf{k}',\mathbf{r},t)\, d\mathbf{k}'\right]\left[\frac{V_c}{8\pi^3}[1-f(\mathbf{k},\mathbf{r},t)]\, d\mathbf{k}\right] S(\mathbf{k}',\mathbf{k}) \qquad (1.3.14)$$

he first factor in Eq. (1.3.13) is the number of electrons in $d\mathbf{k}$, and the cond factor is the number of available states in $d\mathbf{k}'$. The difference in the $_c/4\pi^3$ and $V_c/8\pi^3$ factors is that electrons of either spin may be scattered *ut* of a particular region of phase space, but only half of the available states the receiving region, i.e. those with identical spin, are available for -scattering.

The *net* scattering rate *into* $d\mathbf{k}$ is

$$-\frac{V_c}{4\pi^3}\frac{V_c}{8\pi^3}\int_{\mathbf{k}'} [f(1-f')S - f'(1-f)S']\, d\mathbf{k}\, d\mathbf{k}' \qquad (1.3.15)$$

here $f \equiv f(\mathbf{k},\mathbf{r},t)$, $f' \equiv f(\mathbf{k}',\mathbf{r},t)$, $S \equiv S(\mathbf{k},\mathbf{k}')$, and $S' \equiv S(\mathbf{k}',\mathbf{k})$. This uantity must be equal to $(V_c/4\pi^3)\, d\mathbf{k}(\partial f/\partial t)_{\text{coll}}$, so that

$$\left[\frac{\partial f}{\partial t}\right]_{\text{coll}} = -\frac{V_c}{8\pi^3}\int [f(1-f')S - f'(1-f)S']\, d\mathbf{k}' \qquad (1.3.16)$$

We now return to the Boltzmann equation, Eq. (1.2.1), under steady-ate conditions $(\partial f/\partial t = 0)$, and spatial homogeneity $(\nabla_r f = 0)$. If $\mathbf{B} = 0$, ien

$$\dot{\mathbf{k}} \cdot \nabla_k f = \frac{e}{\hbar}\mathbf{E} \cdot \nabla_k f = \left[\frac{\partial f}{\partial t}\right]_{\text{coll}} \qquad (1.3.17)$$

is usual to expand f into a series of Legendre polynomials $P_n(\cos\theta)$ and ien approximate the series with the first two terms. That is,

$$f(\mathbf{k}) = \sum_n f_n(\mathscr{E})P_n(\cos\theta) \simeq f_0(\mathscr{E}) + f_1(\mathscr{E})\cos\theta$$

here θ is the angle between $\mathbf{k}$ and $\mathbf{E}$. By substituting the approximation $= f_0 + f_1\cos\theta$ into Eq. (1.3.17), we may obtain equations for f_0 and f_1. efore doing this, however, we may note that the magnitude of f_1 might be pected to be proportional to E, the driving field, since $f_1 = 0$ if $E = 0$. hus, $f_1 E$ will be of -der E^2, and thus negligible for low electric fields. We

will also ignore $f_1(E)f_1(E')$ terms. With these approximations

$$\left[\frac{\partial f}{\partial t}\right]_{\text{coll}} = -\frac{V_c}{8\pi^3}\int \{[f_0(1-f_0')S - f_0'(1-f_0)S']\, d\mathbf{k}'$$

$$-\frac{V_c}{8\pi^3}\int f_1\cos\theta[1-f_0'+f_0'S'] - f_1'\cos\theta'[1-f_0+f_0S]\}\, d\mathbf{k}' \qquad (1.3.18)$$

But the first integral vanishes because $(\partial f/\partial t)_{\text{coll}} = 0$ if $\mathbf{E} = 0$. Also, we will assume that $S(\mathbf{k},\mathbf{k}') = S(\mathbf{k}',\mathbf{k})$, which implies that $S(\mathbf{k},\mathbf{k}') = S(|\mathbf{k}'-\mathbf{k}|)$. In this case

$$\left[\frac{\partial f}{\partial t}\right]_{\text{coll}} = -\frac{V_c}{8\pi^3}\cos\theta\int S\left[f_1\frac{1-f_0'}{1-f_0} - \frac{\cos\theta'}{\cos\theta}f_1'\frac{f_0}{f_0'}\right] d\mathbf{k}' \qquad (1.3.19)$$

Finally, we note that $\cos\theta'$ can be written

$$\cos\theta' = \cos\theta\cos\theta_k - \sin\theta\sin\theta_k\cos\beta$$

where θ_k is the angle between $\mathbf{k}$ and $\mathbf{k}'$, and β is the angle between the plane containing $\mathbf{k}$ and $\mathbf{k}'$, and the plane containing $\mathbf{k}$ and $\mathbf{E}$. The integration over β from 0 to 2π will cause the terms containing $\cos\beta$ to vanish, so that

$$\left[\frac{\partial f}{\partial t}\right]_{\text{coll}} = -\frac{V_c}{8\pi^3}\cos\theta\int S\left[f_1\frac{1-f_0'}{1-f_0} - \cos\theta_k f_1'\frac{f_0}{f_0'}\right] d\mathbf{k}' \qquad (1.3.20)$$

It is of interest to write Eq. (1.3.20) in a *relaxation-time* form. That is, we set

$$\left[\frac{\partial f}{\partial t}\right]_{\text{coll}} = -\frac{f-f_0}{\tau(\mathscr{E})} = -\frac{f_1\cos\theta}{\tau(\mathscr{E})}$$

which implies that

$$\frac{1}{\tau(\mathscr{E})} = \frac{V_c}{8\pi^3}\int S\left[\frac{1-f_0'}{1-f_0} - \cos\theta_k\frac{f_1'f_0}{f_1f_0'}\right] d\mathbf{k}' \qquad (1.3.21)$$

It is clear that $\tau(\mathscr{E})$ is not a useful concept if $\mathscr{E}' \neq \mathscr{E}$, for then $f_1' \neq f_1$, and τ is a function of the perturbation strength f_1. Thus, for inelastic scattering, the relaxation time is not a useful quantity. In this case, it is necessary to deal with the full Boltzmann equation:

$$\frac{e}{\hbar}\mathbf{E}\cdot\nabla_k f_1(\mathscr{E}) = -\frac{V_c}{8\pi^3}\cos\theta\int S(\mathbf{k},\mathbf{k}')\left[f_1(\mathscr{E})\frac{1-f_0'(\mathscr{E})}{1-f_0(\mathscr{E})}\right.$$

$$\left. - \cos\theta_k f_1'(\mathscr{E}')\frac{f_0(\mathscr{E})}{f_0(\mathscr{E}')}\right] d\mathbf{k}' \qquad (1.3.22)$$

which must be solved for $f_1(\mathscr{E})$ by numerical methods. Such methods are discussed in detail in other works (Rode, 1975; Nag, 1980) and will not be further mentioned in this section.

For elastic scattering, we have $\mathscr{E}' \simeq \mathscr{E}$ so that $f_0(\mathscr{E}') \simeq f_0(\mathscr{E})$, and $f_1(\mathscr{E}') \simeq f_1(\mathscr{E})$. Then Eq. (1.3.21) becomes

$$\frac{1}{\tau(\mathscr{E})} = \frac{V_c}{8\pi^3}\int S(\mathbf{k},\mathbf{k}')(1-\cos\theta_k)\,d\mathbf{k}' \qquad (1.3.23)$$

By comparison with Eq. (1.3.10) we see that

$$\frac{1}{\tau(\mathscr{E})} = \frac{V_c}{8\pi^3}\int \frac{2\pi}{\hbar} A^2(|\mathbf{k}-\mathbf{k}'|)G(\mathbf{k},\mathbf{k}')(1-\cos\theta)\delta(\mathscr{E}_{\mathbf{k}}-\mathscr{E}_{\mathbf{k}'})\,d\mathbf{k}' \qquad (1.3.24)$$

for defect scattering, and

$$\frac{1}{\tau(\mathscr{E})} = \frac{V_c}{8\pi^3}\sum_{+,-}\int \frac{2\pi}{\hbar}\{A^2(|\mathbf{k}-\mathbf{k}'|)G(\mathbf{k},\mathbf{k}')(1-\cos\theta) \times \delta(\mathscr{E}_{\mathbf{k}}-\mathscr{E}_{\mathbf{k}'})(n_{\mathbf{q}}+\tfrac{1}{2}\pm\tfrac{1}{2})\}\,d\mathbf{k}' \qquad (1.3.25)$$

for lattice scattering, where θ_k has been redesignated as θ, and where

$$A(\mathbf{q}) = \frac{1}{V_c}\int \Delta V\, e^{-i\mathbf{q}\cdot\mathbf{r}}\,d\mathbf{r} \qquad (1.3.26)$$

Equations (1.3.24)–(1.3.26) can be solved for the various scattering mechanisms which have a known ΔV. We will solve Eq. (1.3.24) explicitly for one mechanism (ionized-impurity scattering) in order to illustrate the technique, and then simply quote the results for other mechanisms.

1.3.1 Scattering mechanisms in GaAs

A summary of various scattering mechanisms in semiconductors, as outlined by Nag (1980), is given in Fig. 1.3.1. We will not consider carrier-carrier

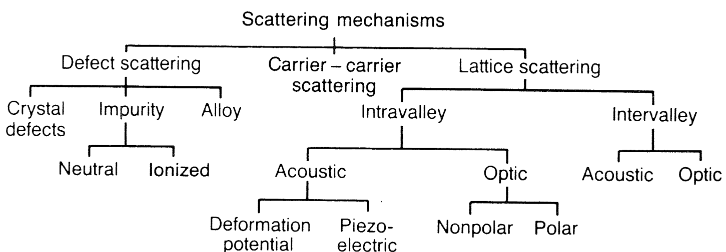

Fig. 1.3.1 An outline of the various possible carrier scattering mechanisms in GaAs. (After Nag (1980). Reproduced by permission of Springer-Verlag, Inc.)

scattering at all, since it is not important except at high carrier concentrations, say, $n > 10^{18}\ \mathrm{cm}^{-3}$. The mechanisms of relevance are listed in Table 1.3.1 along with the energy, mass, and temperature dependencies of τ and

Table 1.3.1 Mass and temperature dependences of τ and μ (nondegenerate electrons)

Mechanism	Relaxation time: Energy dependence	Relaxation time: Mass dependence	Mobility: Temperature dependence	Mobility: Mass dependence
(1) Impurity				
(a) Ionized	$\frac{3}{2}$	$\frac{1}{2}$	$\frac{3}{2}$	$-\frac{1}{2}$
(b) Neutral (Erginsoy)	0	1	0	0
(2) Acoustic phonon				
(a) Deformation	$-\frac{1}{2}$	$-\frac{3}{2}$	$-\frac{3}{2}$	$-\frac{5}{2}$
(b) Piezoelectric	$\frac{1}{2}$	$-\frac{1}{2}$	$-\frac{1}{2}$	$-\frac{3}{2}$
(3) Optical phonon				
(a) Polar	$\sim\frac{1}{2}$	$-\frac{1}{2}$	—	$-\frac{3}{2}$
(b) Nonpolar	$\sim-\frac{1}{2}$	$-\frac{3}{2}$	$-\frac{3}{2}$ $(kT \gg \hbar\omega_0)$	$-\frac{5}{2}$
(4) Localized potential				
(a) Alloy	$-\frac{1}{2}$	$-\frac{3}{2}$	$-\frac{1}{2}$	$-\frac{5}{2}$
(b) Space charge	$-\frac{1}{2}$	$\frac{1}{2}$	$-\frac{1}{2}$	$-\frac{1}{2}$
(c) Barrier	$-\frac{1}{2}$	$-\frac{3}{2}$	$-\frac{1}{2}$	$-\frac{5}{2}$
(d) Well	$-\frac{1}{2}$	$\frac{3}{2}$	$-\frac{1}{2}$	$\frac{1}{2}$
(5) Dipole	$\frac{1}{2}$	$-\frac{1}{2}$	$\frac{1}{2}$	$-\frac{3}{2}$

μ. Ionized-impurity scattering will be considered in more detail than the others, because of its importance in materials analysis, and because it illustrates well calculations involving Eq. (1.3.24).

1.3.1.1 *Ionized impurities*

Ionized impurities scatter electrons through their screened coulomb potential:

$$\Delta V = \frac{Ze^2}{4\pi\epsilon r} e^{-r/\lambda_D} \tag{1.3.27}$$

where Ze is the ionic charge, and λ_D is the Debye length: in the non-degenerate case, $\lambda_D^2 = \epsilon kT/e^2 n$ for free-electron screening alone, or $\lambda_D^2 = \epsilon kT/e^2\{n + (n + N_A)[1 - (n + N_A)/N_D]\}$ if the donors are not completely ionized. Then

$$\begin{aligned} A(\mathbf{q}) &= \frac{1}{V_c}\int \frac{Ze^2}{4\pi\epsilon r} e^{-r/\lambda_D} e^{-i\mathbf{q}\cdot\mathbf{r}}\, d\mathbf{r} \\ &= \frac{Ze^2}{4\pi\epsilon r}\int_0^\infty \frac{e^{-r/\lambda_D}}{r}\int_0^{2\pi}\int_0^{\pi} e^{-iqr\cos\theta} r^2 \sin\theta\, d\theta\, d\phi\, dr \\ &= \frac{Ze^2}{2\epsilon V_c}\int_0^\infty r e^{-\lambda_D/r}\, dr \int_{-1}^{1} e^{-iqrx}\, dx \\ &= \frac{Ze^2}{\epsilon V_c}\frac{1}{q^2 + \lambda_D^{-2}} \end{aligned} \tag{1.3.28}$$

It is of interest to note here that the 'bare' (unscreened) $A(\mathbf{q})$ is $A(\mathbf{q}) = Ze^2/\epsilon V_c q^2$, so that the 'screening factor' must be $q^2/(q^2 + \lambda_D^{-2})$.

The lowest conduction band in GaAs has s-like wave functions near $\mathbf{k} = 0$ so that $G(\mathbf{k}, \mathbf{k}') \simeq 1$. Also, the total potential is $N_I V_c \Delta V$, if the ionized-impurity concentration is N_I. Then Eq. (1.3.24) becomes

$$\frac{1}{\tau_{ii}(\mathscr{E})} = \frac{N_I V_c^2}{8\pi^3}\int \frac{2\pi}{\hbar}\frac{Z^2 e^4}{\epsilon^2 V_c^2}\frac{(1-\cos\theta)}{[|\mathbf{k}-\mathbf{k}'|^2 + \lambda_D^{-2}]^2}\delta(\mathscr{E}_{\mathbf{k}} - \mathscr{E}_{\mathbf{k}'})\, d\mathbf{k}' \tag{1.3.29}$$

We let

$$\begin{aligned} d\mathbf{k}' &= k'^2 \sin\theta\, d\theta\, d\phi\, d\mathbf{k}' \\ &= k'^2 \sin\theta\, d\theta\, d\phi \frac{m^*}{\hbar^2}\frac{1}{k'} d\mathscr{E}' \end{aligned}$$

since $\mathscr{E}' = \hbar^2 k'^2/2m^*$ for a parabolic band, and also write

$$|\mathbf{k} - \mathbf{k}'|^2 = k^2 + k'^2 - 2kk'\cos\theta$$

The in[illegible]tion over ϕ gives a factor 2π, and the $\delta(\mathscr{E} - \mathscr{E}')$ implies that $k = k'$, for the parabolic band. Thus,

$$\begin{aligned} \frac{1}{\tau_{ii}(\mathscr{E})} &= \frac{N_I Z^2 e^4 m^*}{8\pi\epsilon^2\hbar^3}\frac{1}{k^3}\int_{-1}^{1}\frac{(1-x)\, dx}{[1 - x + 1/2k^2\lambda_D^2]^2} \\ &= \frac{N_I Z^2 e^4 m^*}{8\pi\epsilon^2\hbar^3}\frac{1}{k^3}\left[\ln(1 + 4k^2\lambda_D^2) - \frac{4k^2\lambda_D^2}{1 + 4k^2\lambda_D^2}\right] \end{aligned} \tag{1.3.3}$$

By letting $k^2 = 2m^*\mathscr{E}/\hbar^2$ Eq. (1.3.30) becomes

$$\begin{aligned} \frac{1}{\tau_{ii}(\mathscr{E})} &= \frac{N_I Z^2 e^4[\ln(1 + y') - y'/(1 + y')]}{16\sqrt{2}\pi\epsilon^2 m^{*1/2}\mathscr{E}^{3/2}} \\ &\equiv a_{ii}^{-1}\mathscr{E}^{-3/2}[\ln(1 + y') - y'/(1 + y')] \end{aligned} \tag{1.3.3}$$

where $y' = 8\epsilon m^*(kT)\mathscr{E}/\hbar^2 e^2 n$. Equation (1.3.31) is the well-known Brook[s-] Herring formula, which usually is considered to be valid if $y' \gg 1$, i.e. high enough T or low enough n. However, Meyer and Bartoli (1981a) ha[ve] shown that a more accurate criterion for validity is $ka_0/2 \gg 1$, where a_0 [is] the Bohr radius.

The mobility associated with B–H ionized-impurity scattering is

$$\begin{aligned} \mu_{ii} &= \frac{e\langle\tau_{ii}(\mathscr{E})\rangle}{m^*} = \frac{e}{m^*}\frac{\int_0^\infty \tau_{ii}(\mathscr{E})\mathscr{E}^{3/2}\frac{\partial f_0}{\partial\mathscr{E}}\, d\mathscr{E}}{\int_0^\infty \mathscr{E}^{3/2}\frac{\partial f_0}{\partial\mathscr{E}}\, d\mathscr{E}} \\ &= \frac{e}{m^*}a_{ii}\frac{\int_0^\infty \mathscr{E}^3[\ln(1 + y') - y'/(1 + y')]^{-1}\frac{\partial f}{d\mathscr{E}}\, d\mathscr{E}}{\int_0^\infty \mathscr{E}^{3/2}\frac{\partial f_0}{\partial\mathscr{E}}\, d\mathscr{E}} \end{aligned} \tag{1.3.3}$$

We first consider non-degenerate statistics. Then $\partial f_0/\partial\mathscr{E} \propto \exp(-\mathscr{E}/kT)$ [so] that

$$\begin{aligned} \mu_{ii} &= \frac{e}{m^*}a_{ii}\frac{\int_0^\infty \mathscr{E}^3 e^{-\mathscr{E}/kT}[\ln(1 + y') - y'/(1 + y')]^{-1}\, d\mathscr{E}}{\int_0^\infty \mathscr{E}^{3/2} e^{-\mathscr{E}/kT}\, d\mathscr{E}} \\ &\simeq \frac{e}{m^*}a_{ii}\frac{\Gamma(4)}{\Gamma(\frac{5}{2})}(kT)^{3/2}[\ln(1 + y) - y/(1 + y)]^{-1} \\ &= \frac{128\sqrt{2}\pi^{1/2}\epsilon^2(kT)^{3/2}}{N_I Z^2 e^3 m^{*1/2}[\ln(1 + y) - y/(1 + y)]} \end{aligned} \tag{1.3.3}$$

where $y = 24\epsilon m^*(kT)^2/\hbar^2 e^2 n$. This value of y is obtained by realizing th[at] the bracketed term in the integral varies slowly with $\mathscr{E}$, and thus can [be] replaced by its value at the integrand maximum, i.e. a[t] $\mathscr{E} \simeq 3kT$. Note th[at] μ_{ii} in Eq. (1.3.33) varies with temperature as $T^{3/2}$, an[d thi]s ionized-impuri[ty]

scattering almost always dominates at a low enough temperature in any semiconductor.

For degenerate statistics, $\partial f_0/\partial \mathscr{E} \simeq \delta(\mathscr{E} - \mathscr{E}_F)$ in Eq. (1.3.32), and thus $\mu_{ii} = e\tau_{ii}(\mathscr{E}_F)/m^*$. For this case,

$$k^2 \simeq k_F^2 \simeq 2m^*\mathscr{E}_F/\hbar^2 \simeq (3\pi^2 n)^{2/3}$$

and the generalized form of λ_D^2 then becomes

$$\lambda_D^2 = \frac{\epsilon kT\mathscr{F}_{1/2}(\eta)}{e^2 n\mathscr{F}_{-1/2}(\eta)} \rightarrow \frac{\epsilon kT}{e^2 n}\frac{\eta_F^{3/2}\Gamma(\frac{3}{2})}{\eta_F^{1/2}\Gamma(\frac{5}{2})} = \frac{\epsilon kT}{e^2 n}\frac{2}{3}\frac{\mathscr{E}_F}{kT} = \frac{2}{3}\frac{\epsilon\mathscr{E}_F}{e^2 n} \qquad (1.3.34)$$

where $\eta_F \equiv \mathscr{E}_F/kT \gg 1$. Thus, μ_{ii} becomes

$$= \frac{24\pi^3\epsilon^2\hbar^3 n}{N_I Z^2 e^3 m^{*2}[\ln(1+y_F) - y_F/(1+y_F)]} \qquad (1.3.35)$$

where $y_F = 3^{1/3}4\pi^{8/3}\epsilon\hbar^2 n^{1/3}/e^2 m^*$. Note that μ_{ii} for the degenerate case is more strongly dependent on m^* than that for the nondegenerate case, and also has no explicit dependence on T.

Numerical values for τ_{ii} and μ_{ii} in GaAs are as follows (cf. Table 1.3.2):

$$\tau_{ii}(\mathscr{E}) = 7.08 \times 10^6 \frac{\mathscr{E}^{3/2}(\text{eV})}{N_I(\text{cm}^{-3})Z^2[\ln(1+y) - y/(1+y)]}\ \text{s} \qquad (1.3.36)$$

Table 1.3.2 Constants used for mobility formulas (valued at 300 K, where applicable)

Quantity	Magnitude	Units	Reference
$\hbar$	1.055×10^{-34}	J-s	Nag, 1980
T_{po}	419	K	Nag, 1980
ϵ(300 K)	$12.91(8.84 \times 10^{-12})$	F/m	Nag, 1980
ϵ_∞(300 K)	$10.91(8.84 \times 10^{-12})$	F/m	Nag, 1980
e	1.602×10^{-19}	C	Nag, 1980
m^*(4 K)	$0.066(9.109 \times 10^{-31})$	kg	Rode, 1975
$c_L \equiv \rho s^2$	1.45×10^{11}	N/m²	Nag, 1980
$P \equiv (h_{pz}^2/\rho s^2\epsilon)^{1/2}$	0.052	unitless	Nag, 1980
E_1	9.3	eV	Nolte *et al.*, 1987
k	1.380×10^{-23}	J/deg	Nag, 1980

where

$$y = 4.29 \times 10^{17}\frac{\mathscr{E}(\text{eV})T}{n(\text{cm}^{-3})} \qquad (1.3.37)$$

and

$$\mu_{ii}(T)_{\text{nondegen}} = 2.12 \times 10^{18}\frac{T^{3/2}}{N_I(\text{cm}^{-3})Z^2[\ln(1+y) - y/(1+y)]}\frac{\text{cm}^2}{\text{V-s}} \qquad (1.3.38)$$

where

$$y = 1.11 \times 10^{14}\frac{T^2}{n(\text{cm}^{-3})} \qquad (1.3.$$

Also,

$$\mu_{ii}(T)_{\text{degen}} = 7.56 \times 10^3\frac{n(\text{cm}^{-3})}{N_I(\text{cm}^{-3})Z^2[\ln(1+y) - y/(1+y)]}\frac{\text{cm}^2}{\text{V-s}} \qquad (1.3.$$

where

$$y = 9.98 \times 10^{-6}[n(\text{cm}^{-3})]^{1/3} \qquad (1.3.$$

Before leaving the subject of ionized-impurity scattering, we sho discuss some of the approximations implicit in the analysis. First of scattering theory has been well developed in terms of a partial-wa phase-shift analysis, which yields a scattering cross-section σ_s as sho below:

$$\sigma_s = \frac{4\pi}{k^2}\sum_{l=0}^{\infty}(l+1)\sin^2(\delta_l - \delta_{l+1}) \qquad (1.3.$$

where δ_l is the phase shift of the lth partial wave. The Brooks–Herr scattering theory, described in this section, is based on the Born approxin tion, which requires that $\delta_l \ll 1$, for all l. The criterion for the validity this approximation is generally given as $4k^2\lambda_D^2 \gg 1$ (or roughly, $y \gg$ although Meyer and Bartoli (1981a) have shown that $ka_0/2 \gg 1$ is a m accurate criterion. If the Born approximation is not valid, then Eq. (1.3. must be used, with enough phase shifts included to get the desired accura For GaAs, it turns out that the Brooks–Herring mobility can be off as mu as 10% at 300 K, 20% at 77 K, and 30% at 10 K, depending upon Accurate numbers may be obtained from the tables supplied by Meyer a Bartoli (1981a).

Another problem, the loss of free-carrier screening, arises at very l temperatures, or in semi-insulating GaAs at any temperature. When screening is present, then the scattering cross-section diverges at l scattering angles, as may be seen in Eq. (1.3.28) by letting $\lambda_D \rightarrow \infty$, a $q \simeq |\mathbf{k} - \mathbf{k}'| \rightarrow 0$. Conwell and Weisskopf, (1950) solved this problem ir rather arbitrary manner by cutting off the potential at a radius correspor ing to half the average distance between impurities. Their analysis then l to the formula

$$\mu_{iiCW} = 2.12 \times 10^{18}\frac{T^{3/2}}{N_I(\text{cm}^{-3})Z^2\ln(1+y)}\frac{\text{cm}^2}{\text{V-s}} \qquad (1.3.$$

where

$$y = 5.37 \times 10^{18}\frac{T^2}{[N_I(\text{cm}^{-3})]^{2/3}} \qquad (1.3.$$

As can be seen, the Conwell–Weisskopf formula is nearly the same as t Brooks–Herring formula, except for the screening term, $\ln(1+y)$.

A third problem which can arise is multi-ion scattering; i.e., if the scattering centers are close enough together, then an incoming electron might 'feel' the potentials of more than one center at a time. Note that the Conwell–Weisskopf formulation explicitly avoids this problem by always cutting off the potential at a point less than the impurity separation distance. Ridley (1977) has argued that the Brooks–Herring and Conwell–Weisskopf formulations can indeed be reconciled if this 'third-body interference' is taken into account. A more complete discussion of this whole problem is given by Meyer and Bartoli (1985).

1.3.1.2 *Neutral impurities*

When an electron passes close to a neutral atom, momentum can be transferred through a process in which the free electron exchanges with a bound electron on the atom. For a *hydrogenic* donor, Erginsoy (1950) has calculated that $\tau_{ni}(\mathscr{E}) = m^*/20N_n\hbar a_0$, independent of energy, so that

$$\mu_{ni} = \frac{e}{20N_n\hbar a_0} = \frac{e^3m^*}{80\pi N_n\hbar^3\epsilon}$$
$$= 7.42 \times 10^{19}/N_n(\mathrm{cm}^{-3})\,\frac{\mathrm{cm}^2}{\mathrm{V\text{-}s}} \qquad (1.3.45)$$

where a_0 is the effective Bohr radius of the donor and N_n is the concentration of neutral impurities. Basically, Erginsoy considered only the zeroth partial wave ($l = 0$) in the general cross-section formula (Eq. (1.3.42)) and used some approximate phase-shift results from Massey and Moiseiwitsch (1950). Later, Sclar (1956) considered the additional 'resonant' scattering due to the possibility of negative-ion formation and derived a formula

$$\frac{1}{\tau_{ni}(\mathscr{E})} = \frac{\pi N_n e^4}{2^{1/2}m^{*1/2}\mathscr{E}^{3/2}}[\ln(1 + k\lambda_D)^2 - 1/(1 + k^{-2}\lambda_D^{-2})] \qquad (1.3.46)$$

which can be compared to the Erginsoy formula as follows (McGill and Baron, 1975):

$$\mu_{ni}(\mathrm{Sclar}) = 0.82\mu_{ni}(\mathrm{Erginsoy})\left[\frac{2}{3}\left[\frac{kT}{E_D^-}\right]^{1/2} + \frac{1}{3}\left[\frac{E_D^-}{kT}\right]^{1/2}\right] \qquad (1.3.47)$$

where $E_D^- = 0.283$ meV is the binding energy of the negative ion. McGill and Baron (1975) have improved on both of these formulations by carrying out the phase-shift calculation, Eq. (1.3.42), up to $l = 2$ terms. Their results, which used more accurate phase shifts, are compared to the others in Fig. 1.3.2 (McGill and Baron, 1975); here they have explicitly related the mobility to the binding energy of the donor electron. Note that since $\mu_{ni} \propto a_0^{-1} \propto$ [illegible] the ground-state binding energy, a deep donor will not scatter elec[illegible]ns very effectively. It turns out that for the hydrogenic donor

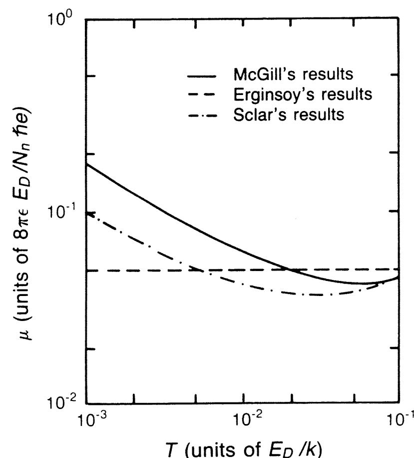

Fig. 1.3.2 Conductivity mobility (in reduced units) vs. temperature (in reduced units) for neutral impurity scattering, according to the theories of Erginsoy (1950), Sclar (1956), and McGill and Baron (1975). (After McGill and Baron (1975). Reproduced by permission of The American Institute of Physics)

in GaAs, which has $E_D \simeq 5$ meV, the various formulas differ little above 5 K. Other workers (Blagosklonskaya *et al.*, 1970; Schwartz, 1961) have obtained results similar to those of McGill and Baron (1975).

Meyer and Bartoli (1981b) have used some of these results and others to develop an analytical formula which is accurate to 7% for $\mathscr{E}/E_D \lesssim 0.5$. Their result is

$$\tau_{ni}(\mathscr{E}) = \frac{m^*}{A(x)N_n\hbar a_0} \qquad (1.3.48)$$

where $x = \mathscr{E}/E_D = (ka_0)^2$, and

$$A(x) = \frac{35.2}{x^{1/2}}\frac{(1 + e^{-50x})(1 + 80.6x + 23.7x^2)}{(1 + 41.3x + 133x^2)}\left[\tfrac{1}{3}\ln(1 + x) - \frac{(1 + x/2 - x^2/6)}{(1 + x)^3}\right] \qquad (1.3.49)$$

This relationship for τ_{ni} is probably the best one to use when adding up the various $\tau_j^{-1}(\mathscr{E})$ for energy averaging (Eq. (1.2.27)). Note that $A(x) \simeq 20$ from $x = 0.05$ to 1.0, in agreement with Erginsoy.

1.3.1.3 *Acoustic phonons: deformation potential*

The acoustic-mode lattice vibrations induce changes in la[illegible]e spacing, which change the band gap from point to point. Since the crys[illegible] is 'deformed' at

iterative technique is highly accurate but does not reduce to analytical form. The variational technique, on the other hand, can be written in closed form up to a certain accuracy, but evidently takes far more calculational effort to attain a given accuracy than the iterative method. Ziman (1960) has written out the first two variational terms in the expansion of mobility in terms of Bessel functions, as solved by Howarth and Sondheimer (1953). (Note that Ziman appears to have inverted a factor $3/\pi^{1/2}2^{7/2}$ in his Eq. (10.5.17).) Putley (1960) writes the Howarth and Sondheimer relationship in the following form (after multiplication by 4π to put into MKS units):

$$\mu_{po} = \frac{2^{9/2}\pi^{1/2}}{3}\frac{\hbar^2(kT)^{1/2}(e^{T_{po}/T}-1)\chi(T_{po}/T)}{e(kT_{po})m^{*3/2}(\epsilon_\infty^{-1}-\epsilon^{-1})}$$
$$= 1.04\times10^5\frac{T^{1/2}(e^{T_{po}/T}-1)\chi(T_{po}/T)}{T_{po}}\frac{\mathrm{cm}^2}{\mathrm{V\text{-}s}} \quad (1.3.56)$$

where $\chi(T_{po}/T)$ is a slowly varying function of T, shown in Fig. 1.3.3. In

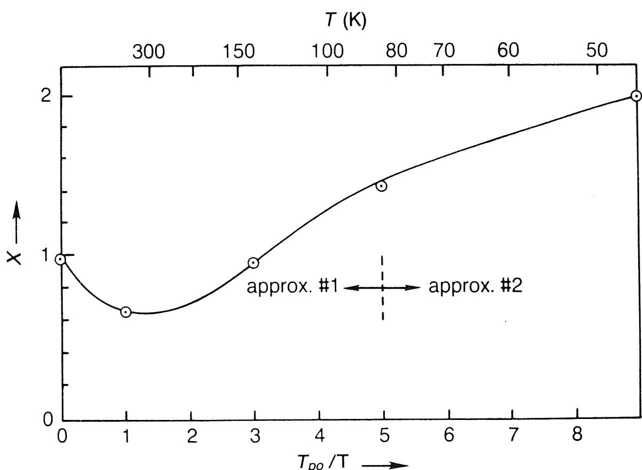

Fig. 1.3.3 The slowly varying function $\chi(T_{po}/T)$ in the polar-optical-mode scattering formula (Eq. (1.3.56)) as a function of T_{po}/T. The points are from Putley (1960), following the variational theory of Howarth and Sondheimer (1953). The solid line is an analytical fit given by Eqs. (1.3.57) and (1.3.58)

this figure, the six points given by Putley are shown as circles, whereas the solid line is an approximation, as follows:

approx. #1: $0 \le T_{po}/T \le 5 \quad (84\,\mathrm{K} \le T \le \infty)$

$$\chi(T_{po}/T) = 1 - 0.5841(T_{po}/T) + 0.2920(T_{po}/T)^2 - 0.037164(T_{po}/T)^3 + 0.0012016(T_{po}/T)^4 \quad (1.3.57)$$

approx. #2: $5 \le T_{po}/T \le \infty \quad (0 \le T \le 84\,\mathrm{K})$

$$\chi(T_{po}/T) = \frac{3\pi^{1/2}}{8}\left[\frac{T_{po}}{T}\right]^{1/2} \quad (1.3.58)$$

As can be seen, the maximum deviation of the line from the points is about 4%. By using Eq. (1.3.58), the low-temperature limit of μ is

$$\mu_{po}(T<84\,\mathrm{K}) = 2^{3/2}\pi\frac{\hbar^2(e^{T_{po}/T}-1)}{e(kT_{po})^{1/2}m^{*3/2}(\epsilon_\infty^{-1}-\epsilon^{-1})}$$
$$= 3.386\times10^3(e^{T_{po}/T}-1)\frac{\mathrm{cm}^2}{\mathrm{V\text{-}s}} \quad (1.3.59)$$

For purposes of energy averaging, it would be useful to be able to define an *effective* relaxation time. We suggest the following:

$0 \le T_{po}/T \le 5$:

$$\tau_{po}(\mathscr{E}) = 2^{3/2}\pi\frac{\hbar^2(e^{T_{po}/T}-1)\chi(T_{po}/T)}{e^2(kT_{po})m^{*1/2}(\epsilon_\infty^{-1}-\epsilon^{-1})}\mathscr{E}^{1/2}$$
$$= 6.74\times10^{-13}(e^{T_{po}/T}-1)\chi(T_{po}/T)[\mathscr{E}(\mathrm{eV})]^{1/2}\,\mathrm{s} \quad (1.3.60)$$

$5 \le T_{po}/T \le \infty$:

$$\tau_{po}(\mathscr{E}) = 2^{3/2}\pi\frac{\hbar^2(e^{T_{po}/T}-1)}{e^2(kT_{po})^{1/2}m^{*1/2}(\epsilon_\infty^{-1}-\epsilon^{-1})}$$
$$= 1.28\times10^{-13}(e^{T_{po}/T}-1)\,\mathrm{s} \quad (1.3.61)$$

The low-temperature form of τ_{po}, Eq. (1.3.61), is clearly the one required to give the mobility shown in Eq. (1.3.59), since the $(e^{T_{po}/T}-1)$ term in the mobility does not result from energy averaging. The rationale in suggesting Eqs. (1.3.60) and (1.3.61) for τ_{po} is as follows. In the mobility formula, Eq. (1.3.56), the most rapidly varying term is $(e^{T_{po}/T}-1)$, followed by $T^{1/2}$ and $\chi(T_{po}/T)$, in that order. Fortunately, the $(e^{T_{po}/T}-1)$ term does not result from energy averaging, and thus will simply be repeated in the formula for τ_{po}. At low temperatures, i.e. $T_{po}/T \gg 1$, the product $T^{1/2}\chi(T_{po}/T)$ is independent of temperature, and thus τ_{po} at low temperatures must be independent of energy. At high temperatures, say $T_{po}/T < 5$, $\chi(T_{po}/T)$ varies from unity by only about 40%, while $T^{1/2}$ varies by a factor 2, from 80 to 320 K. Thus, for *very rough* calculations it seems reasonable to carry over the $\chi(T_{po}/T)$ term to τ_{po}, and let the $T^{1/2}$ term be represented by $\mathscr{E}^{1/2}$.

Other approximations for $\tau_{po}(\mathscr{E})$ exist in the literature. For example, Harrison and Hauser (1976) have given such a formula, although it appears to hold only for $\mathscr{E} \gg kT_{po}$.

1.3.1.6 *Optical phonons: non-polar*

The optical-mode lattice vibrations can produce a perturbing potential through local changes in the band gap, just as was found with the acoustic

these points, the potential is called the deformation potential. The corresponding relaxation time can be written

$$\tau_{dp}(\mathscr{E}) = \frac{\pi \hbar^4 \rho s^2}{\sqrt{2}\, E_1^2 m^{*3/2} (kT)} \mathscr{E}^{-1/2}$$
$$= 1.88 \times 10^{-8} [E_1(\text{eV})]^{-2} T^{-1} [\mathscr{E}(\text{eV})]^{-1/2}\ \text{s} \qquad (1.3.50)$$

where ρ is the crystal density, s is the properly averaged velocity of sound, and E_1 is the deformation potential. Here $\rho s^2 \equiv c_l$, the longitudinal elastic constant, about $14.5 \times 10^{10}\ \text{N/cm}^2$ in GaAs. Also, the best value of $|E_1|$ in GaAs is about 9.3 eV (Nolte *et al.*, 1987). The corresponding mobility is

$$\mu_{dp} = \frac{e\langle \tau_{\text{def}}(\mathscr{E})\rangle}{m^*} = \frac{2\sqrt{2}\pi^{1/2} \hbar^4 \rho s^2 e}{3E_1^2 m^{*5/2} (kT)^{3/2}}$$
$$= 4.03 \times 10^{10} [E_1(\text{eV})]^{-2} T^{-3/2} \frac{\text{cm}^2}{\text{V-s}} \qquad (1.3.51)$$

Note that $\mu_{dp} \propto T^{-3/2}$, so that this mechanism tends to dominate at high temperatures. Also, it varies strongly with m^*, so that the scattering rate ($\propto \tau^{-1}$) is stronger for holes than electrons.

The value of $|E_1|$, the hydrostatic, acoustic-mode, band-edge deformation potential, has been a matter of some uncertainty over the years, with reported values ranging from 6.5 to 17.5 eV, and some numbers even outside of this range. The most generally accepted value up to now seems to have been 7 eV, a value determined from 300 K Hall-mobility measurements on pure samples, which have minimal impurity scattering so that lattice scattering is dominant. The lattice scattering in such samples is primarily due to optic-mode lattice vibrations, but acoustic-mode vibrations must also be considered, and thus E_1 comes into play. Evidently, the commonly accepted value of the lattice-limited *Hall* mobility has been about $9500\ \text{cm}^2/\text{V-s}$, giving a conductivity mobility of about $8000\ \text{cm}^2/\text{V-s}$. However, in literally hundreds of Hall-effect measurements on pure samples, of various shapes, we have never measured a value as high as $9500\ \text{cm}^2/\text{V-s}$, and believe that about $8000\text{–}8500\ \text{cm}^2/\text{V-s}$ is a more realistic estimate of the lattice-limited Hall mobility. To determine E_1, we have carried out a simultaneous mobility fit of two vapor-phase epitaxial samples (Look and Colter, 1983) over a temperature range 5–400 K. These samples were grown under very similar conditions, except for impurity content. For maximum accuracy, Rode's iterative method (Rode, 1970) was used, and all unknown parameters, including E_1, were studied by sensitivity analysis. The result was that a good fit to both samples, simultaneously, could be achieved only with $|E_1|$ in the 9.0–10.0 eV range, say, 9.5 ± 0.5 eV. A recent theoretical study (Cardona and Christensen, 1987) finds that $E_1 \simeq -8.8$ eV, and an experimental study, using pressure derivatives (Nolte *et al.*, 1987), finds that $E_1 \simeq -9.3$ e[illegible] Thus, it seems that a range about the latter value, say $|E_1| = 9.3 \pm$ [illegible] eV, is consistent with the most recent determinations and

should be the value used in Eqs. (1.3.50) and (1.3.51). Then,

$$\tau_{dp}(\mathscr{E}) = 1.57 \times 10^{-6}\, T[\mathscr{E}(\text{eV})]^{1/2}\ \text{s} \qquad (1.3.52)$$

$$\mu_{dp} = 4.49 \times 10^{8}\, T^{-3/2} \frac{\text{cm}^2}{\text{V-s}} \qquad (1.3.53)$$

1.3.1.4 *Acoustic phonons: piezoelectric potential*

The atomic displacements produced by the acoustic-mode lattice vibrations introduce a second potential if the atoms are partially ionized. This effect, called the piezoelectric effect, occurs in crystals lacking a center of symmetry, which includes all compound semiconductors of course. A relaxation time can be defined for the piezoelectric-potential mechanism because energy changes during the collisions are small. The relaxation time is

$$\tau_{pe}(\mathscr{E}) = \frac{2\sqrt{2}\,\pi \hbar^2 \rho s^2}{(eh_{pz}/\epsilon)^2 m^{*1/2} (kT)} \mathscr{E}^{1/2} = \frac{2\sqrt{2}\,\pi \hbar^2 \epsilon}{e^2 P^2 m^{*1/2} (kT)} \mathscr{E}^{1/2}$$
$$= 1.92 \times 10^{-8}\, T^{-1} [\mathscr{E}(\text{eV})]^{1/2}\ \text{s} \qquad (1.3.54)$$

where h_{pz} is the *piezoelectric constant*, and $P \equiv (h_{pz}^2/\rho s^2 \epsilon)^{1/2}$ is the *piezoelectric coupling coefficient*. In GaAs, P is usually given as 0.052. The mobility for this relaxation time is

$$\mu_{pe} = \frac{e\langle \tau_{pe}(\mathscr{E})\rangle}{m^*} = \frac{16\sqrt{2}\,\pi^{1/2} \epsilon \hbar^2}{3eP^2 m^{*3/2} (kT)^{1/2}}$$
$$= 7.08 \times 10^{6}\, T^{-1/2} \frac{\text{cm}^2}{\text{V-s}} \qquad (1.3.55)$$

At 300 K, the piezoelectric-potential scattering rate is about five times smaller than the deformation-potential rate.

1.3.1.5 *Optical phonons: polar*

The dominant scattering mechanism at 300 K in GaAs is that due to the dipole moments formed by the interaction of the ionic charges on the atoms with the optical-mode lattice vibrations. This mechanism is called polar optical-mode scattering. As mentioned several times earlier, a relaxation-time solution to the Boltzmann equation, i.e.

$$\left[\frac{\partial f}{\partial t}\right]_{\text{coll}} = -\frac{f - f_0}{\tau(\mathscr{E})}$$

is not possible for polar optical-mode scattering, since τ becomes a function of the perturbation strength itself instead of just the energy $\mathscr{E}$ of the electrons. There are several ways to solve the Boltzmann equation for such mechanisms, such as Rode's iterative technique (Rode, [illegible]), or Kohler's variational technique (Kohler, 1948; Sondheimer, 1950; [illegible]an, 1960). The

modes. The deformation potential in this case is called D_0 (energy per unit strain), and the relaxation time is given by

$$\tau_{npo}(\mathscr{E}) = \frac{\sqrt{2}\,\pi\rho\hbar^3\omega_0}{D_0^2 m^{*3/2} n_0[(\mathscr{E}+\hbar\omega_0)^{1/2} + H(\mathscr{E}-\hbar\omega_0)(n_0+1)n_0^{-1}(\mathscr{E}-\hbar\omega_0)^{1/2}]} \tag{1.3.62}$$

where ω_0 is the nonpolar optic-phonon frequency, $H(x)$ is the Heaviside step function, and $n_0 = 1/[\exp(\hbar\omega_0/kT) - 1]$. The corresponding mobility cannot be solved in closed form, but limiting forms can be given:

$$\mu_{npo} = \frac{2\sqrt{2}\pi^{1/2}\rho\hbar^4 e\omega_0^2}{3D_0^2 m^{*5/2}(kT)^{3/2}} \qquad kT \gg \hbar\omega_0 \tag{1.3.63}$$

$$\mu_{npo} = \frac{\sqrt{2\pi}\rho\hbar^4(\hbar\omega_0)^{1/2}e}{D_0^2 m^{*5/2} n_0} \qquad kT \ll \hbar\omega_0 \tag{1.3.64}$$

Unfortunately, it is difficult to know the strength of this interaction in GaAs, because D_0 is not accurately known. However, this mechanism is thought to be significantly weaker than the other lattice-scattering mechanisms.

1.3.1.7 *Short-range interactions: localized-defect, space-charge, and alloy potentials*

Several types of scattering mechanisms may be approximated by short-range potentials which have constant strength over some small volume V_δ and zero strength elsewhere. The simplest such potential is represented by a delta function:

$$\Delta V = V_\delta E_\delta \delta(\mathbf{r} - \mathbf{r}_0)$$

Then $A(\mathbf{q})$ becomes

$$A(\mathbf{q}) = \frac{1}{V_c}\int \Delta V e^{-i\mathbf{q}\cdot\mathbf{r}}\,d\mathbf{r} = \frac{V_\delta}{V_c} E_\delta e^{-i\mathbf{q}\cdot\mathbf{r}_0}$$

and the relaxation time can be written, for a density of scattering centers N,

$$\begin{aligned}
\frac{1}{\tau_\delta(\mathscr{E})} &= \frac{V_c}{8\pi^3} N V_c \int \frac{2\pi}{\hbar}\frac{V_\delta^2 E_\delta^2}{V_c^2} |e^{-i\mathbf{q}\cdot\mathbf{r}_0}|^2 (1-\cos\theta)\delta(\mathscr{E}_\mathbf{k} - \mathscr{E}_{\mathbf{k}'})\,d\mathbf{k}' \\
&= \frac{NV_\delta^2 E_\delta^2}{4\pi^2\hbar}\int_0^\infty\int_0^{2\pi}\int_0^\pi (1-\cos\theta)\delta(\mathscr{E}_\mathbf{k} - \mathscr{E}_{\mathbf{k}'})k'^2 \sin\theta\,d\theta\,d\phi\,dk' \\
&= \frac{NV_\delta^2 E_\delta^2}{\pi\hbar}\int_0^\infty \delta(\mathscr{E}_\mathbf{k} - \mathscr{E}_{\mathbf{k}'})k'^2 \frac{m^*}{\hbar^2 k'}\,d\mathscr{E}' \\
&= \frac{NV_\delta^2 E_\delta^2}{\pi\hbar}\int_0^\infty \frac{\sqrt{2}m^{*3/2}\mathscr{E}^{*1/2}}{\hbar^3}\delta(\mathscr{E}_\mathbf{k} - \mathscr{E}_{\mathbf{k}'})\,d\mathscr{E}' \\
&= \frac{\sqrt{2}}{\pi}\frac{NV_\delta^2 E_\delta^2 m^{*3/2}\mathscr{E}^{1/2}}{\hbar^4}
\end{aligned} \tag{1.3.65}$$

The corresponding mobility, as first derived by Anselm and Askerov (1962), is

$$\begin{aligned}
\mu_\delta &= \frac{e\langle\tau\rangle}{m^*} = \frac{e\pi\hbar^4}{\sqrt{2}NV_\delta^2 E_\delta^2 m^{*5/2}} \frac{\int_0^\infty \mathscr{E} e^{-\mathscr{E}/kT}\,d\mathscr{E}}{\int_0^\infty \mathscr{E}^{3/2} e^{-\mathscr{E}/kT}\,d\mathscr{E}} \\
&= \frac{2^{3/2}\pi^{1/2}}{3}\frac{e\hbar^4}{NV_\delta^2 E_\delta^2 m^{*5/2}(kT)^{1/2}}
\end{aligned} \tag{1.3.66}$$

1.3.1.7.1 *Alloy potential.*

Although not applicable to GaAs by itself, alloy scattering is important in some of the III–V ternaries and quaternaries, and thus should be mentioned here. The nature of the term $NV_\delta^2 E_\delta^2$ for alloy scattering can be determined from the following argument (Mott and Jones, 1958). The mean potential energy in a lattice composed of two binary compounds, A and B, is $V = \alpha V_A + (1-\alpha)V_B$, where α is the fraction of compound A. The scattering potential at an A unit is then

$$V - V_A = (1-\alpha)(V_B - V_A) \equiv E_A$$

and at a B unit,

$$V - V_B = \alpha(V_A - V_B) \equiv E_B$$

The number of A units is $N_c\alpha$ and the number of B units $N_c(1-\alpha)$, where N_c is the number of primitive cells per unit volume. Then the term $NV_\delta^2 E_\delta^2$ in Eq. (1.3.66) becomes

$$\begin{aligned}
NV_\delta^2 E_\delta^2 &= V_c^2[N_c\alpha E_A^2 + N_c(1-\alpha)E_B^2] \\
&= V_c^2 N_c[\alpha(1-\alpha)^2(V_B - V_A)^2 + (1-\alpha)\alpha^2(V_B - V_A)^2] \\
&= V_c^2 N_c \alpha(1-\alpha)(V_B - V_A)^2 \\
&= V_c\alpha(1-\alpha)(V_B - V_A)^2 \equiv V_c\alpha(1-\alpha)E_{AB}^2
\end{aligned} \tag{1.3.67}$$

where the final step makes use of the fact that $N_c V_c = 1$. Thus,

$$\mu_{al} = \frac{2^{3/2}\pi^{1/2}}{3}\frac{e\hbar^4}{V_c\alpha(1-\alpha)E_{AB}^2 m^{*5/2}(kT)^{1/2}} \tag{1.3.68}$$

where $E_{AB} \equiv |V_A - V_B|$. The quantity $V_A - V_B$ has variously been taken as the difference in band gaps between compounds A and B (Makowski and Glicksman, 1973), the difference in electron affinities (Harrison and Hauser, 1976), and the conduction-band discontinuity (for electrons). A recent study by Basu *et al.* (1986) in $Ga_{0.47}In_{0.53}As$ found that E_{AB} experimentally fell in the range 0.7–1.0 eV, whereas the first two interpretations of E_{AB} suggested above would have predicted 1.1 and 0.8 eV respectively. Thus, it may be difficult to select the best interpretation of E_{AB} from mobility data alone.

For this example, if we estimate $m^* = 0.046m_e$, $V_c = 5.0 \times 10^{-29}$ m^3, and

$E_{AB} \simeq 1$ eV, then $\mu_{al} = 4.5 \times 10^4$ cm²/V-s at 300 K, and 8.8×10^4 cm²/V-s at 77 K. A glance at the magnitudes of other scattering mechanisms in Table 1.3.3 suggests that alloy scattering would be an important mechanism at both temperatures, and in fact, would dominate the scattering at 77 K in a pure sample.

Table 1.3.3 Relative magnitudes of *conductivity* mobilities in GaAs at 300 K and 77 K for various scattering mechanisms (nondegenerate electrons). The values are calculated from the respective formulas in Section 1.3.1, which make use of the constants in Table 1.3.2

Mechanism	Mobility (cm²/V-s) 300 K	77 K
(1) Impurity		
(a) Ionized ($n = 10^{16}$ cm^{-3}, $N_I = 2 \times 10^{16}$ cm^{-3})	9.34×10^4	2.24×10^4
(b) Neutral ($N_n = 2 \times 10^{16}$ cm^{-3}) (Erginsoy formula)	3.71×10^5	3.71×10^5
(2) Acoustic phonon		
(a) Deformation	8.96×10^4	6.89×10^5
(b) Piezoelectric	4.09×10^5	8.07×10^5
(3) Optical phonon		
(a) Polar	8.64×10^3	7.77×10^5
(b) Nonpolar (constants unknown)	—	—
Total mobility (Matthiessen's rule)		
(a) exclude neutral-impurity scattering	7.14×10^3	2.06×10^4
(b) exclude *all* impurity scattering	7.73×10^3	2.51×10^5

1.3.1.7.2 Potential barrier. Consider a square-well potential: $V(r) = V_0$, for $r < a$, and $V(r) = 0$ for $r > a$. Then, in the limit $ka \ll 1$, it can be shown that $V_\delta E_\delta$ in Eq. (1.3.66) simply becomes $(4\pi/3)a^3 V_0$ (Podor, 1983). Thus,

$$\mu_{\text{bar}} = \frac{3}{2^{5/2}\pi^{3/2}} \frac{e\hbar^4}{Na^6 V_0^2 m^{*5/2}(kT)^{1/2}} \tag{1.3.69}$$

and $\tau_{\text{bar}}(\mathscr{E})$ is given by Eq. (1.3.65) with the same substitution for $V_\delta E_\delta$. Note in Eq. (1.3.69) the strong dependence on the radius of the potential.

1.3.1.7.3 Potential well. In this case, the electron can be trapped, with a binding energy E_B. The relaxation time can be written, for $\mathscr{E} \ll E_B$,

$$\tau_{\text{well}}(\mathscr{E}) = \frac{3}{2^{5/2}\pi^2} \frac{m^{*3/2} E_B}{\hbar^2 N} \mathscr{E}^{-1/2} \tag{1.3.70}$$

and μ then becomes (Chattopadhyay, 1981)

$$\mu_{\text{well}} = \frac{1}{2^{3/2}\pi^{5/2}} \frac{eE_B m^{*1/2}}{\hbar^2 N (kT)^{1/2}} \tag{1.3.71}$$

1.3.1.7.4 Space-charge potential. The relaxation time for an impenetrable region, such as a space-charge region, with cross section σ_{sc}, is easily derived:

$$\frac{1}{\tau_{sc}} = N\sigma_{sc} v = N\sigma_{sc} \frac{\hbar k}{m^*} = N\sigma_{sc} \frac{\hbar}{m^*} \frac{\sqrt{(2m^*\mathscr{E})}}{\hbar}$$
$$= 2^{1/2} \frac{N\sigma_{sc}}{m^{*1/2}} \mathscr{E}^{1/2} \tag{1.3.72}$$

and the mobility can then be written

$$\mu_{sc} = \frac{2^{3/2}}{3\pi^{1/2}} \frac{e}{N\sigma_{sc} m^{*1/2}(kT)^{1/2}} \tag{1.3.73}$$

Often, when this mechanism is invoked, the whole quantity $N\sigma_{sc}$ is taken as the fitting parameter since it is difficult to determine either factor separately.

1.3.1.7.5 Comparison of $T^{-1/2}$ mechanisms. The four scattering mechanisms discussed above all have mobilities varying as $T^{-1/2}$, and thus are impossible to separate by temperature dependence alone. Fortunately, as shown in Table 1.3.1, some of them differ greatly in their mass dependences, and may possibly be separated on this basis. However, it is important to recognize that the $T^{-1/2}$ dependence is not very unique (cf. the piezoelectric mechanism, also), and thus one must be very careful in assigning a particular scattering mechanism when this temperature dependence is observed. Another pitfall is that the mobility may simply be in a transition region, from lattice scattering to impurity scattering, when it appears to show a $T^{-1/2}$ variation. Thus, the magnitudes of the various mechanisms must be estimated in order to make a reasonable analysis.

1.3.1.8 Dipoles

If two impurity or defect ions of opposite charge are fairly close together, then they may scatter electrons as a dipole, rather than as two monopoles. In analogy with Eq. (1.3.27), the screened dipole potential is

$$\Delta V = \frac{\mathbf{q}_d \cdot \mathbf{r}}{4\pi\epsilon r^3}\left(1 + \frac{r}{\lambda_D}\right) e^{-r/\lambda_D} \tag{1.3.74}$$

where $\mathbf{q}_d$ is the dipole moment ($q = e^* l$, where e^* is the ionic charge and l is the distance between charges), and λ_D is the screening length. This potential leads (Dimitrov, 1976) to a relaxation time, for the *unscreened* case ($\lambda_D \to \infty$), of

$$\frac{1}{\tau_{\text{dip}}(\mathscr{E})} = \frac{1}{2^{3/2} 3\pi} \frac{m^{*1/2} e^2 N q_d^2}{\hbar^2 \epsilon^2} \mathscr{E}^{-1/2} \tag{1.3.75}$$

and a mobility, for non-degenerate electrons, of

$$\mu_{dip} = 2^{9/2}\pi^{1/2}\frac{\hbar^2\epsilon^2(kT)^{1/2}}{m^{*3/2}eNq_d^2} = 3.53\times 10^7 \frac{T^{1/2}}{[l(\text{cm})]^2 N(\text{cm}^{-3})}\frac{\text{cm}^2}{\text{V-s}} \quad (1.3.76)$$

where it is assumed that the dipole consists of two ions of charge e separated by distance l. If there is a distribution of l, then l^2 should be averaged over the distribution.

As an example, assume that there are 10^{18} dipoles having $l \simeq 5$ Å, about one lattice distance. Then at $T = 300$ K, $\mu_{dip} \simeq 2.4\times 10^5$ cm^2/V-s, denoting a rather weak mechanism. If however, $l = 50$ Å, then $\mu_{dip} = 2.4\times 10^3$ cm^2/V-s, a strong contribution, although we have neglected screening, which would weaken the scattering. Note that the whole idea of two charges acting as a dipole in the electron scattering process requires that $l < k^{-1} \lesssim \hbar/(2m^*kT)^{1/2} \simeq 50$ Å at 300 K. It is doubtful that dipole scattering has much effect in GaAs under most circumstances.

1.3.2 The analysis of mobility data

Mobility data are commonly used to estimate impurity or defect concentrations in semiconductor materials. The relevant parameters which determine the scattering strengths of the various perturbing potentials are listed in Table 1.3.4. It is usually assumed that the scattering strengths of the lattice-phonon mechanisms are already known; such an assumption is fairly accurate for GaAs, and even for some of the III–V ternary compounds at the present time. The procedure for determining the unknown parameters can then be approached with various levels of sophistication, as discussed below.

Table 1.3.4 Fitting parameters from mobility formulas

Parameter	Equations
Ionized impurity concentration: N_I	(1.3.36)–(1.3.44)
Neutral impurity concentration: N_n	(1.3.45)–(1.3.49)
Alloy-potential factor: $V_c\alpha(1-\alpha)E_{AB}^2$	(1.3.68)
Potential-barrier factor: $Na^6V_0^2$	(1.3.69)
Potential-well factor: E_B/N	(1.3.71)
Space-charge-potential factor: $N\sigma_{sc}$	(1.3.73)
Dipole-potential factor: Nq_d^2	(1.3.76)

1.3.2.1 *Matthiessen's rule*

When several scattering mechanisms are simultaneously present, then the mobility is given by $\mu = e\langle\tau\rangle/m^*$, where

$$\langle\tau\rangle = \left\langle \frac{1}{\tau_1^{-1}+\tau_2^{-1}+\tau_3^{-1}+\cdots}\right\rangle \quad (1.3.77)$$

If all the relaxation times are independent of energy, as would be the case with degenerate electrons, then

$$\tau^{-1} = \tau_1^{-1}+\tau_2^{-1}+\tau_3^{-1}+\cdots$$

or

$$\mu^{-1} = \mu_1^{-1}+\mu_2^{-1}+\mu_3^{-1}+\cdots \quad (1.3.78)$$

Equation (1.3.78) is known as Matthiessen's rule, and it is widely applied in semiconductors as a first approximation. Usually it is assumed that lattice scattering and ionized-impurity scattering are the dominant mechanisms in GaAs, and that the 300 K lattice-limited *Hall* mobility is known (about 8000–8500 cm^2/V-s). Then, if the electrons are nondegenerate, Eqs. (1.3.38) and (1.3.39) give

$$\frac{1}{\mu_{meas}} - \frac{1}{8000} = \frac{1}{\mu_{ii}} = \frac{N_I(\text{cm}^{-3})Z^2[\ln(1+y) - y/(1+y)]}{2.12\times 10^{18}\,T^{3/2}} \quad (1.3.79)$$

where $y = 1.11\times 10^{14}\,T^2/n$ (cm^{-3}). Since μ_{meas} and n are known, and $Z = 1$, in most cases, the value of N_I can be calculated. At 77 K, a lattice-limited *Hall* mobility of about 2.8×10^5 cm^2/V-s should be used (Table 1.3.3). For degenerate electrons, Matthiessen's rule is exact, except that Eqs. (1.3.40) and (1.3.41) should be used for μ_{ii}. The formulas for other mechanisms can be similarly determined.

At this point it is worthwhile mentioning a common problem, which is that reasons other than microscopic scattering often limit the mobility in GaAs, especially at room temperature. For example, geometry, contact size and inhomogeneity are three factors which can have such an influence. Because of this problem, Eq. (1.3.79) should not be applied at room temperature unless μ_{meas} is *significantly* less than 8000 cm^2/V-s, say $\mu_{meas} \lesssim$ 5000 cm^2/V-s; otherwise the resulting N_I may be quite inaccurate.

1.3.2.2 *Wolfe–Stillman method*

The second level of sophistication for GaAs analysis is the empirical Wolfe–Stillman method (Wolfe *et al.*, 1970; Stillman and Wolfe, 1976), which can be applied if the donors are shallow enough that a 77 K

number of n vs. T curves, 4 to 100 K, with the charge-balance equation, to be described later, and obtained accurate donor and acceptor concentrations, N_D and N_A, respectively. Since the hydrogenic donors in GaAs are very shallow (~5 meV), all the donors (and acceptors too, of course) are ionized at 77 K, so that $N_I = N_D + N_A$. These workers then found that an empirical curve, with

$$(N_D + N_A)[\ln(6.94 \times 10^{17}/n_{77}) - 1]$$

as a parameter, could accurately predict the true $(N_D + N_A)$, as obtained by the statistical method. The square-bracketed term in the parameter is easily recognized as the Brooks–Herring screening factor for the case $y \gg 1$. The curve is reproduced in Fig. 1.3.4 (Wolfe *et al.*, 1970). Because the donors

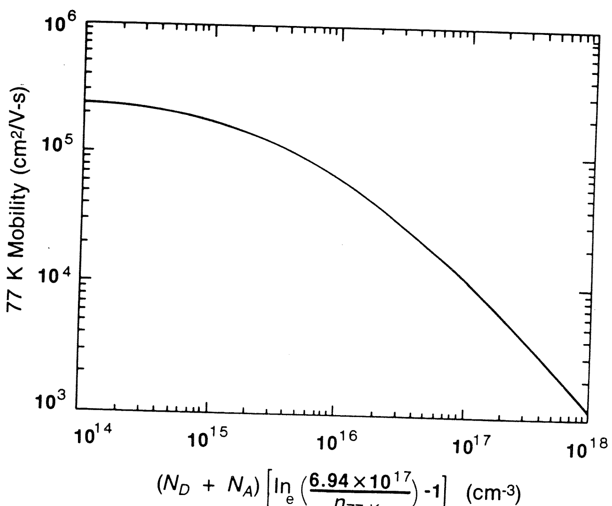

Fig. 1.3.4 The 77 K electron Hall mobility in GaAs vs. an ionized-impurity-concentration expression. The curve was derived empirically. (After Wolfe *et al.* (1970). Reproduced by permission of The American Institute of Physics)

are fully ionized at 77 K, the relationship $n = N_D - N_A$ also holds, so that N_D and N_A can be determined separately.

The Wolfe–Stillman method has proved to be extremely useful for conductive samples in the 10^{14}–$10^{17}\,\text{cm}^{-3}$ range, since very important information can be obtained with a minimum of effort. Two caveats should be pointed out, however: (1) the Hall r-factor was not taken into account in this work, which can result in a 5–30% error (cf. Fig. 1.2.1); and (2) at low compensation ratios, say $N_A/N_D \lesssim 0.2$, the value of N_A is often very inaccurate (so mes even negative!), although the sum, $N_D + N_A$, should not be greatly aиected.

1.3.2.3 *Relaxation-time energy averaging*

A further level of sophistication involves energy averaging of the total scattering rate, i.e.

$$\mu_{\text{meas}} = \frac{e\langle\tau\rangle}{m^*} = \frac{4}{3\pi^{1/2}}\frac{e}{m^*}\int_0^\infty (\tau_1^{-1} + \tau_2^{-1} + \tau_3^{-1} + \cdots)^{-1}\mathscr{E}^{3/2}e^{-\mathscr{E}/kT}\,d\mathscr{E} \quad (1.3.80)$$

The undetermined parameters (Table 1.3.4) in the τ_i are varied until Eq. (1.3.80) is satisfied at each temperature. The accuracy of this method is hurt somewhat by the fact that the relaxation time for polar optical-mode scattering, Eqs. (1.3.60) and (1.3.61), are only approximate; however, at low temperatures, $T < 85$ K, the problem is minimized because (1) the relaxation time is more accurate, and (2) the mechanism is becoming very weak anyway. Equation (1.3.80) can be easily set up on a small computer with common integration subroutines.

1.3.2.4 *Full numerical calculations: comparison with approximate methods*

For maximum accuracy at $T > 85$ K, for which polar optical-mode scattering is important, it is necessary to numerically solve the Boltzmann equation. Several methods are currently in vogue: (1) variational technique; (2) matrix technique; (3) iterative technique; and (4) Monte Carlo technique. The relative merits of each of these methods is discussed at length in Nag's book (Nag, 1980), and, in fact, computer programs for the latter two are given in the appendices of that book. (Note that some errors do exist in these programs.) The iterative technique (Rode, 1970) is perhaps the most popular at this time because it is known to be rapidly convergent. The variational technique, however, has the advantage that analytical formulas can be derived for the first few levels of approximation.

In Table 1.3.5, we compare the values obtained from a numerical method (iterative solution of the Boltzmann equation, with Brooks–Herring ionized-impurity scattering) with those obtained by an approximate method, which consists of using the various mobility formulas presented in Section 1.3.1 and combining them by Matthiessen's rule. The values of the various constants which are typically used in GaAs scattering formulas are presented in Table 1.3.2. When these constants are used with the accurate numerical method mentioned above, a value of $1.03 \times 10^4\,\text{cm}^2/\text{V-s}$ is obtained for μ_H (300 K), and this value is significantly higher than what is observed; i.e., in literally hundreds of measurements in n-type GaAs, with $n < 10^{15}\,\text{cm}^{-3}$, we have never observed $\mu_H > 8.5 \times 10^3\,\text{cm}^2/\text{V-s}$, and we believe that this is also the case in most other laboratories. To determine 'better' constants we have simultaneously fitted the Hall mob‧‧ties in two pure vapor-phase epitaxial GaAs layers (Fig. 1.4.7), and have . .d that the best fit is obtained if the ionized-impurity scattering rate is multiplied by

Table 1.3.5 A comparison of calculated mobilities under various conditions. The 'approximate method' refers to the use of the equations in Section 1.3.1, the constants in Table 1.3.2, and the application of Matthiessen's rule: The 'numerical method' is an iterative fit of the Boltzmann equation. The 'best fit' includes the appropriate constants discussed in the text, which best fit the data shown in Fig. 1.4.7.

	μ (300 K)	μ_H (300 K)	μ (77 K)	μ_H (77 K)
Case 1. $n = 10^{16}$, $N_I = 2 \times 10^{16}$ cm^{-3}				
$N_n = 0$				
Approximate method:				
Table 1.3.2	7.12×10^3		2.06×10^4	
'Best fit'	6.10×10^3		1.51×10^4	
Wolfe–Stillman				1.6×10^4
Numerical method:				
Table 1.3.2	6.59×10^3	7.16×10^3	1.72×10^4	2.26×10^4
'Best fit'	5.04×10^3	5.48×10^3	1.28×10^4	1.68×10^4
Case 2. $n = 10^{12}$ cm^{-3}; $N_I = N_n = 0$				
Approximate method:				
Table 1.3.2	7.73×10^3		2.51×10^5	
'Best fit'	6.72×10^3		2.87×10^5	
Numerical method:				
Table 1.3.2	8.50×10^3	1.03×10^4	2.34×10^5	2.45×10^5
'Best fit'	6.85×10^3	8.34×10^3	2.72×10^5	2.85×10^5

scattering rate by 0.4, and the polar-optical scattering rate by 1.18; these results are designated 'best fit' in Table 1.3.5. It must be emphasized, however, that the changes described here have no particular theoretical significance, and must simply be viewed as fitting parameters. In fact, it is well known that the Brooks–Herring theory itself is inadequate in certain temperature and impurity-concentration ranges (Meyer and Bartoli, 1981a), and that multiple-impurity scattering and nonrandom impurity scattering may have to be considered at higher impurity concentrations (Lancefield *et al.*, 1987). Nevertheless, the 'best fit' data seem to agree fairly well with experimental results that can be checked by other means, say by a fit to the charge-balance equation. For example, as shown in Table 1.3.5, the agreement with the Wolfe–Stillman (W–S) method (Fig. 1.3.4) is good at $n = 10^{16}$ and $N_I = 2 \times 10^{16}$ cm^{-3}, although the 'best fit' mobilities become higher than the W–S mobilities at lower concentrations.

Because 77 K is such a useful characterization temperature, we give in Table 1.3.6 a detailed compilation of μ_H vs. n_H values for various values of the compensation factor N_I/n_H. The error resulting from the use of the Born approximation will be less than 10% for $n_H < 10^{17}$ cm^{-3} and $n_H > 10^{18}$ cm^{-3}, and less than 20% for $10^{17} \lesssim n_H \lesssim 10^{18}$ cm^{-3} (Meyer and Bartoli, 1981a). The magnitudes of other errors, as discussed earlier, are not known at this time, but the table should still be valuable for comparative purposes.

It is also of interest to calculate the temperature dependence of the maximum mobility which could be expected in GaAs. In Fig. 1.3.5 we show the experimental ...

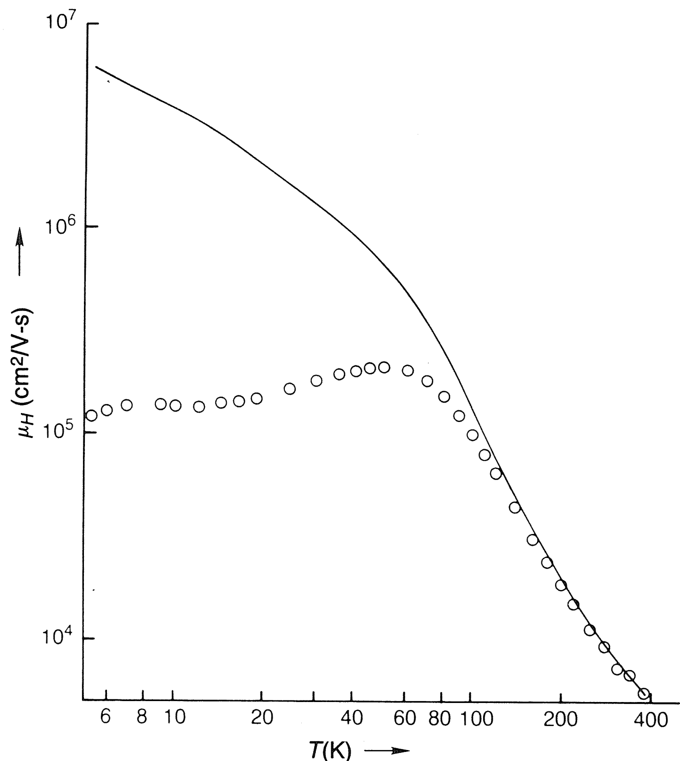

Fig. 1.3.5 The experimental Hall mobility μ_H vs. temperature T for a relatively pure, epitaxial GaAs layer. (After Look and Colter (1983).) Also shown (solid line) is the theoretical lattice-limited mobility which results from setting $N_I = N_n = 0$, in the same sample. (After Sizelove and Look (1988))

1.4.7), and the theoretical μ_H with N_I and N_n set equal to zero, but with the correct values of n included for screening purposes. It is seen that the 4.2 K Hall mobility is about 7.3×10^6 cm^2/V-s, a value which has never been approached in bulk GaAs, but which has nearly been equaled (5×10^6 cm^2/V-s at 2 K) in an AlGaAs/GaAs heterostructure (English *et al.*, 1987). In such a material, which will be discussed more fully in Section 1.3.4, the donors which provide the electrons reside in the AlGaAs, far from the electrons in the pure GaAs. Furthermore, the electrons in the GaAs typically have a relatively large Fermi wave vector and strong screening, so that the background impurities in the GaAs are not as effective in reducing the mobility.

As is further seen in Table 1.3.5, the 'approximate method' gives values of μ which are close enough to the 'best fit' numerical values to constitute a useful technique, especially considering how easy it is to use. However, in most cases it is probably just as convenient to use Table 1.3.6 or the

Table 1.3.6 Low-field Hall mobilities (cm²/V-s) at $T = 77.2\,\mathrm{K}$ for various values of $n_H(\mathrm{cm}^{-3})$ and $N_I/n_H = (N_D^+ + N_A^-)/n_H$. (Note that n_H is the *measured concentration*: $n_H = (eR)^{-1}$)

$n_H(\mathrm{cm}^{-3})$	N_I/n_H 1	2	3	4	5
1×10^{12}	2.85×10^5	2.84×10^5	2.82×10^5	2.80×10^5	2.79×10^5
2	2.84	2.81	2.78	2.75	2.73
5	2.79	2.73	2.67	2.62	2.57
1×10^{13}	2.73	2.62	2.53	2.46	2.39
2	2.62	2.46	2.34	2.23	2.15
5	2.40	2.15	1.97	1.84	1.72
1×10^{14}	2.16	1.84	1.63	1.48	1.35
2	1.86	1.49	1.27	1.11	9.88×10^4
5	1.40	1.02	8.05×10^4	6.73×10^4	5.77
1×10^{15}	1.06	7.08×10^4	5.34	4.30	3.60
2	7.66×10^4	4.70	3.40	2.66	2.19
5	4.66	2.63	1.84	1.41	1.15
1×10^{16}	3.10	1.68	1.16	8.85×10^3	7.19×10^3
2	2.05	1.08	7.42×10^3	5.68	4.61
5	1.21	6.38×10^3	4.38	3.36	2.73
1×10^{17}	8.59×10^3	4.52	3.10	2.37	1.92
2	6.41	3.35	2.28	1.73	1.40
5	4.64	2.37	1.61	1.21	9.8×10^2
1×10^{18}	3.82	1.94	1.30	9.8×10^2	7.9
2	3.24	1.64	1.10	8.3	6.6
5	2.68	1.36	9.1×10^2	6.8	5.5
1×10^{19}	2.34	1.18	7.9	5.9	4.8

$n_H(\mathrm{cm}^{-3})$	N_I/n_H 6	7	8	9	10
1×10^{12}	2.78×10^5	2.76×10^5	2.75×10^5	2.74×10^5	2.72×10^5
2	2.70	2.68	2.66	2.64	2.62
5	2.53	2.49	2.46	2.42	2.39
1×10^{13}	2.33	2.28	2.23	2.19	2.14
2	2.07	2.00	1.94	1.88	1.83
5	1.63	1.54	1.47	1.41	1.35
1×10^{14}	1.25	1.17	1.10	1.03	9.78×10^4
2	8.93×10^4	8.16×10^4	7.52×10^4	6.97×10^4	6.50
5	5.06	4.50	4.06	3.70	3.39
1×10^{15}	3.09	2.71	2.42	2.18	1.99
2	1.86	1.62	1.43	1.29	1.17
5	9.71×10^3	8.41×10^3	7.42×10^3	6.65×10^3	6.03×10^3
1×10^{16}	6.06	5.25	4.64	4.16	3.77
2	3.90	3.38	2.99	2.68	2.43
5	2.31	2.00	1.76	1.58	1.43
1×10^{17}	1.62	1.40	1.23	1.10	9.9×10^2
2	1.17	1.01	8.9×10^2	7.9×10^2	7.1
5	8.1×10^2	7.0×10^2	6.1	5.5	4.9
1×10^{18}	6.6	5.6	4.9	4.4	4.0
2	5.5	4.7	4.2	3.7	3.3
5	4.6	3.9	3.4	3.0	2.7
1×10	4.0	3.4	3.0	2.7	2.4

1.3.3 Inhomogeneity effects on mobility

Every researcher in electrical measurements has encountered samples which exhibit a mobility much below that which can be explained by impurity or defect scattering. On the other hand, there are a few cases in which the mobility is too high (Wolfe and Stillman, 1975a), but such examples are rare. We will be concerned here with inhomogeneous regions which are large compared with the mean free path of the electrons being scattered. Indeed, much smaller regions may simply act as random-scattering centers, so that the theory of Section 1.3.1.7.4 (Eq. (1.3.73)) could be applied. In this section, we will consider two sources of inhomogeneity, both of which affect the magnitude and temperature dependence of the mobility.

1.3.3.1 Spherical conducting inclusions

We assume that a sample of normal conductivity σ and mobility μ has a fraction f of its volume filled with cylindrical inclusions of conductivity σ_0 and the same mobility, μ. Then Voronkov *et al.* (1971) have shown that the *apparent* conductivity is given by

$$\sigma_{\mathrm{app}} = \sigma\left[1 + \frac{3(\sigma_0 - \sigma)}{\sigma_0 + 2\sigma} f\right] \tag{1.3.81}$$

and the Hall coefficient by

$$\sigma_{\mathrm{app}}^2 R_{\mathrm{app}} = \sigma\mu\left[1 + \frac{9\sigma(\sigma_0\mu_0 - \sigma\mu)}{\mu(\sigma_0 + 2\sigma)^2} f\right] \tag{1.3.82}$$

For the case of nonconducting inclusions, i.e., $\sigma_0/\sigma \to 0$, these equations give

$$\mu_{\mathrm{app}} = \mu\frac{1 - 9f/4}{1 - 3f/2} \qquad \sigma_0/\sigma \to 0 \tag{1.3.83}$$

and, for high-conducting inclusions, i.e., $\sigma_0/\sigma \to \infty$, μ_{app} becomes

$$\mu_{\mathrm{app}} = \frac{\mu}{1 + 3f} \qquad \sigma_0/\sigma \to \infty \tag{1.3.84}$$

where these relationships hold only for $f \ll 1$. It is clear that the measured mobility can be considerably less than the microscopic mobility of the host material. Other examples are given by Juretschke *et al.* (1956) and Herring (1960).

1.3.3.2 Potential fluctuations due to compensation

The random distributions of charged impurities and defects give rise to spatial variations of the bands (Shklovskii and Efros, 1971; Efros *et al.*, 1979; Yanchev *et al.*, 1979; Pistoulet *et al.*, 1984). A sch tic view of this phenomenon is given in Fig. 1.3.6 (Pistoulet *et al.*, 1984), in which the mean

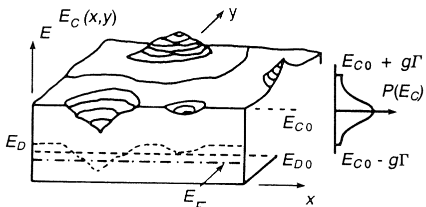

Fig. 1.3.6 A schematic diagram of the conduction band due to potential fluctuations. The various quantities are defined in the text. (After Pistoulet *et al.* (1984). Reproduced by permission of The American Institute of Physics)

conduction-band energy is $\mathscr{E}_{C0}$, and the standard deviation is $\Gamma/\sqrt{2}$. Here it is assumed that the probability distribution for $\mathscr{E}_C$ is a gaussian, given by

$$P(\mathscr{E}_C) = (\Gamma\sqrt{\pi})^{-1} \exp[-(\mathscr{E}_C - \mathscr{E}_{C0})^2/\Gamma^2] \qquad (1.3.85)$$

except that the distribution is truncated at $E_{C0} \pm g\Gamma$, where $g \simeq 2$ or 3, to avoid the effects of very high hills or deep wells. The average total density of nondegenerate electrons n_0 in the conduction band is

$$n_0 = (\Gamma\sqrt{\pi})^{-1} N_C e^{(\mathscr{E}_F - \mathscr{E}_{C0})/kT} \int_{\mathscr{E}_{C0}-g\Gamma}^{\mathscr{E}_{C0}+g\Gamma} e^{(\mathscr{E}_{C0}-\mathscr{E}_C)/kT} e^{-(\mathscr{E}_{C0}-\mathscr{E}_C)^2/\Gamma^2} \, d\mathscr{E}_C \qquad (1.3.86)$$

where N_C is the effective conduction-band density of states (Eq. (C.1.14)). For conductivity, the important parameter is the density of electrons n_{f0} with $\mathscr{E} > \mathscr{E}_{C0}$; this expression can be approximated by

$$n_{f0} = N_C \exp[(\mathscr{E}_F - \mathscr{E}_{C0})/kT] \exp[\beta\Gamma/2kT] \qquad (1.3.87)$$

where $\beta \simeq 0.083$ for $g = 3$. The ratio n_{f0}/n_0 then becomes

$$\frac{n_{f0}}{n_0} = \exp[-(\Gamma/2kT)^{(2-\delta\Gamma/kT)}] \qquad (1.3.88)$$

where $\delta = 0.035$ for $g = 3$. The d.c. conductivity is given by

$$\sigma = q n_{f0} \mu_0 = q n_0 \mu_D \qquad (1.3.89)$$

where $\mu_D = (n_{f0}/n_0)\mu_0$ is the *apparent* drift mobility of the *total* carrier population. Thus, both μ and n are modified from their expected values according to Eqs. (1.3.88) and (1.3.89) respectively.

As an example, we show in Fig. 1.3.7 the effects of band fluctuations on Arrhenius plots for undoped, SI GaAs, with Γ and compensation ratio ($K \equiv N_D^+/N_D = [EL2]^+/[EL2]$) as parameters (Pistoulet *et al.*, 1984). For small K and large Γ, the activation energy E_{D0} can be much different from its expected value of 0.76 eV (i.e. its value for $\Gamma = 0$). Whether or not the

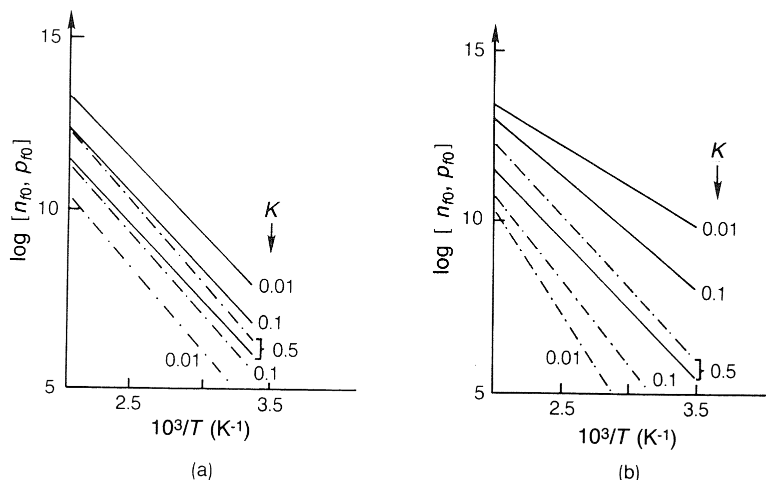

Fig. 1.3.7 The concentrations of electrons n_{f0} (solid lines) and holes p_{f0} (dotted-dashed lines), which carry the current, in an inhomogeneous sample as a function of inverse temperature T^{-1} and compensation ratio $K \equiv N_D^+/N_D$. (a) $\Gamma = 0$ meV, and (b) $\Gamma = 150$ meV. As can be seen, the Arrhenius plots, and thus activation energies, are strongly affected by K and Γ. (After Pistoulet *et al.* (1984). Reproduced by permission of The American Institute of Physics)

fluctuation mechanism has much practical importance in SI GaAs is difficult to assess. For example, in our laboratory, most of the undoped SI wafers have measured E_{D0}s of 0.76 ± 0.01 eV. Thus, the fluctuations seem to have little effect. The case for Cr-doped GaAs, which exhibits mixed conductivity, is discussed by Pistoulet and Hamamdjian (1987).

1.3.4 Scattering in two dimensions

In the materials we have considered so far, the size of the electronic wave function is much smaller than any of the sample dimensions, so that quantum size effects are negligible. The relevant scale here is the de Broglie wavelength, given by

$$\lambda_{deB} = \frac{h}{p} \simeq \frac{h}{\sqrt{(2m^*\mathscr{E})}} \qquad (1.3.90)$$

where $\mathscr{E}$ is the kinetic energy of the electron. At $T = 300$ K, for example, a thermalized electron would have $\mathscr{E} \simeq 0.026$ eV, and therefore a λ_{deB} of about 300 Å. However, an important new class of materials has arisen in the last few years in which the electrons are 'self-confined' in inversion layers which have typical thicknesses of about 100 Å. In such cases the electrons are quantized along the small dimension, and are free to move only along the remaining two dimensions. Hence, the scattering is also in two dimensions, and the matrix elements given in Eq. (1.3.5) must be modified

Consider a prototype heterostructure, $Al_xGa_{1-x}As/GaAs$, with an energy-band diagram as shown in Fig. 1.3.8. The doped $Al_xGa_{1-x}As$

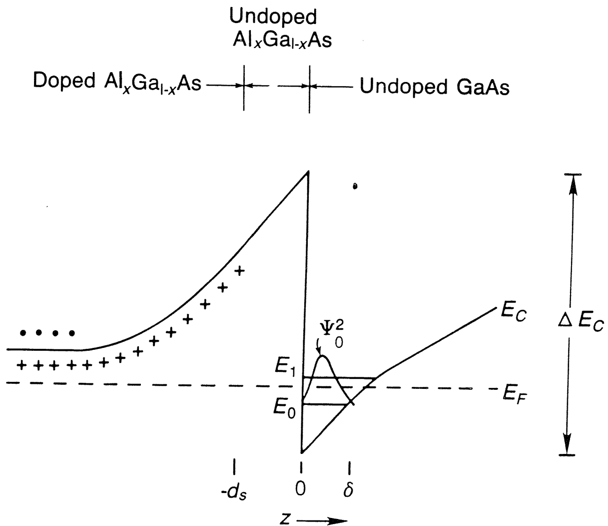

Fig. 1.3.8 The conduction-band diagram for a heterostructure junction. The two lowest sub-band energies, E_0 and E_1, are shown along with the electron density ψ_0^2 of the lowest sub-band. The effective thickness of the two-dimensional electron gas is approximately δ

typically has a donor concentration $N_D \gtrsim 10^{18}\,\mathrm{cm}^{-3}$, while the undoped $Al_xGa_{1-x}As$ and GaAs are much purer. Because of the conduction-band discontinuity ΔE_c between the two materials, electrons in the doped $Al_xGa_{1-x}As$ will transfer to the GaAs conduction band, which has a lower electron energy. However, the resulting positive charge (ionized donors) in the $Al_xGa_{1-x}As$ will bend that band upward in the direction toward the interface. Since the electric field must be continuous across the interface (assuming a negligible change in dielectric constant, and the absence of interface charge), the GaAs band will continue upward at the same slope, although gradually bending back toward the horizontal because of the negative charge (free electrons) which have transferred from the $Al_xGa_{1-x}As$. Thus, a roughly triangular well is formed, and the motion in the z-direction is quantized, forming sub-bands of energy E_0, E_1, E_2, etc. However, the motion in the x- and y-directions is still free.

The electron density in the well region depends on the shapes of the wave functions for the various sub-bands, which are given, in two dimensions, by

$$\psi_{n,\mathbf{k}_\parallel}(\mathbf{r}_\parallel, z) = \zeta_n(z)e^{i\mathbf{k}_\parallel\cdot\mathbf{r}_\parallel} \tag{1.3.91}$$

where $\mathbf{k}_\parallel = \hat{\mathbf{i}}k_x + \hat{\mathbf{j}}k_y$ and $\mathbf{r}_\parallel = \hat{\mathbf{i}}x + \hat{\mathbf{j}}y$. The corresponding subband energies

are

$$E_n(\mathbf{k}_\parallel) = E_n + \frac{\hbar^2 k_\parallel^2}{2m^*} \tag{1.3.92}$$

The $\zeta_n(z)$ can be determined from a variational solution of the Schroedinger equation. The result for the lowest sub-band is (Stern and Howard, 1967; Stern, 1972):

$$\zeta_0(z) = (\tfrac{1}{2}b^3z^2)^{1/2}e^{-bz/2} \tag{1.3.93}$$

where

$$b = \left[\frac{12m^*e^2}{\epsilon\hbar^2}\right]^{1/3}(n_{As} + \tfrac{11}{32}n_s)^{1/3} \tag{1.3.94}$$

in MKS units. Here n_s is the sheet electron density in the two-dimensional region, and n_{As} is the sheet depletion concentration (mainly acceptors) in that same region. For $n_{As} \simeq 0$, and $n_s \simeq 5\times10^{11}\,\mathrm{cm}^{-2}$, we get $b \simeq 34$ Å, which gives an indication of the small extent of the wave function.

To calculate the mobility, we must begin with the matrix element of Eq. (1.3.2):

$$M(\mathbf{k}, \mathbf{k}') = \int_{\substack{\text{Unit}\\\text{cell}}} \psi_{\mathbf{k}'}^*(\mathbf{r})\,\Delta V\,\psi_{\mathbf{k}}(\mathbf{r})\,d\mathbf{r} \tag{1.3.95}$$

where the potential ΔV is usually expanded in a Fourier series:

$$\Delta V = \sum_{\mathbf{q}} A(\mathbf{q})e^{i\mathbf{q}\cdot\mathbf{r}}$$
$$= \sum_{\mathbf{q}} A(\mathbf{q}_\parallel, q_z)e^{i\mathbf{q}_\parallel\cdot\mathbf{r}_\parallel}e^{iq_z z} \tag{1.3.96}$$

Note that in the three-dimensional case, discussed previously, the wave functions were given by $\psi_{\mathbf{k}}(\mathbf{r}) = U_{\mathbf{k}}(\mathbf{r})\exp(i\mathbf{k}\cdot\mathbf{r})$, where $\mathbf{k}$ is the *three*-dimensional wave vector. In that case, (Eq. 1.3.95) vanishes unless $\mathbf{q} = \mathbf{k}' - \mathbf{k}$, which is a statement of momentum conservation. However, the two-dimensional case gives, for an *intra*-sub-band transition ($n \to n$),

$$M_{2D}(\mathbf{k}, \mathbf{k}') = \sum_{\mathbf{q}} \int \zeta_n^*(z)e^{i\mathbf{k}_\parallel\cdot\mathbf{r}_\parallel}A(\mathbf{q}_\parallel, q_z)e^{i\mathbf{q}_\parallel\cdot\mathbf{r}_\parallel}e^{iq_z z}\zeta_n(z)e^{i\mathbf{k}_\parallel\cdot\mathbf{r}_\parallel}\,d\mathbf{r}$$
$$= \sum_{q_z} A(|\mathbf{k}_\parallel - \mathbf{k}'_\parallel|, q_z)\int \zeta_n^*(z)\zeta_n(z)e^{iq_z z}\,dz$$
$$= \sum_{q_z} A(|\mathbf{k}_\parallel - \mathbf{k}'_\parallel|, q_z)I_{nn}(q_z) \tag{1.3.97}$$

Remember that the three-dimensional matrix element (Eq. (1.3.5)) was given by

$$M_{3D}(\mathbf{k}, \mathbf{k}') = A\big(|\mathbf{k} - \mathbf{k}'|\big)\int U_{\mathbf{k}'}^*(\mathbf{r})U_{\mathbf{k}}(\mathbf{r})\,d\mathbf{r}$$
$$= A(|\mathbf{k} - \mathbf{k}'|)I(\mathbf{k}, \mathbf{k}') \tag{1.3.98}$$

where $I(\mathbf{k}, \mathbf{k}')$, the overlap integral, was approximately unity for s-like wave functions. Thus, the two-dimensional matrix element differs from the three-dimensional matrix element by the factor $I_{nn}(q_z)$. For the variational wave function of Eq. (1.3.93),

$$|I_{00}(q_z)|^2 = \frac{b^6}{(b^2 + q_z^2)^3} \tag{1.3.99}$$

Another difference between two- and three-dimensional scattering is in the screening factor. In the three-dimensional case, the screening factor can be easily inferred from Eq. (1.3.28):

$$S_{3D}(q) = \frac{A(\mathbf{q})}{A_s(\mathbf{q})} = \frac{q^2 + \lambda_D^{-2}}{C}\frac{C}{q^2} = 1 + \frac{1}{\lambda_D^2 q^2} = 1 + \frac{e^2 N}{\epsilon k T q^2} \tag{1.3.100}$$

where $C = Ze^2/\epsilon V_c$ and N is simply equal to the free carrier concentration n if the electrons are nondegenerate and if all donors and acceptors are fully ionized. Equation (1.3.28) was derived (see, e.g., Nag, 1980) from the three-dimensional Poisson equation, by allowing the charge to depend upon the potential, which has spherical symmery. In the two-dimensional case, the potential does not have spherical symmetry and the resulting screening factor is entirely different (Stern and Howard, 1967; Grinberg and Shur, 1985; Lei *et al.*, 1985). Following the treatment of Hirakawa and Sakaki (1986) we write S_{2D} as

$$S_{2D} = 1 + \frac{e^2 F(q_\parallel)\Pi(q_\parallel)}{2\epsilon q_\parallel} \tag{1.3.101}$$

where

$$F(q_\parallel) = \int_0^\infty \int_0^\infty \zeta^2(z)\zeta^2(z')e^{-q_\parallel |z-z'|}\,dz\,dz' \tag{1.3.102a}$$

and (Maldague, 1978)

$$\Pi(q_\parallel, T, z) = \int_0^\infty \frac{\Pi(q_\parallel, 0, \xi')}{4kT\cosh^2[(\xi - \xi')/2kT]}\,d\xi' \tag{1.3.102b}$$

where ξ is the Fermi energy and $\Pi(q, 0, \xi)$ is the polarizability function at $T = 0$:

$$\Pi(q_\parallel, 0, \xi) = \frac{m^*}{\pi\hbar^2}\{1 - H(q_\parallel - 2k_F)[1 - (2k_F/q_\parallel)^2]^{1/2}\} \tag{1.3.103}$$

where $H(x)$ is the Heaviside step function and k_F is the Fermi wave vector. For elastic scattering processes, the matrix elements (Eq. (1.3.97)) should be divided by S_{2D}. Various specific cases are considered below. For the variational wave function of Eq. (1.3.93) $F(q_\parallel)$ becomes

$$F(q_\parallel) = \frac{b(8b^2 + 9bq_\parallel + 3q_\parallel^2)}{8(b + q_\parallel)^3}$$

1.3.4.1 *Ionized-impurity scattering*

For charged defects and impurities, the scattering rate is given by (Ando *et al.*, 1982; Hirakawa and Sakaki, 1986):

$$\frac{1}{\tau_{ii,2D}} = \frac{m^* Z^2 e^4}{8\pi\hbar^3\epsilon^2}\int (1 - \cos\theta)\,d\theta \int N_I(z_I)\left[\frac{F(q_\parallel, z_I)}{q_\parallel S(q_\parallel)}\right]^2 dz_I \tag{1.3.104}$$

where $N_I(z_I)$ is the ionized-impurity concentration at position z_I, and

$$F(q_\parallel, z_I) = \int \zeta^2(z)e^{-q|z_I - z|}\,dz$$

Here

$$\begin{aligned} q_\parallel = |\mathbf{k}_\parallel - \mathbf{k}'_\parallel| &= (k_\parallel^2 + k_\parallel'^2 - 2k_\parallel k'_\parallel \cos\theta)^{1/2} \\ &\simeq 2^{1/2}k_\parallel(1 - \cos\theta)^{1/2} \simeq 2k_\parallel \sin(\theta/2) \\ &\simeq 2\sqrt{2}m^{*1/2}\hbar^{-1}[\mathscr{E}(k_\parallel) - \mathscr{E}_0]^{1/2}\sin(\theta/2) \end{aligned} \tag{1.3.105}$$

for electrons in the *lowest* sub-band. Note that the constant in front of Eq. (1.3.104) is the same as that for the three-dimensional case (Eq. (1.3.30)). However, one of the big differences in the two- and three-dimensional ionized-impurity scattering rates is the $F(q_\parallel, z_I)$ term, which can be quite small if the donors are separated from the two-dimensional electrons, as shown in Fig. 1.3.8. It is mainly this fact which makes possible the extremely high mobilities observed in structures that have large spacer thicknesses, d_s (English *et al.* 1987; Harris *et al.*, 1986). However, the screening factor $S(q_\parallel)$ can also significantly affect the ionized-impurity scattering, as is shown in the μ_{ii} vs. n_s data of Fig. 1.3.9. Here the two-dimensional sheet carrier concentration n_s is varied by applying a gate voltage, as will be discussed later. The reason that μ_{ii} is less than $10^6\,\mathrm{cm^2/V\text{-}s}$ in this case, even at $n_s \simeq 10^{12}\,\mathrm{cm^{-2}}$, is the relatively small spacer, $d_s \simeq 45$ Å.

1.3.4.2 *Acoustic-mode deformation-potential scattering*

Following Price (1982) and Hirakawa and Sakaki (1986), the scattering rate for this mechanism is given by

$$\frac{1}{\tau_{dp}} = \frac{3bE_1^2 m^* kT}{32\pi\hbar^3 c_L}\int \frac{1 - \cos\theta}{S^2(q_\parallel)}\,d\theta \tag{1.3.106}$$

where E_1 is the deformation potential (per unit strain), and c_L is the longitudinal elastic constant (c_L is analogous to ρs_L^2 in Eq. (1.3.50)). Equation (1.3.106) makes use of the variational wave function, Eq. (1.3.93). With values of $c_L = 1.44 \times 10^{11}\,\mathrm{N/m^2}$ and $E_1 \simeq 13.5$ eV (Mendez *et al.*, 1984), Hirakawa and Sakaki obtained values of μ_{dp} vs. n_s as shown in Fig. 1.3.9. However, a value of 9.3 eV for E_1 seems to be more acceptable, at present, so that the μ_{dp} curves in Fig. 1.3.9 should be raised by about a

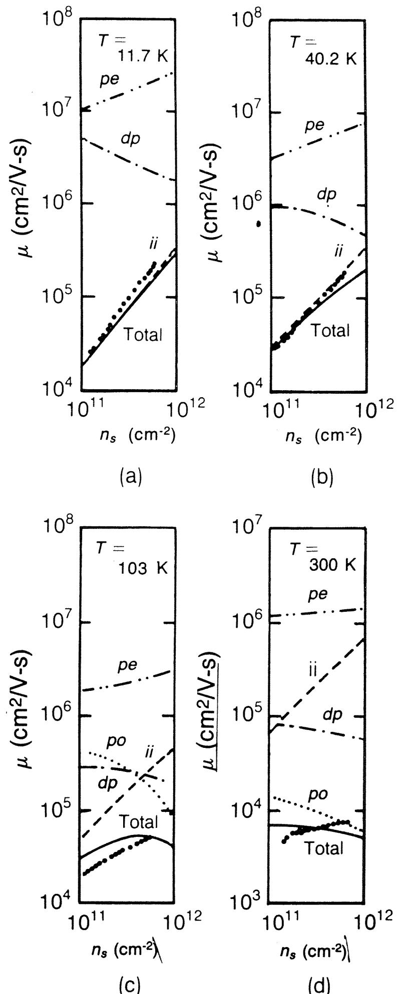

Fig. 1.3.9 The two-dimensional electron mobility μ vs. sheet carrier concentration n_s at various temperatures in an AlGaAs/GaAs heterojunction. The lines are theoretical results, as discussed in Section 1.3.4. (After Hirakawa and Sakaki (1986). Reproduced by permission of The American Institute of Physics)

factor 2. Such a change would indeed seem to give better overall agreement with the theory and experiment. There are also questions regarding the screening of the deformation potential by two-dimensional electrons (Walukiewicz, 1988). These problems must be considered further.

1.3.4.3 *Acoustic-mode piezoelectric-potential scattering*

Again following Price (1984) and Hirakawa and Sakaki (1986), this mechanism gives, for the variational wave function,

$$\frac{1}{\tau_{pe}} = \frac{(eh_{14})^2 m^* kT}{4\pi\hbar^3} \int (1-\cos\theta) \frac{1}{q_\parallel S^2(q_\parallel)} \left[\frac{9}{32c_L} f_L(y) + \frac{13}{32c_T} f_T(y)\right] d\theta \tag{1.3.107}$$

where h_{14} is the relevant component of the piezoelectric tensor (h_{14} is analogous to h_{pz}/ϵ of Eq. (1.3.54)), c_T is the transverse elastic constant ($c_T \simeq \rho s_T^2$), and

$$f_L(y) = \frac{1 + 6y + 12y^2 + 2y^3}{(1+y)^6} \tag{1.3.108a}$$

$$f_T(y) = \frac{13 + 78y + 72y^2 + 82y^3 + 36y^4 + 6y^5}{13(1+y)^6} \tag{1.3.108b}$$

where $y = q/b$. The n_s dependence of μ_{pe} is shown in Fig. 1.3.9, with the following values of the constants: $h_{14} = 1.2 \times 10^9$ V/m and $c_T = 0.49 \times 10^{11}$ N/m^2. Note that if μ_{dp} is increased by a factor 2 in these figures, as suggested earlier, then τ_{pe}^{-1} competes favorably with τ_{dp}^{-1} at the lower temperatures. In fact, in that case the combination of these two lattice-scattering mechanisms would give a mobility of about 5×10^6 cm^2/V-s at $T = 11.7$ K (Fig. 1.3.9a), which is very close to the maximum which has been observed so far (English *et al.*, 1987). Interestingly enough, it is also close to the three-dimensional lattice-limited mobility, as shown in Fig. 1.3.5. Thus, the two-dimensional acoustic-mode lattice scattering is not greatly different than that in three dimensions. This conclusion also holds for polar optical-mode scattering, discussed below.

1.3.4.4 *Polar optical-mode scattering*

To be able to give a relaxation time for polar optical-mode scattering, an inelastic process, we must ignore the 'in-scattering' term. In this approximation (Hirakawa and Sakaki, 1986),

$$\frac{1}{\tau_{po}} = \frac{m^* e^2 \hbar\omega_{L0}}{8\pi^2\hbar^3} \frac{(\epsilon_\infty^{-1} - \epsilon^{-1})}{[1 - f_0(\mathscr{E})]} \int (1-\cos\theta)\{[1 - f_0(\mathscr{E} + \hbar\omega_{L0})] N_q \mathbf{I}(q_{\parallel+}) + [1 - f_0(\mathscr{E} - \hbar\omega_{L0})] H(\mathscr{E} - \hbar\omega_{L0})(N_q + 1)\mathbf{I}(q_{\parallel-})\}\, d\theta \tag{1.3.109}$$

where $\hbar\omega_{LO} \simeq 36.5$ meV is the longitudinal-optical phonon energy ($\hbar\omega_{LO} = kT_{po}$),

$$f_0(\mathscr{E}) = 1/\{1 + \exp[(\mathscr{E} - \mathscr{E}_F)/kT]\} \qquad N_q = 1/[\exp(\hbar\omega_{LO}/kT) - 1]$$

$q_{\parallel +}$ and $q_{\parallel -}$ are the two-dimensional scattering wave vectors for absorption and emission, respectively, and

$$\mathbf{I}(q_{\parallel \pm}) = \int \frac{|I(q_z)|^2}{q_{\parallel \pm}^2 + q_z^2} \, \mathrm{d}q_z \tag{1.3.110}$$

1.3.4.5 Calculation of mobilities

To calculate the total mobility, the various relaxation rates are added,

$$\tau^{-1} = \tau_{ii}^{-1} + \tau_{dp}^{-1} + \tau_{pe}^{-1} + \tau_{po}^{-1}$$

and then averaged according to

$$\mu = \frac{e\langle\tau\rangle}{m^*} = \frac{e}{m^*} \frac{\int_0^\infty \tau(\mathscr{E})\mathscr{E}(\partial f_0(\mathscr{E})/\partial\mathscr{E})\,\mathrm{d}\mathscr{E}}{\int_0^\infty \mathscr{E}(\partial f_0(\mathscr{E})/\partial\mathscr{E})\,\mathrm{d}\mathscr{E}} \tag{1.3.111}$$

where the $q_\parallel$ dependence has been converted to an $\mathscr{E}$ dependence by Eq. (1.3.105). Note that the $\mathscr{E}^{3/2}$ weighting factor in the three-dimensional case has become $\mathscr{E}$ in the two-dimensional case because the two-dimensional density of states is independent of energy. The results for the individual mobilities as well as the total mobility are shown in Fig. 1.3.9 (Hirakawa and Sakaki, 1986).

As is seen, the theoretical μ_{po} decreases quite strongly with n_s, even at 300 K, whereas the experimental data (Hirakawa and Sakaki, 1986) show an opposite dependence on n_s. Vinter (1984) performed a calculation in which the in-scattering terms, as well as inter-sub-band scattering terms were included, but screening was neglected. His results are shown in Fig. 1.3.10, and it is seen that μ_{po} is nearly independent of n_s at 300 K. The experimental data (Hirakawa and Sakaki, 1986; Look *et al.*, 1987) suggest that the weaker n_s dependence is more accurate. For an n_s of about 5×10^{11} cm^{-2}, both calculations give $\mu_{po} \simeq 10^4$ cm^2/V-s, which is quite close to the three-dimensional value, given in Table 1.3.3. It is interesting that both of the two-dimensional calculations discussed in this section, and the three-dimensional calculation discussed earlier, all give nearly the same value of μ_{dp} at 300 K, in spite of the fact that different deformation potentials were used in these calculations, ranging from 9.3 to 13.5 eV. (The 7 eV value quoted in Vinter (1984) is a misprint; it should read 10 eV.) Evidently some of the other differences in the calculations cancel each other out. For μ_{pe}, Vinter's two-dimensional calculation is quite close to the three-dimensional value (Table 1.3.3) at 77 K, but Hirakawa and Sakaki's two-dimensional

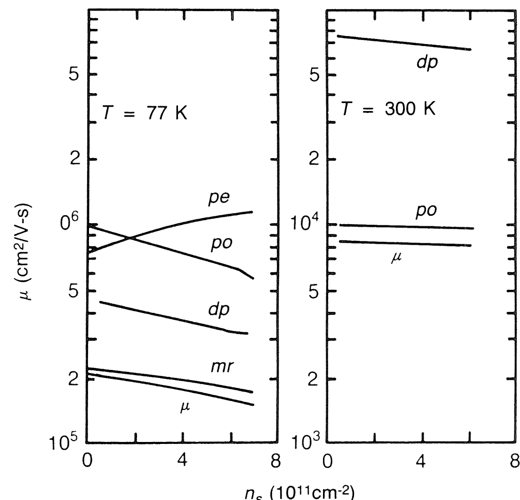

Fig. 1.3.10 The calculated two-dimensional electron mobilities for various scattering mechanisms (Section 1.3.4) in an AlGaAs/GaAs heterojunction at 300 and 77 K. The line designated 'μ' results from an accurate numerical calculation of the total mobility (Section 1.3.2.4), while that designated '*mr*' results from an application of Matthiessen's rule (Section 1.3.2.1). (After Vinter (1984). Reproduced by permission of The American Institute of Physics)

value is about a factor 2 higher. However, the overall conclusion is that lattice scattering is not greatly different in two and three dimensions, over a rather large temperature range, roughly 5–300 K. This conclusion is reinforced by comparing the three-dimensional calculation, illustrated in Fig. 1.3.5, with the two-dimensional experimental data of English *et al.* (1987). The main differences in two- and three-dimensional scattering result from the ionized-impurity contributions.

1.4 SEMICONDUCTOR STATISTICS: CARRIER CONCENTRATION

The carrier concentration is related to the physical parameters by means of statistical theory, just as the mobility was related through the use of scattering theory. Blakemore (1983) has written an excellent book on this latter subject, and Look (1981) has given a derivation of the relevant equations and has summarized the earlier contributions (Landsberg, 1952; Guggenheim, 1953; Landsberg, 1956; Champness, 1956; Shockley and Last, 1957; Teitler and Wallis, 1960; Clark, 1980). It is well known that the

energy distribution function for electrons in an energy band is described by

$$f(\mathscr{E}) = \frac{1}{1 + e^{(\mathscr{E} - \mathscr{E}_F)/kT}} \tag{1.4.1}$$

where $f(\mathscr{E})$ is the distribution function and $\mathscr{E}_F$ is the Fermi energy. However, the proper distribution functions for localized levels, such as impurities or defects, are not as well known. It is often assumed that a generalized distribution function can be written as

$$f(\mathscr{E}) = \frac{1}{1 + Ke^{(\mathscr{E} - \mathscr{E}_F)/kT}} \tag{1.4.2}$$

where K is a *degeneracy factor*. In the past most researchers have used one or three values for K: $K = 1$ for band electrons; $K = \frac{1}{2}$ for electrons on a donor center; and $K = 4$ for electrons on an acceptor center. In fact, the actual situation is not that simple, and some of the complexities are discussed in Section 1.4.2, along with simple rules that allow determination of the proper degeneracy factor. Because of these and other problems in the understanding of distribution functions, a detailed derivation of the relevant equations is carried out in Appendix C. Only the results will be presented in this section.

1.4.1 Donors and acceptors

Consider the group-IV impurity Si placed on a Ga site (Si_{Ga}) in the GaAs lattice. The Si has four electrons in its outer shell, whereas the Ga it replaced had only three. Thus, only three of the four Si electrons are needed for bonding purposes, and the fourth spreads out into a large (~100 Å) orbit, bound to the positive Si core by only about 5 meV. Thus, at temperatures $kT > 5$ meV, or $T > 60$ K, a large fraction of these electrons are 'donated' to the conduction band.

Conversely, consider the group-II impurity Cd placed on the same Ga site. Since Cd has only two outer-shell electrons, it will attempt to 'accept' an electron from a donor impurity in order to satisfy all the bonding requirements. The accepted electron, in this case, will be bound by about 1.49 eV, and a temperature greater than 17 000 K(!) would be required to dislodge it.

There could, of course, be more complicated cases. For example, Ag on a Ga site could accept two electrons, although the second electron may not necessarily be bound, i.e., its energy level may lie above the conduction-band minimum. A case in point is Cr_{Ga}, which can bind the first electron with about 0.7 eV. The excitation of this electron to the conduction band is described by the equation $Cr^{2+} + 0.7\,\text{eV} \rightarrow Cr^{3+} + e_{CB}$, which is denoted by (2+/3+). Note here that Cr^{3+} specifies the *neutral* Cr_{Ga} configuration; in some work the neutral state is specified by Cr^0. Cr has yet another acceptor level, (+/2+), but this level is about 0.1 eV above the conduction

band, and thus is unstable to auto-ionization (Hennel *et al.*, 1981). Finally, Cr has a donor level, (3+/4+), about 0.3 eV above the valence band (Look *et al.*, 1982).

We also must consider defects as well as impurities. For example, As_{Ga} is a very important defect (related to EL2) that should have two electrons available for donation. Also, the Ga vacancy, V_{Ga}, would seemingly want to accept up to three electrons to satisfy bonding requirements. There is a multitude of literature on both experimental and theoretical investigations of these levels. Reviews covering material up through 1983 have been written by Neumark and Kosai (1983), and by Blakemore and Rahimi (1984), and more recent theoretical work has been carried out by Baraff and Schluter (1985, 1986) and others.

It is clear from this brief discussion that various centers can be quite complex, even exhibiting both donor and acceptor nature. Thus, we must not speak merely of *donors* and *acceptors*, but rather of donor and acceptor *transitions*. A *donor transition* occurs when a neutral center loses an electron, or a positively-charged center gains or loses an electron, while an *acceptor transition* occurs when a neutral center gains an electron, or a negatively charged center gains or loses an electron. Often the word 'level' is used to refer to the energy of a particular transition; here, we will use 'level' synonomously with 'transition'.

1.4.2 Occupation probability

We suppose that there is a density N_k of type-k centers, with various possible charge states $l = 0, 1, 2, \ldots, l_k$, and excited states $m_l = 0, 1, 2, \ldots, m_{kl}$ within each charge state. Let the density of N_k centers which have charge-state l and excited state m_l be donated by n_{klm}, and their degeneracy by g_{klm}. Then, it is shown in Appendix C that

$$\frac{n_{klm}}{N_k} \equiv f(\mathscr{E}_{klm}) = \frac{1}{1 + \sum\limits_{l',m' \neq l,m} \frac{g_{kl'm'}}{g_{klm}} \exp\left([\mathscr{E}_{klm} - \mathscr{E}_{kl'm'} - (l - l')\mathscr{E}_F]/kT\right)} \tag{1.4.3}$$

where the summation restriction means that $l' \neq l$ and $m' \neq m$, *at the same time*. Note, incidently, that Eq. (1.4.3) can be quite different from the simple version of $f(\mathscr{E})$, Eq. (1.4.2). In particular, there is often no value of K which can properly give the temperature dependence of $f(\mathscr{E})$.

The energies in Eq. (1.4.3) are measured with respect to the valence-band edge, in order to keep them all positive (except for the case of a degenerate hole gas). Let $\mathscr{E}_0$ represent the energy of the highest state that is still resonant with the valence band, and let $\mathscr{E}_1$ represent the next higher state, created by adding an electron. The additional energy necessary to create $\mathscr{E}_1$ from $\mathscr{E}_0$ is not really $\mathscr{E}_1 - \mathscr{E}_0$, but $\mathscr{E}_1 - \mathscr{E}_{VB}$, because part of the energy, i.e.,

$\mathscr{E}_{VB} - \mathscr{E}_0$, is already available in the system. Thus, we can effectively set $\mathscr{E}_0 = \mathscr{E}_{VB}$. Therefore, $\mathscr{E}_1 - \mathscr{E}_0$ is the energy necessary to add one electron to the center, $\mathscr{E}_2 - \mathscr{E}_0$, two electrons, $\mathscr{E}_3 - \mathscr{E}_0$, three electrons, etc. Now it is extremely important to note that we do not measure these *multi-electron* energies in experiments, but instead we measure *single-electron* transition energies, defined as $E_1 \equiv \mathscr{E}_1 - \mathscr{E}_0$, $E_2 \equiv \mathscr{E}_2 - \mathscr{E}_1$, $E_3 = \mathscr{E}_3 - \mathscr{E}_2, \ldots, E_l = \mathscr{E}_l - \mathscr{E}_{l-1}$. However, it is easier to present the theory in terms of the multi-electron energies.

Some applications of Eq. (1.4.3) are given below.

1.4.2.1 *The degeneracy factor: band states vs. donor states*

A model of rather general importance in semiconductor statistics is based on a 'box' which can hold zero, one, or two electrons, illustrated in Fig. 1.4.1. For example, this model can be applied to a band state, with

$\mathscr{E}_2 = 2\mathscr{E}_1$ — $g_2 = 1$; $\mathscr{E}_1$ — $g_1 = 2$; $\mathscr{E}_0 = 0$ — $g_0 = 1$ (a) band states

$\mathscr{E}_2 \gg 2\mathscr{E}_1$ — $g_2 = 1$; $\mathscr{E}_1$ — $g_1 = 2$; $\mathscr{E}_0 = 0$ — $g_0 = 1$ (b) *s*-like donor states

Fig. 1.4.1 A schematic diagram of the major difference between (a) band states and (b) *s*-like donor states as it affects their respective degeneracy factors. (It is the assumption $\mathscr{E}_2 \gg \mathscr{E}_1$ that leads to the famous degeneracy factor of $\frac{1}{2}$ for donor states)

(k_x, k_y, k_z) quantum numbers, or an *s*-like donor state, with its own appropriate quantum numbers, since each of these states can hold up to two electrons because of spin degeneracy. We ignore excited states (i.e. within a given charge state) and suppress the index k, so that the summation is over $l = 0$, 1, and 2, with corresponding degeneracies $g_0 = 1$, $g_1 = 2$, and $g_2 = 1$ (see Fig. 1.4.1). Then Eq. (1.4.3) yields

$$n_0 = \frac{N}{1 + \dfrac{g_1}{g_0} e^{(\mathscr{E}_0 - \mathscr{E}_1 + \mathscr{E}_F)/kT} + \dfrac{g_2}{g_0} e^{(-\mathscr{E}_2 + 2\mathscr{E}_F)/kT}}$$

$$= \frac{N}{1 + 2e^{(-\mathscr{E}_1 + \mathscr{E}_F)/kT} + e^{(-\mathscr{E}_2 + 2\mathscr{E}_F)/kT}} \quad (1.4.4)$$

$$n_1 = \frac{N}{1 + \frac{1}{2}e^{(\mathscr{E}_1 - \mathscr{E}_F)/kT} + \frac{1}{2}e^{(\mathscr{E}_1 - \mathscr{E}_2 + \mathscr{E}_F)/kT}} \quad (1.4.5)$$

$$n_2 = \frac{N}{1 + e^{(\mathscr{E}_2 - 2\mathscr{E}_F)/kT} + 2e^{(\mathscr{E}_2 - \mathscr{E}_1 - \mathscr{E}_F)/kT}} \quad (1.4.6)$$

where we have set $\mathscr{E}_0 = 0$.

1.4.2.1.1 *Band states.*

For band states, the wave functions are large, spread throughout the crystal. Thus, the electron–electron repulsion is small, and we expect that $\mathscr{E}_2 \simeq 2\mathscr{E}_1$. The *average* number of electrons is then given by

$$n_{av} = n_1 + 2n_2 = \frac{N}{1 + \frac{1}{2}e^{(\mathscr{E}_1 - \mathscr{E}_F)/kT} + \frac{1}{2}e^{(-\mathscr{E}_1 + \mathscr{E}_F)/kT}} + \frac{2N}{1 + e^{(2\mathscr{E}_1 - 2\mathscr{E}_F)/kT} + 2e^{(\mathscr{E}_1 - \mathscr{E}_F)/kT}}$$

$$= \frac{N}{1 + \frac{1}{2}x + \frac{1}{2}\dfrac{1}{x}} + \frac{2N}{1 + x^2 + 2x}$$

$$= \frac{2N(1+x)}{1 + x^2 + 2x} = \frac{2N}{1+x} = \frac{2N}{1 + e^{(\mathscr{E}_1 - \mathscr{E}_F)/kT}} \quad (1.4.7)$$

where we have used $x \equiv \exp(\mathscr{E}_1 - \mathscr{E}_F)/kT$. This is just the expected result, since the *total* number of states, because of spin, is twice the number of (k_x, k_y, k_z) band states. Thus, we have derived Eq. (1.4.1), since $f(\mathscr{E}) = n_{av}/2N$.

1.4.2.1.2 *Donor states.*

The *s*-like donor states can be described by exactly the same model, except that now the electron–electron repulsion is very strong, because of the wave-function localization. Therefore, it is expected that $\mathscr{E}_2 \gg 2\mathscr{E}_1$, and we can let $\exp(\mathscr{E}_2/kT) \to \infty$, and $\exp(-\mathscr{E}_2/kT) \to 0$. Then n_{av} becomes

$$n_{av} = n_1 + 2n_2 = \frac{N}{1 + \frac{1}{2}e^{(\mathscr{E}_1 - \mathscr{E}_F)/kT} + 0} + \frac{2N}{1 + \infty + \infty}$$

$$= \frac{N}{1 + \frac{1}{2}e^{(\mathscr{E}_1 - \mathscr{E}_F)/kT}} \quad (1.4.8)$$

Here we have derived the well-known Fermi function for shallow, *s*-like donors, i.e. Eq. (1.4.2) with $K = \frac{1}{2}$. Note that the degeneracy factor of $\frac{1}{2}$ arises simply because of the strong electron–electron repulsion assumed, which keeps the two-electron state from ever being occupied at normal temperatures.

Often, the *ionized* donor density n^+ is the quantity used in calculations. It

is easy to see that

$$n^+ = N - n^0 = N - n_{av} = \frac{N}{1 + 2e^{-(\mathscr{E}_1 - \mathscr{E}_F)/kT}} \tag{1.4.9}$$

where the degeneracy factor is now 2. Equation (1.4.9) illustrates the fact that the 'value' of the degeneracy factor depends on whether the *occupied* or *unoccupied* state is being considered. The occupied state is neutral and the unoccupied state is charged, for single-level *donors*, while the opposite is true for single-level *acceptors*. This potential ambiguity must be considered when reading the literature.

It is more usual to relate donor energies to the conduction band. Then, $\mathscr{E}_{1CB} = \mathscr{E}_1 - \mathscr{E}_G \equiv -E_D$, where E_D is the donor *activation* energy, a positive quantity. Also, we can let $\mathscr{E}_{FCB} = \mathscr{E}_F - \mathscr{E}_G \equiv -E_F$. Then Eq. (1.4.9) becomes

$$n^+ = \frac{N}{1 + 2e^{-(\mathscr{E}_{1CB} - \mathscr{E}_{FCB})/kT}} = \frac{N}{1 + 2e^{(E_D - E_F)/kT}} \tag{1.4.10}$$

1.4.2.2 *Excited states of shallow donors*

A neutral shallow donor in GaAs has a spectrum of excited states just as a hydrogen atom does. However, it is likely that the *occupied* state has excited states within the band gap. Then, the *unoccupied* state density is given by

$$\begin{aligned} n_{D0} &= \frac{N_D}{1 + \sum_{m'} \frac{g_{D1m'}}{g_{D00}} e^{(-\mathscr{E}_{D1m'} + \mathscr{E}_F)/kT}} \\ &= \frac{N_D}{1 + \frac{g_{D10}}{g_{D00}} e^{(-\mathscr{E}_{D10} + \mathscr{E}_F)/kT} \sum_{m'} \frac{g_{D1m'}}{g_{D10}} e^{(\mathscr{E}_{D10} - \mathscr{E}_{D1m'})/kT}} \\ &= \frac{N_D}{1 + \frac{g_{D10}}{g_{D00}} e^{(-\mathscr{E}_{D10} + \mathscr{E}_F)/kT}(1 + F)} \end{aligned} \tag{1.4.11}$$

where

$$F = \sum_{m' \neq 0} \frac{g_{D1m'}}{g_{D00}} e^{(\mathscr{E}_{D10} - \mathscr{E}_{D1m'})/kT} \tag{1.4.12}$$

Equation (1.4.11) has been applied to the study of shallow donors in GaAs (Eddolls *et al.*, 1967; Carballes *et al.*, 1969) by setting

$$\mathscr{E}_{D1m'} - \mathscr{E}_{D10} = \mathscr{E}_{D10}[1 - (m' + 1)^{-2}] \quad \text{and} \quad g_{D1m'}/g_{D10} = (m' + 1)^2$$

in analogy the case for the hydrogen atom. Although the data in these studies could indeed be fitted much better with the $(1 + F)$ term included,

the model itself suffers from the neglect of such important factors as wave-function overlap, which begins to affect the excited states before the ground state, as N_D increases. As discussed by Stillman and Wolfe (1976), and illustrated in Fig. 1.4.2, it is reasonable to treat the overlapping excited

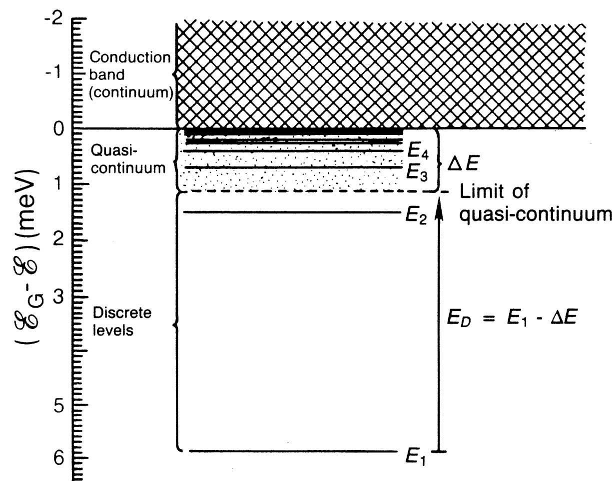

Fig. 1.4.2 Excited states of hydrogenic donors in GaAs. The activation energy of an *isolated* donor is E_1, but at higher donor concentrations the activation energy is reduced to $E_1 - \Delta E$, due to overlap of the excited-state wave functions and the consequent formation of a quasi-continuum of width ΔE. (After Stillman and Wolfe (1976). Reproduced by permission of Elsevier Sequoia SA)

states, of width ΔE, as part of the band continuum, which has the effect of reducing $\mathscr{E}_G - \mathscr{E}_{D10}$ and also reducing the number of excited states which should be included. The correct number of excited states can be determined from the data of Fig. 1.4.3 (Stillman and Wolfe, 1976), which relates the *measured* E_D to the doping concentration N_D. Thus, for example, if $N_D > 10^{15}$ cm^{-3}, no excited states should be included in the analysis.

In fact, the decrease of the effective E_D with increasing N_D (and N_A also) is a complicated problem, which has been described in terms of screening, band tailing, impurity-band formation, potential fluctuations, and other phenomena. (See, e.g., Neumark and Schroder, 1981; Fedders, 1982; Lowney, 1986; Bennett and Lowney, 1987.) For example, consider the data in Fig. 1.4.4 (Stillman and Wolfe, 1976), from which E_D is normally measured by the $\ln n$ vs. T^{-1} slope at low temperature. Not only does the measured E_D decrease with increasing n, but also the curves begin to turn back up at low temperatures, for $n > 5 \times 10^{14}$ cm^{-3}. Thi havior is due to conduction in the donor levels themselves, rather than the conduction

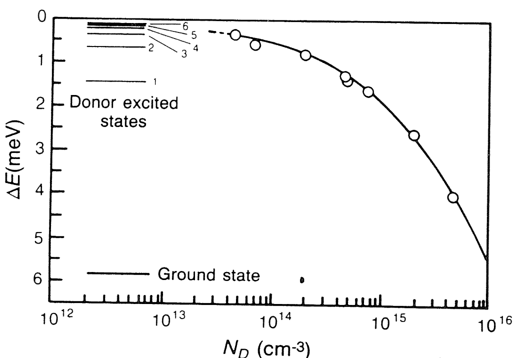

Fig. 1.4.3 The width ΔE of the quasi-continuum as a function of donor concentration N_D. Note that for $N_D \gtrsim 8 \times 10^{14}\,\mathrm{cm}^{-3}$, the quasi-continuum encompasses all states but the ground state. (After Stillman and Wolfe (1976). Reproduced by permission of Elsevier Sequoia SA)

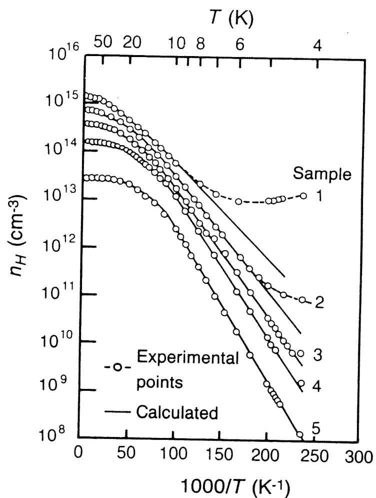

Fig. 1.4.4 Experimental (points) and theoretical (solid lines) variations of the electron Hall concentration n_H as a function of inverse temperature T^{-1} for several samples of different concentrations. Note that the activation energy (the low-temperature slope) decreases as N_D increases. (After Stillman and Wolfe (1976). Reproduced by permission of Elsevier Sequoia SA)

band (Emel'yanenko *et al.*, 1973; Velichko *et al.*, 1979; Sites and Nedoluha, 1981; Benzaquen and Walsh, 1984). A stronger example of heavy-doping effects is given in Fig. 1.4.5. Note that at very high carrier concentrations,

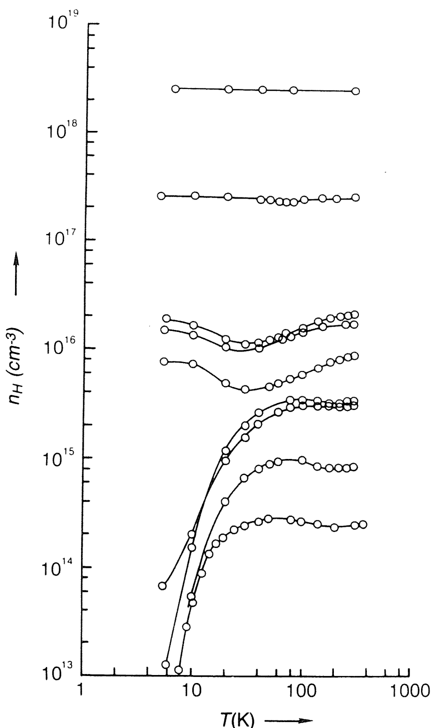

Fig. 1.4.5 The Hall electron concentration n_H vs. temperature T for a range of concentrations. At the mid-$10^{15}\,\mathrm{cm}^{-3}$ range, impurity-banding effects become evident at low temperatures. Above $10^{18}\,\mathrm{cm}^{-3}$, n_H is temperature- independent

the impurity band formed from the donor levels has merged with the conduction band, and the conductivity is indicative of a degenerate electron gas, i.e. the electrical properties are nearly temperature-independent. It is clear that carrier-concentration data, especially at low temperatures, need to be analyzed very carefully before any conclusions are drawn.

1.4.3 Charge-balance equation

Although we can write precise expressions for the occupation probabilities by means of Eq. (1.4.3), the actual magnitudes depend on a knowledge of

the Fermi energy $\mathscr{E}_F$. This quantity is usually obtained by solving the charge-balance equation for the problem. In simple terms, the negative charges must balance the positive charges, or

$$n + \sum_k N_{Ak}^- = p + \sum_k N_{Dk}^+ \tag{1.4.13}$$

where only single-level centers ($l = 0$ or 1) are being considered at this point. In practice, the great majority of samples are analyzed by one of two equations which are given below.

1.4.3.1 *n-type sample; donor dominant*

Here we assume that $n \gg p$ and, over the temperature range of interest, $\mathscr{E}_F$ remains *more* than a few kT from every level except one, a donor, which we will call the *dominant* donor. Then, only that particular donor's Fermi function is temperature-dependent, and the rest of the donors and acceptors satisfy the following equalities: (1) $N_{Ak}^- = N_{Ak}$ if $\mathscr{E}_{Ak1} < \mathscr{E}_F$; (2) $N_{Ak}^- = 0$ if $\mathscr{E}_{Ak1} > \mathscr{E}_F$; (3) $N_{Dk}^+ = N_{Dk}$ if $\mathscr{E}_{Dk1} > \mathscr{E}_F$; and (4) $N_{Dk}^+ = 0$ if $\mathscr{E}_{Dk1} < \mathscr{E}_F$. (The definition of '>' here means a few kT greater.) These temperature-independent terms can all be lumped together, since they cannot be fitted separately anyway, into a term N_A^{net}:

$$N_A^{\text{net}} = \sum_{\substack{k \\ \mathscr{E}_{Ak} < \mathscr{E}_F}} N_{Ak} - \sum_{\substack{k \\ \mathscr{E}_{Dk} > \mathscr{E}_F}} N_{Dk} \tag{1.4.14}$$

Then Eq. (1.4.13) becomes

$$n + N_A^{\text{net}} = N_D^+ = n_{D0} = \frac{N_D}{1 + \dfrac{g_{D1}}{g_{D0}} e^{(-\mathscr{E}_{D1} + \mathscr{E}_F)/kT}} \tag{1.4.15}$$

To put the exponential term in a more tractable form, we can write $\mathscr{E}_1 = \mathscr{E}_G + \mathscr{E}_{1CB} = \mathscr{E}_G - E_D$, where E_D is the (positive) activation energy, and

$$n = N_C e^{(\mathscr{E}_F - \mathscr{E}_G)/kT} \tag{1.4.16}$$

where N_C is the effective conduction-band density of states, if Boltzmann statistics apply. At this stage, we can either solve Eq. (1.4.15) for $\mathscr{E}_F$ or write the whole equation in terms of n, by using Eq. (1.4.16) for $\mathscr{E}_F$ in the last term. In the latter case, Eq. (1.4.15) becomes

$$n + N_A^{\text{net}} = \frac{N_D}{1 + \dfrac{g_{D1}}{g_{D0}} \dfrac{n}{N_C} e^{E_D/kT}} = \frac{N_D}{1 + n/\phi_D} \tag{1.4.17}$$

where

$$\phi_D = \frac{g_{D0}}{g_{D1}} N_C e^{-E_D/kT}$$
$$= \frac{g_{D0}}{g_{D1}} N_C' e^{\alpha_D/k} T^{3/2} e^{-E_{D0}/kT} \tag{1.4.18}$$

where $N_C' = 2(2\pi m^* k)^{3/2}/h^3$, and $E_D = E_{D0} - \alpha_D T$. (A linear temperature dependence for E_D is usually sufficient over a reasonable temperature range.) A plot of n vs. T then has four fitting parameters: N_D, N_A^{net}, E_{D0}, and $(g_{D0}/g_{D1}) \exp(\alpha_D/k)$. It is sometimes convenient to write a quadratic equation in n from Eq. (1.4.17); the solution is

$$n = \tfrac{1}{2}(\phi_D + N_A^{\text{net}}) \left\{ \left[1 + \frac{4\phi_D(N_D - N_A^{\text{net}})}{(\phi_D + N_A^{\text{net}})^2} \right]^{1/2} - 1 \right\} \tag{4.4.19}$$

Three limiting cases are important here.

1.4.3.1.1 Low temperature, with $\phi_D \ll N_A^{\text{net}}$, $(N_A^{\text{net}})^2/(N_D - N_A^{\text{net}})$. In this case, the square-root term in Eq. (1.4.19) can be expanded to give

$$n \simeq \tfrac{1}{2}(\phi_D + N_A^{\text{net}}) \frac{2\phi_D(N_D - N_A^{\text{net}})}{(\phi_D + N_A^{\text{net}})^2}$$
$$= (N_D - N_A^{\text{net}})\phi_D = (N_D - N_A^{\text{net}}) \frac{g_{D0}}{g_{D1}} N_c' e^{\alpha_D/k} T^{3/2} e^{-E_{D0}/kT} \tag{1.4.20}$$

Thus, a plot of $\ln(n/T^{3/2})$ vs. $1/T$ should give a straight line with slope $-E_{D0}/k$.

1.4.3.1.2 Low temperature, with $\phi_D \gg N_A^{\text{net}}$; $\phi_D \ll (N_D - N_A^{\text{net}})$. The important distinction here is that $\phi_D \gg N_A^{\text{net}}$ even while $\phi_D \ll (N_D - N_A^{\text{net}})$, which can occur only for extremely small N_A^{net}. In this case, the second term in the square-root bracket is $\gg 1$, and n becomes

$$n = \tfrac{1}{2}\phi_D \frac{2(N_D - N_A^{\text{net}})^{1/2}}{\phi_D^{1/2}} = (N_D - N_A^{\text{net}})^{1/2} \phi_D^{1/2}$$
$$= (N_D - N_A^{\text{net}})^{1/2} \left[\frac{g_{D0}}{g_{D1}} N_C' e^{\alpha_D/k} \right]^{1/2} T^{3/4} e^{-E_{D0}/2kT} \tag{1.4.21}$$

Note that now a plot of $\ln(n/T^{3/4})$ vs. $1/T$ has a slope of $-E_{D0}/2k$, rather than $-E_{D0}/k$. Such an occurrence is very improbable in GaAs, because it is difficult to make material with low enough N_A/N_D, say with $N_A/N_D < 0.1$ (Wolfe and Stillman, 1975b). However, there are a few cases in which N_A/N_D is smaller, and one of these is presented in Fig. 1.4.6 (Look and Colter, 1983). Here sample RR-126 has a normal compensation ratio (0.28) while sample RR-98 has a much smaller ratio (0.06). N that RR-98 has a distinct region with a slope -2.3 meV$/k$, as well as a region with the

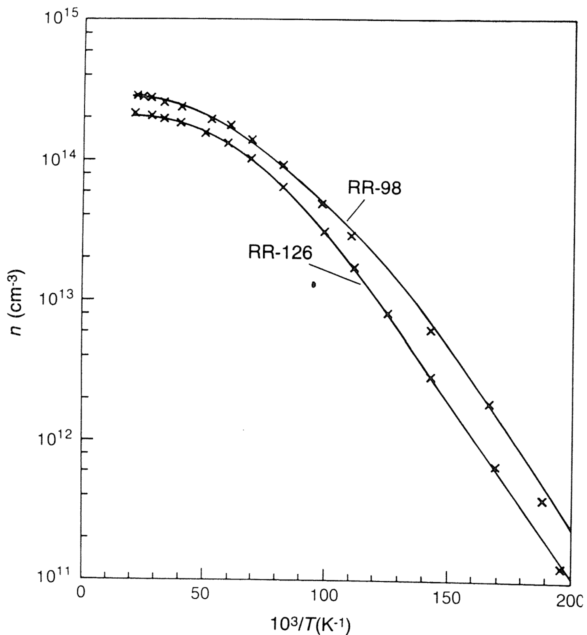

Fig. 1.4.6 The electron concentration n vs. inverse temperature T for two GaAs epitaxial layers, one of normal compensation (RR-126), and one of low compensation (RR-98). The solid lines are least-squares fits by Eq. (1.4.17), with the following parameters: RR-126: $N_D = 3.2 \times 10^{14}\,\text{cm}^{-3}$, $N_A = 1.1 \times 10^{14}\,\text{cm}^{-3}$, $E_{D0} = 4.3$ meV, $(g_0/g_1)\exp(\alpha/k) \simeq 1$; RR-98: $N_D = 3.1 \times 10^{14}\,\text{cm}^{-3}$, $N_A = 2.5 \times 10^{13}\,\text{cm}^{-3}$, $E_{D0} = 4.7$ meV, $(g_0/g_1)\exp(\alpha/k) \simeq 1$. (After Look and Colter (1983). Reproduced by permission of The American Institute of Physics)

expected slope, $-4.7\,\text{meV}/k$. The reason is that ϕ_D indeed is larger than N_A^{net} over a small region, $80 < T < 120$ K, but then becomes smaller than N_A^{net} for $T < 80$ K. The other sample, RR-126, has no region for which $\phi_D > N_A^{\text{net}}$ and thus the slope is $-4.3\,\text{meV}/k$ over the whole low-temperature range. (Note that $E_D(\text{RR-126}) < E_D(\text{RR-98})$ because of screening, as discussed earlier).

The low value of N_A for sample RR-98 also affects the shape of the mobility curve, as seen in Fig. 1.4.7 (Look and Colter, 1983). As was found in Eq. (1.3.33) the mobility due to ionized-impurity scattering varies as $T^{3/2}/N_I = T^{3/2}/(2N_A + n)$. At very low T, such that $n \ll N_A$, μ increases with T, as $T^{3/2}$. At somewhat higher T, around 10 K, $n \sim N_A$, and n is increasing much faster than $T^{3/2}$; therefore, μ decreases with T. At still higher T, about 20 K, n begins to saturate and increases more slowly than $T^{3/2}$; thus, μ again begins to increase with T. Finally, above 80 K, lattice scattering becomes

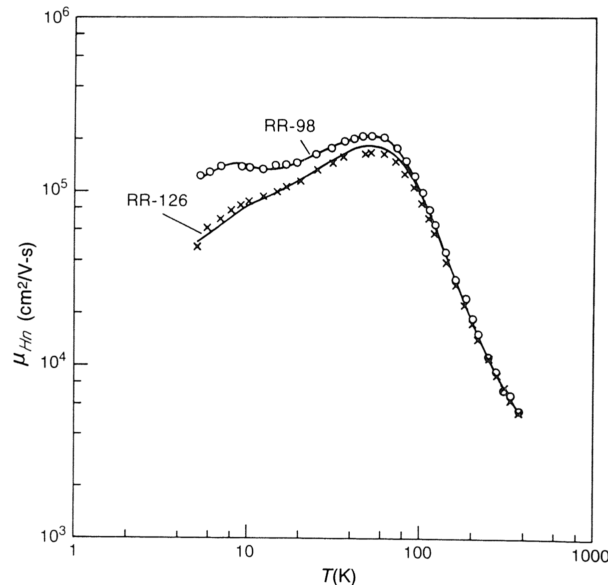

Fig. 1.4.7 The electron Hall mobility μ_H vs. temperature T for the two samples shown in Fig. 1.4.6. The solid lines represent least-squares fits by a numerical solution of the Boltzmann equation (Section 1.3.2.4) with the following fitting parameter, N_A: RR-126: $N_A = 7.8 \times 10^{13}\,\text{cm}^{-3}$; RR-98: $N_A = 1.5 \times 10^{13}\,\text{cm}^{-3}$. (After Look and Colter (1983). Reproduced by permission of The American Institute of Physics)

dominant, and μ decreases with T. Thus, μ vs. T exhibits a double maximum in RR-98, but not in RR-126, which has a larger value of N_A.

1.4.3.1.3 High temperature, with $\phi_D \gg N_A^{\text{net}}$, $N_D - N_A^{\text{net}}$. In this case, the square-root term can again be expanded, with the result

$$n = \tfrac{1}{2}(\phi_D + N_A^{\text{net}})\frac{2\phi_D(N_D - N_A^{\text{net}})}{(\phi_D + N_A^{\text{net}})^2} \simeq N_D - N_A^{\text{net}} \tag{1.4.22}$$

Thus, at higher temperatures, n approaches a constant, $N_D - N_A^{\text{net}}$, because all of the uncompensated donor electrons have been excited into the conduction band. This region is clearly seen in Figs. 1.4.4 and 1.4.6.

1.4.3.2 n-type sample; acceptor dominant

The fact that a sample is n-type does not guarantee that a donor is dominant, i.e., that $\mathscr{E}_F$ is near a donor, but only that $n > p$, or

$$\sum_k N_{Dk}^{+} > \sum_k N_{Ak}^{-}$$

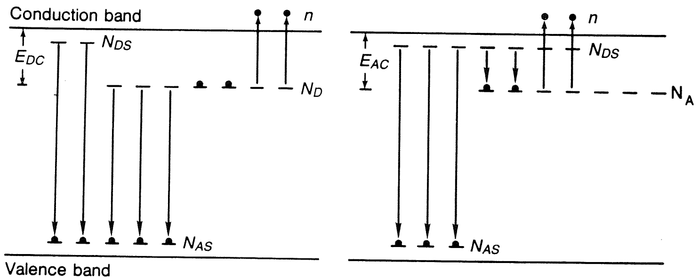

Fig. 1.4.8 A schematic illustration of how a deep level of a given energy and concentration can be either (a) a donor or (b) an acceptor (N_D or N_A), and yet give the same free electron concentration n. For this to happen, the shallow-level concentrations, N_{DS} and N_{AS}, must be different in the two cases. (After Look and Sizelove (1987). Reproduced by permission of The American Institute of Physics)

Thus, we could imagine a situation like that illustrated in Fig. 1.4.8 (Look and Sizelove, 1987), in which electrons supplied to acceptors N_A from shallow donors N_{DS} are being thermally excited to the conduction band. The charge-balance equation is now

$$n + N_A^- = n + n_{A1} = \sum_{\substack{k \\ \mathscr{E}_{Dk} \gg \mathscr{E}_F}} N_{Dk} - \sum_{\substack{k \\ \mathscr{E}_{Ak} \ll \mathscr{E}_F}} N_{Ak} \equiv N_D^{\text{net}} \tag{1.4.23}$$

or

$$n - N_D^{\text{net}} = \frac{N_A}{1 + \frac{g_{A0}}{g_{A1}} e^{(\mathscr{E}_{A1} - \mathscr{E}_F)/kT}} = \frac{N_A}{1 + \phi_A^{CB}/n} \tag{1.4.24}$$

where

$$\phi_A^{CB} = \frac{g_{A0}}{g_{A1}} N'_C e^{\alpha_A/k} e^{-E_{A0}^{CB}/kT} \tag{1.4.25}$$

Although ϕ_A^{CB} here has exactly the same form as ϕ_D (Eq. (1.4.18)), it seems at first glance that the entire equation, Eq. (1.4.24), has a significantly different n-dependence than that of Eq. (1.4.17), and thus, that it should be possible by a goodness-of-fit criterion to tell whether a donor or acceptor is dominant. In fact, it can be rigorously shown that such a decision is impossible to make by an n vs. T fit alone, and that this impossibility holds not only for the simple single-level centers discussed here, but also for centers of any complexity (Look, 1987b). As shown in Table 1.4.1, the only fitting p[illegible]meter that is different in any sense is the temperature-indepen[illegible] concentration, and unless some knowledge of N_{AS} and N_{DS} is

Table 1.4.1 Comparison of donor and acceptor fits (compare Fig. 1.4.8)

Fitting parameter	Donor fit (Eqs. (1.4.17), (1.4.18))	Acceptor fit (Eqs. (1.4.24), (1.4.25))
Activation energy of dominant center	E_D	E_A^{CB}
Concentration of dominant center	N_D	N_A
Temperature-independent concentration	$N_{AS} - N_{DS}$	$N_{AS} - N_{DS} - N_A$
Degeneracy term	$(g_0/g_1)N'_c \exp(\alpha/k)$	$(g_0/g_1)N'_c \exp(\alpha/k)$

available from *other* sources (say from mobility, or analytical measurements), it is impossible to use this term as an indicator of whether the dominant center is a donor or an acceptor.

1.4.3.3 *p-type sample; acceptor dominant*

For a p-type sample, $p \gg n$, and thus the charge-balance equation becomes

$$N_A^- = n_{A1} = p + N_D^{\text{net}} \tag{1.4.26}$$

or

$$p + N_D^{\text{net}} = \frac{N_A}{1 + \frac{g_{A0}}{g_{A1}} e^{(\mathscr{E}_{A1} - \mathscr{E}_F)/kT}} = \frac{N_A}{1 + p/\phi_A} \tag{1.4.27}$$

where

$$\phi_A = \frac{g_{A1}}{g_{A0}} N'_V e^{\alpha_A/k} T^{3/2} e^{-E_{A0}/kT} \tag{1.4.28}$$

Here, $N'_V = 2(2\pi m_p^* k)^{3/2}/h^3$, and E_A is assumed to obey $E_A = E_{A0} - \alpha_A T$. Note that the statistics here (a dominant acceptor in a p-type sample) are precisely those of a dominant donor in an n-type sample, except that the degeneracy factor g_{A1}/g_{A0} is inverted.

1.4.4 Degeneracy factors

In order to determine the various g_{lm}, we need to know something about the states being considered, especially their symmetries. Band states and s-like donor states were illustrated in Fig. 1.4.1, and it was seen that the values of g_0, g_1, and g_2 were 1, 2, and 1 respectively. A slightly more complicated example is that of a shallow acceptor, made up of Γ-point valence-band type functions, which consist of s-like an[illegible] p-like functions. Consider the acceptor Cd_{Ga}, which results in seven elect[illegible], in the primitive cell. In parts (a) and (b) of Fig. 1.4.9, it is assumed that the $p_+ \equiv p_x + ip_y$,

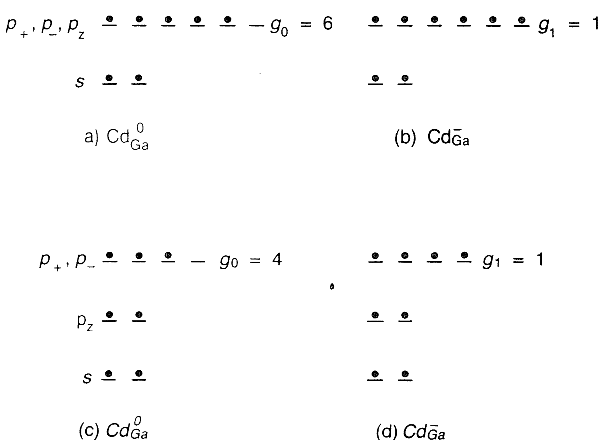

Fig. 1.4.9 Various possible degeneracies which can result from the impurity states Cd^0_{Ga} and Cd^-_{Ga}, depending on the assumptions about energy splittings

$p_- \equiv p_x - ip_y$, and p_z functions are all degenerate, so that together they can hold six electrons. The Cd^0_{Ga} charge state will supply five electrons to this manifold, so that $g_{A0} = 6!/5!\,1! = 6$, and the Cd^-_{Ga} charge states supplies six electrons, so that $g_{A1} = 6!/6! = 1$. Then the degeneracy factor in Eq. (1.4.28) is $g_{A1}/g_{A0} = \frac{1}{6}$.

On the other hand, the p_z functions are often split off from the other p-like states by more than a few kT, giving the situation shown in (c) and (d) of Fig. 1.4.9. In this case, $g_{A0} = 4!/3!\,1! = 4$ and $g_{A1} = 4!/4! = 1$, so that $g_{A1}/g_{A0} = \frac{1}{4}$. This latter value is the acceptor degeneracy factor usually quoted in the literature for single-level acceptors, but it should be realized that a definite model is implicitly assumed by its use.

Next consider Cu_{Ga}, a double-level acceptor, which results in six electrons in the primitive cell. The energy arrangement suggested in (c) and (d) of Fig. 1.4.9 would lead to $g_{A0} = 4!/2!\,2! = 6$, $g_{A1} = 4!/3!\,1! = 4$, and $g_{A2} = 4!/4! = 1$. If $\mathscr{E}_F$ is near the $(-/0)$ level, and the $(2-/-)$ level is much higher in energy, then Eq. (1.4.27) will adequately describe the situation, with $g_{A1}/g_{A0} = \frac{2}{3}$; this value has also been used in several works dealing with double-level acceptors.

Finally, two common centers that make GaAs semi-insulating are Cr and EL2. The Cr^{3+}/Cr^{2+} acceptor transition, i.e. $(-/0)$, has a degeneracy factor $g_{A1}/g_{A0} = \frac{5}{4}$, as determined from the symmetry of the states involved. The situation for EL2, on the other hand, is not as clear. If EL2 consists *mainly* of As_{Ga}, with only a small energy perturbation from an associated defect which is presumed to exist, then Fig. 1.4.1 would apply with $g_{D0} = 1$, $g_{D1} = 2$, and $g_{D2} = 1$. If the upper donor level, $(0/+)$, and lower donor level, $(+/2+)$, are well separated in energy, then the former, if dominant, would

have a degeneracy factor of $g_{D0}/g_{D1} = \frac{1}{2}$, and the latter, $g_{D1}/g_{D2} = 2$. However, the actual lower symmetry (than tetrahedral) of the Ga_{As}–X defect complex may disturb the energy scheme enough that the degeneracy factors will not be those given above.

1.4.5 A general formulation

A completely general charge-balance equation has been derived in Appendix C:

$$n = p + \sum_{k,l=0,m}^{l=l_{Dk}+l_{Ak}} (l_{Dk} - l)n_{klm} \qquad (1.4.29)$$

where n_{klm} has already been defined in Eq. (1.4.3). Here, l_{Dk} is the maximum number of donor transitions a given center may have, and l_{Ak} the maximum number of acceptor transitions, all within the band gap of course. Most impurities and defects are pure donors ($l_{Ak} = 0$) or pure acceptors ($l_{Dk} = 0$), but there are exceptions. As an example, suppose a hypothetical center k had three donor levels ($l_{Dk} = 3$) and two acceptor levels ($l_{Ak} = 2$). Then, l would range from 0 to 5, giving six charge states and five possible transitions. (The $l = 6$ state in this example would be unstable with respect to auto-ionization; i.e. the sixth electron would transfer to the bottom of the conduction band unless $\mathscr{E}_F$ were very high in the band.) The neutral state in this case would have $l = 3$. A complete outline of the various possible transitions is given in Table 1.4.2. The $l = 0$ state is chosen on the basis that

Table 1.4.2 Data for a hypothetical center k with three donor levels ($l_{kD} = 3$) and two acceptor levels ($l_{kA} = 2$), all in their respective ground states ($m_l = 0$)

l	Number of electrons	Charge	Total energy	Transition energy	Transition notation	Transition designation
(6)	$(n_0 + 6)$	(-3)	$(\mathscr{E}_{k60})$			
				$(\mathscr{E}_{k60} - \mathscr{E}_{k50})$	$(3-/2-)$	Triple acceptor (unstable)
5	$n_0 + 5$	-2	$\mathscr{E}_{k50}$			
				$\mathscr{E}_{k50} - \mathscr{E}_{k40}$	$(2-/-)$	Double acceptor
4	$n_0 + 4$	-1	$\mathscr{E}_{k40}$			
				$\mathscr{E}_{k40} - \mathscr{E}_{k30}$	$(-/0)$	Single acceptor
3	$n_0 + 3$	0	$\mathscr{E}_{k30}$			
				$\mathscr{E}_{k30} - \mathscr{E}_{k20}$	$(0/+)$	Single donor
2	$n_0 + 2$	$+1$	$\mathscr{E}_{k20}$			
				$\mathscr{E}_{k20} - \mathscr{E}_{k10}$	$(+/2+)$	Double donor
1	$n_0 + 1$	$+2$	$\mathscr{E}_{k10}$			
				$\mathscr{E}_{k10} - \mathscr{E}_{k00}$	$(2+/3+)$	Triple donor
0	n_0(core)	$+3$	$\mathscr{E}_{k00}$			

a greater-than-bandgap energy would be required to excite an electron from this 'core' state to the conduction band. Note again that the *measured* quantities are the *transition* energies, not the *total* energies. Since the transition energy is $E_l = \mathscr{E}_l - \mathscr{E}_{l-1}$, we can write the $\mathscr{E}_l$ as follows:

$$\mathscr{E}_l \equiv \mathscr{E}_l - \mathscr{E}_0 = E_l + E_{l-1} + E_{l-2} + \cdots E_1 \tag{1.4.30}$$

Equation (1.4.29) can be written in another way to show the symmetry with respect to donors and acceptors. We add and subtract the following term from the right-hand side of Eq. (1.4.29):

$$\sum_{\substack{k \\ \text{acceptors}}} l_{Ak} N_{Ak} = \sum_{\substack{k,l=0,m \\ \text{acceptors}}}^{l=l_{Ak}} l_{Ak} n_{klm} = \sum_{\substack{k,l=0,m \\ \text{acceptors}}}^{l=l_{Dk}+l_{Ak}} l_{Ak} n_{klm} \tag{1.4.31}$$

The final step in Eq. (1.4.31) follows because $l_{Dk} = 0$ for acceptors. Then Eq. (1.4.29) becomes

$$n = p + \sum_{k,l=0,m}^{l=l_{Dk}+l_{Ak}} (l_{Dk} + l_{Ak} - l) n_{klm} - \sum_k l_{Ak} N_k \tag{1.4.32}$$

But n, p, and the first summation are all entirely symmetrical with respect to whether a particular center k has l_{Dk} donor states and l_{Ak} acceptor states, or vice versa. Then, since the last term is temperature-independent, an n vs. T fit will give exactly the same values of N_k, $\mathscr{E}_{klm}$ and g_{klm}, whether centers are assumed to be donors or acceptors. The only change will be in the *interpretation* of N^{net}, which comprises of the last summation plus the temperature-independent parts of the first summation.

1.4.6 Fits to carrier concentration vs. temperature

The major use of Eq. (1.4.29) or (1.4.32) is to fit n(or p) vs. T data. Usually, n is determined from the Hall coefficient, i.e., $n = r/eR_H$, and r may be obtained from the mobility. A self-consistent procedure is outlined below:

(1) Measure R_H and σ vs. T.
(2) Initially, let $r = 1$ for all T, so that $n_{(1)} = 1/eR_H$.
(3) Let $\mu_{(1)} = \mu_H = |R\sigma|$, and find values of $N_{I(1)}$ and other undetermined constants such that Eq. (1.3.80) (or equivalent) is satisfied for $\mu_{(1)}$. Note that $n_{(1)}$ will be used in the screening factor for τ_{ii} (Eq. (1.3.36)), and the other scattering mechanisms.
(4) By using the expressions for the various τ_i found in Step 3, calculate $r_{(1)}$ from $r = \langle\tau^2\rangle/\langle\tau\rangle^2$, or equivalent. Then get a new set of values for n: $n_{(2)} = r_{(1)}/eR_H$.
(5) Go to Step 3, except now $\mu_{(2)} = \mu_H/r(1)$. Continue.

Usually, o. ɔr two iterations are sufficient for this procedure to converge and give accurate values of n vs. T. Then Eq. (1.4.29) can be applied, as

illustrated in several examples below. However, it should be remembered that the *measured n* depends on the *electrical* thickness, which in turn depends on the *actual n*, because of depletion. (Section 1.1.9.2; Chandra *et al.*, 1979; Lepkowski *et al.*, 1987). This correction should be included in the iterations, for maximum accuracy.

An example of a self-consistent fit, involving a numerical solution of the mobility $\mu(n)$ to obtain $r(n)$, and a simultaneous solution of $n = r(n)/eR_H$, is illustrated by the data of Figs. 1.4.6 and 1.4.7. The corresponding r vs. T was presented earlier in Fig. 1.2.1.

1.4.6.1 Shallow donor dominant

In n-type GaAs exhibiting very small (~5 meV) activation energies, it is quite certain that the dominant (i.e. 5 meV) level is a donor, because the possibility of other donor levels existing even closer to the conduction band is extremely remote. Good examples of such samples were given in Fig. 1.4.4 and 1.4.6., which clearly are 'single-level' problems, since there is no evidence of other levels having temperature-dependent occupation probabilities over the temperature range considered. Also, $p = n_i^2/n = 5.1 \times 10^{12}\,\text{cm}^{-6}/n$ is very small, i.e., $p \ll n$, so that Eq. (1.4.29) gives

$$\begin{aligned}
n &= \sum_{l=0,m}^{l=1} (1-l) n_{Dlm} + \sum_{\substack{k,l,m \\ \text{acceptor levels} \\ \text{below } \mathscr{E}_F}} (-l) n_{klm} \\
&= \sum_m n_{D00} - N_A^{\text{eff}} \\
&= \frac{N_D}{1 + \sum_{l',m'} \frac{g_{Dl'm'}}{g_{D00}} e^{(\mathscr{E}_{D00} - \mathscr{E}_{Dl'm'} + l'\mathscr{E}_F)/kT}} - N_A^{\text{eff}} \\
&= \frac{N_D}{1 + \sum_{m'} \frac{g_{D1m'}}{g_{D00}} e^{(-\mathscr{E}_{D1m'} + \mathscr{E}_F)/kT}} - N_A^{\text{eff}} \\
&= \frac{N_D}{1 + \frac{g_{D10}}{g_{D00}} e^{(-\mathscr{E}_{D10} + \mathscr{E}_F)/kT}(1+F)} - N_A^{\text{eff}} \\
&= \frac{N_D}{1 + \frac{g_{D10}}{g_{D00}} e^{(E_D - E_F)/kT}(1+F)} - N_A^{\text{eff}} \\
&= \frac{N_D}{1 + \frac{g_{D10}}{g_{D00}} e^{\alpha_D/k} e^{(E_{D0} - E_F)/kT}(1+F)} - N_A^{\text{eff}}
\end{aligned} \tag{1.4.33}$$

where $E_D = \mathscr{E}_G - \mathscr{E}_{D10}$, $E_F = \mathscr{E}_G - \mathscr{E}_F$, F was defined in Eq. (1.4.12), and N_A^{eff} is defined by

$$N_A^{\text{eff}} = \sum_{\substack{k,l,m \\ \text{acceptor levels} \\ \text{below } \mathscr{E}_F}} l n_{klm} = \sum_k l_{Ak} N_k \tag{1.4.34}$$

In Eq. (1.4.34), it is assumed that *all* possible acceptor levels for a given center are below $\mathscr{E}_F$.

The fitting parameters are $E_{D0}(= E_D - \alpha_D T)$, $(g_{D10}/g_{D00}) \exp(\alpha_D/k)$, N_D, F, and N_A^{eff}. Note that usually N_A^{eff} is given as N_A, the total acceptor concentration in the sample. However, the l_{Ak} in Eq. (1.4.34) accounts for the fact that some of them may have multiple charges. There is no way of determining the various components of N_A^{eff}, of course, by an n vs. T fit alone.

Equation (1.4.33) can now be solved for n or $\mathscr{E}_F$ by using

$$n = N_C e^{-(\mathscr{E}_G - \mathscr{E}_F)/kT} = N_C e^{-E_F/kT} = N'_C T^{3/2} e^{-E_F/kT} \tag{1.4.35}$$

in the Boltzmann approximation ($\mathscr{E}_F < \mathscr{E}_G - 3kT$), or, in general,

$$n = N_C \int_0^\infty \frac{(2/\sqrt{\pi}) x^{1/2}\, dx}{1 + \exp[x + E_F/kT]} \tag{1.4.36}$$

where E_F is a positive quantity here if $\mathscr{E}_F$ is *below* the conduction-band edge. The vast majority of n vs. T data in GaAs are fitted with Eq. (1.4.33), although normally the F factor is omitted.

1.4.6.2 *Shallow acceptor dominant*

As in the previous example, when a very small activation energy is measured it can be safely assumed that even shallower levels are absent. In a p-type sample ($p \gg n$), in which there is no evidence from the p vs. T data that multiple-charge states or excited states exist in the dominant center, and also that no other dominant centers exist, Eq. (1.4.29) gives

$$\begin{aligned} 0 &= p + \sum_{l=0,m=0}^{l=1,m=0} (0 - l) n_{Alm} + \sum_{\substack{k,l,m \\ \text{donor levels} \\ \text{above } \mathscr{E}_F}} (l_{Dk} - l) n_{klm} \\ &= p - n_{A10} + \sum_k l_{Dk} N_k \\ &= p - \frac{N_A}{1 + \frac{g_{A00}}{g_{A10}} e^{(\mathscr{E}_{A10} - \mathscr{E}_{A00} - \mathscr{E}_F)/kT}} + N_D^{\text{eff}} \\ &= p - \frac{N_A}{1 + \frac{g_{A00}}{g_{A10}} e^{(E_A - \mathscr{E}_F)/kT}} + N_D^{\text{eff}} \\ &= p - \frac{N_A}{1 + \frac{g_{A00}}{g_{A10}} e^{\alpha_A/k} e^{(E_{A0} - \mathscr{E}_F)/kT}} + N_D^{\text{eff}} \end{aligned} \tag{1.4.37}$$

where E_A is the acceptor activation energy (a positive quantity). Here again, the definition of N_D^{eff} reflects the fact that some of the donors may have multiple levels, and it is assumed that all of these levels are above $\mathscr{E}_F$, in this case. Equation (1.4.37) is solved for p or $\mathscr{E}_F$ by using the relationship

$$p = N_V e^{-\mathscr{E}_F/kT} = N'_V T^{3/2} e^{-\mathscr{E}_F/kT} \tag{1.4.38}$$

in the Boltzmann limit ($\mathscr{E}_F > 3kT$), or

$$p = N_V \int_0^\infty \frac{(2/\sqrt{\pi}) x^{1/2}\, dx}{1 + \exp[x + \mathscr{E}_F/kT]} \tag{1.4.39}$$

in the general case.

1.4.6.3 *Deep centers dominant*

The equations already derived in the previous sections for shallow-level n-type and p-type samples are basically sufficient for deep-level samples also, as long as only single-level deep centers are assumed. The only changes involved are in the definitions of N_A^{eff} and N_D^{eff}, the temperature-independent terms, which must be generalized:

$$\begin{aligned} N_A^{\text{eff}} = -N_D^{\text{eff}} &= \sum_{\substack{k,l,m \\ \text{acceptor levels} \\ \text{below } \mathscr{E}_F}} (l - l_{Dk}) n_{klm} - \sum_{\substack{k,l,m \\ \text{donor levels} \\ \text{above } \mathscr{E}_F}} (l_{Dk} - l) n_{klm} \\ &= \sum_k (l_{Fk} - l_{Dk}) N_{Ak} - \sum_k (l_{Dk} - l_{Fk}) N_{Dk} \\ &= \sum_k (l_{Fk} - l_{Dk}) N_k \end{aligned} \tag{1.4.40}$$

where l_F is defined by the relationship:

$$\mathscr{E}_{l_F} - \mathscr{E}_{l_F - 1} < \mathscr{E}_F - 3kT \tag{1.4.41a}$$

$$\mathscr{E}_{l_F + 1} - \mathscr{E}_{l_F} > \mathscr{E}_F + 3kT \tag{1.4.41b}$$

Here N_{Ak} is a center which is negatively charged (i.e. acceptor-like) at the given value of $\mathscr{E}_F$, but may also exhibit donor transitions at lower values of $\mathscr{E}_F$, and N_{Dk} is a center which is positively charged (donor-like) at the given $\mathscr{E}_F$. For a simple, single-level acceptor, with that level below $\mathscr{E}_F$ (i.e. $\mathscr{E}_1 - \mathscr{E}_0 < \mathscr{E}_F$), $l_D = 0$ and $l_F = 1$, so that its contribution to N_A^{eff} is just N_A. For a double-level acceptor, with both levels below $\mathscr{E}_F$, $l_D = 0$ and $l_F = 2$, so that the contribution to N_A^{eff} is $2N_A$. A triple-level donor, on the other hand, with the two upper levels above $\mathscr{E}_F$ (i.e., $\mathscr{E}_3 - \mathscr{E}_2 > \mathscr{E}_F$, $\mathscr{E}_2 - \mathscr{E}_1 > \mathscr{E}_F$), and the lower level below $\mathscr{E}_F$ (i.e., $\mathscr{E}_1 - \mathscr{E}_0 < \mathscr{E}_F$), would have $l_D = 3$ and $l_F = 1$, so that the contribution to N_A^{net} would be $-2N_D$. Basically, $|l_{Fk} - l_{Dk}|$ gives

1.4.6.4 *General fitting routine*

As shown in Section 1.4.5, we have no hope of determining, from a statistical fit alone, whether a given center k is a donor or an acceptor. The only difference in the charge-balance equation comes in the temperature-independent term, as in obvious from Eq. (1.4.32):

$$\begin{aligned} n &= p + \sum_{k,l=0,m}^{l=l_{Dk}+l_{Ak}} (l_{Dk} + l_{Ak} - l) n_{klm} - \sum_k l_{Ak} N_k \\ &= p + \sum_{\substack{k,l=0,m \\ \text{levels near } \mathscr{E}_F}}^{l=l_{Dk}+l_{Ak}} (l_{Dk} + l_{Ak} - l) n_{klm} \\ &\quad - \sum_{\substack{k \\ \text{levels near } \mathscr{E}_F}} l_{Ak} N_k - \sum_{\substack{j \neq k \\ \text{levels far} \\ \text{from } \mathscr{E}_F}} (l_{Fj} - l_{Dj}) N_j \\ &= p + \sum_{\substack{k,l=0,m \\ \text{levels near } \mathscr{E}_F}}^{l_k} (l_k - l) n_{klm} + N_0 \end{aligned} \qquad (1.4.42)$$

where $l_k = l_{Dk} + l_{Ak}$ is simply the maximum number of electrons a center can hold, for $\mathscr{E}_F < \mathscr{E}_G$. Here $n_{klm} = N_k f(\mathscr{E}_{klm})$, as given by Eq. (1.4.3), and N_0 is independent of temperature over the given range. Note that the centers with index k have transitions (levels) near $\mathscr{E}_F$, while those with index j do not. Thus, the values of N_k can be determined, in principle, by the n vs. T fit, whereas the N_j cannot be determined individually but only as part of the temperature-independent term N_0.

We illustrate the use of Eq. (1.4.42) with an example of two shallow centers (C_1, a single-level donor, and C_4, a single-level acceptor) and two deep single-level centers, C_2 and C_3, with unknown donor or acceptor nature. It is assumed that, as temperature is varied, $\mathscr{E}_F$ covers an energy range that includes C_2 and C_3 but not C_1 and C_4, as illustrated in Fig. 1.4.10. Since both C_2 and C_3 have only one level in the band gap, $l_k = 1$ and $l = 0$ or 1, independent of their donor or acceptor nature. If excited states are assumed absent ($m = 0$), then Eq. (1.4.42) becomes

$$\begin{aligned} n &= p + n_{200} + n_{300} + N_0 \\ &= p + \frac{N_2}{1 + \dfrac{g_{210}}{g_{200}} e^{(-\mathscr{E}_{210} + \mathscr{E}_F)/kT}} + \frac{N_3}{1 + \dfrac{g_{310}}{g_{300}} e^{(-\mathscr{E}_{310} + \mathscr{E}_F)/kT}} + N_0 \end{aligned} \qquad (1.4.43)$$

Here $\mathscr{E}_F$ can be written in terms of n or p, depending on whether $n_{meas} \gg p_m$ [illegible]r vice versa, and p can be written as n_i^2/n, if desired. If $\mathscr{E}_{210}$ and $\mathscr{E}_{310}$ [illegible] assumed to be independent of temperature, then the fitted

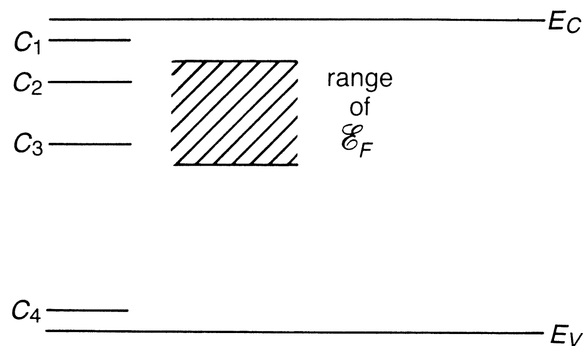

Fig. 1.4.10 A four-level model which can be analyzed with Eq. (1.4.43). Here it is assumed that the Fermi level $\mathscr{E}_F$ varies with temperature over a range which encompasses the energies of centers C_2 and C_3, but not C_1 or C_4

Table 1.4.3 Values of a temperature-independent term N_0 for various D/A choices of centers C_1, C_2, C_3 and C_4. Center C_1 is assumed to have a single-level donor far above $\mathscr{E}_F/(l_{D1} = 1,\ l_{F1} = 0)$, and center C_4 a single-level acceptor far below $\mathscr{E}_F(l_{D4} = 0,\ l_{F4} = 1)$

C_1	C_2	(l_{A2})	C_3	(l_{A3})	C_4	N_0
D	D	0	D	0	A	$N_1 - N_4$
D	D	0	A	1	A	$N_1 - N_4 - N_3$
D	A	1	D	0	A	$N_1 - N_4 - N_2$
D	A	1	A	1	A	$N_1 - N_4 - N_2 - N_3$

parameters will be $\mathscr{E}_{210}$, $\mathscr{E}_{310}$, N_2, N_3, g_{210}/g_{200}, g_{310}/g_{300}, and N_0, where N_0 must be interpreted as shown in Table 1.4.3. Note that it is impossible to determine $N_1 - N_4$ unless the donor/acceptor natures of C_2 and C_3 are known. Sometimes mobility and analytical information can be used to help make those choices.

Often in as-grown, bulk, GaAs, three dominant defect centers are found (Look *et al.* 1983), at energies $\mathscr{E}_C - 0.15$ (or $\mathscr{E}_2 = 1.37\,\text{eV}$), $\mathscr{E}_C - 0.43$ (or $\mathscr{E}_3 = 1.09\,\text{eV}$), and $\mathscr{E}_C - 0.75$ (or $\mathscr{E} = 0.77\,\text{eV}$). The last energy is that of EL2, which dominates in semi-insulating GaAs, while the other two are dominant in more conducting, n-type material. We assume typical concentrations for N_2 and N_3 of about $5 \times 10^{15}\,\text{cm}^{-3}$, and also assume $N_1 - N_4 = -2 \times 10^{15}\,\text{cm}^{-3}$ and degeneracy factors of unity. Then the computer-generated curve of n vs. T for Eq. (1.4.43) is given in Fig. 1.4.11 (Sizelove and Look, 1988). Note that intrinsic conduction (electrons excited from valence band) becomes important above 800 K. [illegible]rtunately, the intrinsic electron excitation can obscure the excitation from EL2.

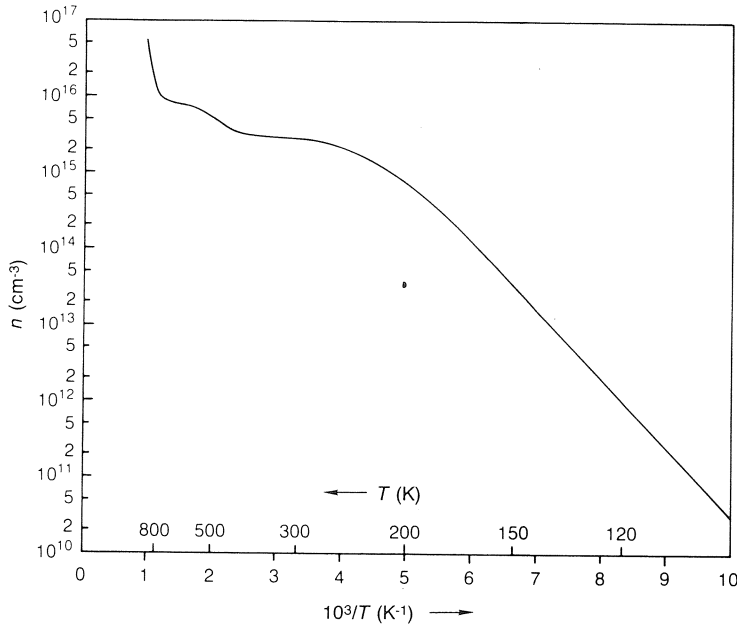

Fig. 1.4.11 A computer-generated curve of electron concentration n vs. inverse temperature T^{-1} for the four-level model of Fig. 1.4.10 and Eq. (1.4.43). It is assumed that C_1 is a donor, and C_4 an acceptor. The various other assumptions are as follows: $N_2 = N_3 = 5 \times 10^{15}\,\text{cm}^{-3}$; $N_0 = 2 \times 10^{15}\,\text{cm}^{-3}$; $\mathscr{E}_2 = 1.37\,\text{eV}$ (or $E_2 = 0.15\,\text{eV}$); $\mathscr{E}_3 = 1.09\,\text{eV}$ (or $E_3 = 0.43\,\text{eV}$); and $g_{21}/g_{20} = g_{31}/g_{30} = 1$. The sharp increase in n at high temperature is due to intrinsic electron excitation. Note that N_0 cannot be interpreted in terms of N_1, N_2, N_3, and N_4 unless the donor/acceptor natures of C_2 and C_3 are known

Data from a pure, vapor-phase epitaxial GaAs layer, irradiated with $1 \times 10^{14}/\text{cm}^2$ 1 MeV electrons, are shown in Fig. 1.4.12 (Sizelove and Look, 1988). It is evident that two centers are contributing to the temperature-dependent electron excitation, so that Eq. (1.4.43) and Table 1.4.3 should apply. The fitted energy values (for $T = 0$) are: $\mathscr{E}_2 = 1.375\,\text{eV}$, or $E_2 = \mathscr{E}_G - \mathscr{E}_2 = 1.519 - 1.375 = 0.144\,\text{eV}$, and $\mathscr{E}_3 = 1.228\,\text{eV}$, or $E_3 = 0.291\,\text{eV}$. These values agree very well with those measured by deep-level transient spectroscopy (Pons and Bourgoin, 1985), in which they are designated, respectively, as $E2$ and $E3$. The value of N_0, $1.0 \times 10^{14}\,\text{cm}^{-3}$, could be interpreted in four different ways, as shown in Table 1.4.3; however, it is known from other work (Look, 1987a) that $E2$ is a donor, so that N_0 is either $N_1 - N_4$ or $N_1 - N_4 - N_3$, where N_1 is the total concentration of donors with $\mathscr{E} > \mathscr{E}_F$, and N_4 is the total concentration of acceptors with $\mathscr{E} < \mathscr{E}_F$. The values of the degeneracy factors, $(g_{k1}/g_{k0}) \exp(\alpha_k/k)$, are both about 0.5, which is somewhat unexpected since a simple, s-like donor

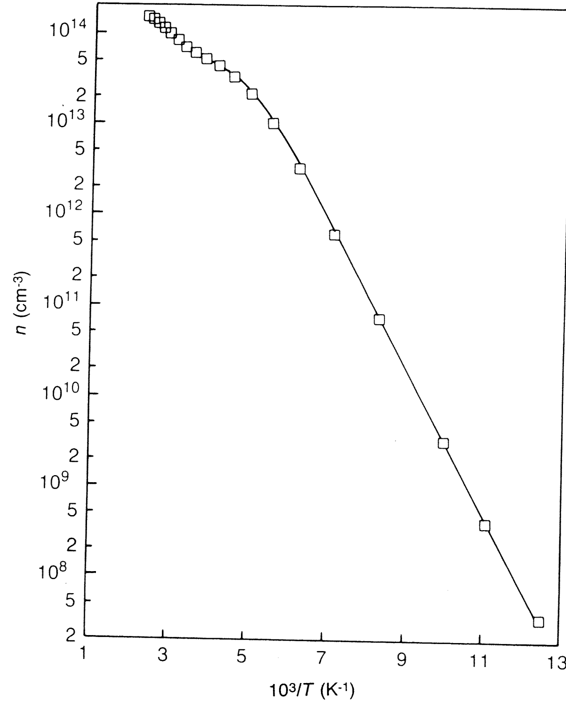

Fig. 1.4.12 The electron concentration n vs. inverse temperature T^{-1} for a pure, epitaxial GaAs layer irradiated with $1 \times 10^{14}\,\text{cm}^{-2}$ 1 MeV electrons. The solid line is a fit by Eq. (1.4.43), with the following parameters: $N_2 = 1.58 \times 10^{14}\,\text{cm}^{-3}$; $N_3 = 1.44 \times 10^{14}\,\text{cm}^{-3}$; $N_0 = 1.03 \times 10^{14}\,\text{cm}^{-3}$; $\mathscr{E}_2 = 1.375\,\text{eV}$ (or $E_2 = 0.144\,\text{eV}$); $\mathscr{E}_3 = 1.228\,\text{eV}$ (or $E_3 = 0.291\,\text{eV}$); and $g_{21}/g_{20} = g_{31}/g_{30} = 0.5$. (After Sizelove and Look (1988))

should give $g_{k1}/g_{k0} \simeq 2$, as shown in Fig. 1.4.1(b). However, the temperature factor α_k must also be taken into account, where α_k here is given by $\mathscr{E}_k = \mathscr{E}_k(T = 0) - \alpha_k T$. Since $\mathscr{E}_k$ is an energy with respect to the *valence* band, a positive α_k implies that the level is moving closer to the valence band, as temperature is increased. In fact, it is more likely that the opposite is true, in which case α_k would be negative, and $\exp(\alpha_k/k) < 1$. Thus, the values of the degeneracy factors could be explained by $g_{k1}/g_{k0} \simeq 2$, and $\exp(\alpha_k/k) \simeq \frac{1}{4}$, but there is no way of knowing this for sure without separate determinations of these quantities. Indeed, there is some evidence from emission and capture measurements (Pons and Bourgoin, 1985) that $\alpha_2 \simeq 0$, and $\alpha_3 \simeq -1.7k$, over restricted temperature ranges. If these values are accurate, then $g_{21}/g_{20} \simeq 0.5$ and $g_{31}/g_{30} \simeq 2.7$; however, further investigation needs to take place before any firm conclusions can be drawn in this matter.

ECTRICAL CHARACTERIZATION F GaAs MATERIALS AND DEVICES

VID C. LOOK
ight State University, USA

wofold purpose runs through this book: firstly to summarize the present ctrical-measurement data in GaAs materials and devices, and secondly to scribe in detail the techniques used to obtain these data. Hall effect, gnetoresistance, C–V, DLTS, PICTS, and contact-resistance TLM analysis covered using numerous examples, figures and tables. As well as describing se techniques, *David Look* explains their theoretical basis in order to provide ders with as complete an understanding of the presented data as possible.

ctrical Characterization of GaAs Materials and Devices also includes erage of recently developed characterization techniques such as mobility filing in MESFETs and MODFETs, and magneto-TLM analysis. Special phasis has been given to topics which in the past have often been neglected, h as impurity and defect Fermi functions, degeneracy factors, and multi-d conduction. It has also been given to relatively new subjects such as the plication of magnetoresistance to determine carrier mobility in device uctures.

ntents: Series Preface; Preface; 1 The Hall Effect and Magnetoresistance; lagnetoresistance in Ungated Structures: Contact Resistance Patterns and nn Diodes; 3 Capacitance and Magnetoresistance in Gated Structures: Field-ect Transistors; 4 Capacitance and Conductance Effects from Deep Traps; pendices; Symbols; References; Index

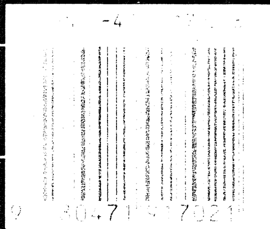

HN WILEY & SONS
ichester · New Y · Brisbane · Toronto · Singapore

LOOK

ELECTRICAL CHARA... OF GaAs MATERIALS AND D...

TK 7871.15 .G3 L66 1989

WILEY

ELECTRICA CHARACTERIZATIO OF Ga MATERIA AND DEVIC

DAVID C. LO

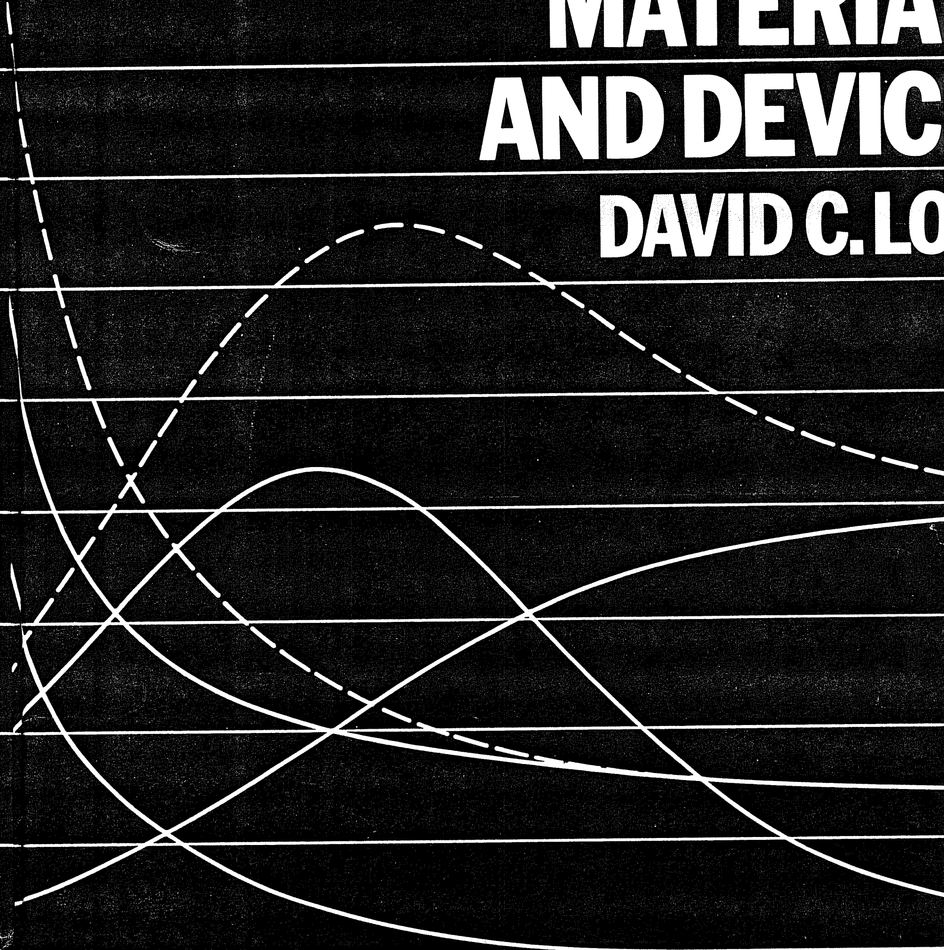

DESIGN AND MEASUREMENT IN ELECTRONIC ENGINEERINC